PERFORMANCE IMPROVEMENT OF PERMANENT MAGNET AC MOTORS

A Dissertation

by

LEILA PARSA

Submitted to the Office of Graduate Studies of
Texas A&M University
in partial fulfillment of the requirements for the degree of

DOCTOR OF PHILOSOPHY

May 2005

Major Subject: Electrical Engineering

PERFORMANCE IMPROVEMENT OF PERMANENT MAGNET AC MOTORS

A Dissertation

by

LEILA PARSA

Submitted to Texas A&M University
in partial fulfillment of the requirements
for the degree of

DOCTOR OF PHILOSOPHY

Approved as to style and content by:

Hamid A. Toliyat (Chair of Committee)	
Mehrdad Ehsani (Member)	Shankar P. Bhattacharyya (Member)
Reza Langari (Member)	Chanan Singh (Head of Department)

May 2005

Major Subject: Electrical Engineering

ABSTRACT

Performance Improvement of Permanent Magnet AC Motors. (May 2005)

Leila Parsa, B.S., Khaje Nasir Toosi University of Technology, Tehran, Iran;

M.S., Iran University of Science and Technology, Tehran, Iran

Chair of Advisory Committee: Dr. Hamid A. Toliyat

Multi-phase motors have several advantages over the traditional three-phase motors. In this study, the additional degrees of freedom available in five-phase permanent magnet motors have been used for three purposes: 1) enhancing the torque producing capability of the motor, 2) improving the reliability of the system, and 3) better adjusting of the torque and flux linkages of the five-phase direct torque controlled system.

1) Due to the fact that space and time harmonics of the same orders will contribute positively to output torque, a five-phase permanent magnet motor with quasi-rectangular back-EMF waveform is supplied with combined fundamental and third harmonic of currents. For modeling and analysis of the motor a $d_1q_1d_3q_30$ frame of reference is defined where d_1q_1 rotates at the synchronous speed and d_3q_3 rotates at the three times synchronous speed. Based on the mathematical model in the $d_1q_1d_3q_30$ frame of reference, it is shown that this system while having a higher torque density with respect to a conventional permanent magnet synchronous machine, is also compatible with vector control algorithm.

2) A resilient current control of the five-phase permanent motor with both sinusoidal and trapezoidal back-EMF waveforms under asymmetrical fault condition is proposed. In this scheme, the stator MMF is kept unchanged during healthy and faulty condition. Therefore, the five-phase permanent magnet motor operates continuously and steadily without additional hardware and just by modifying the control algorithm in case of loss of up to two phases. The feature is of major importance in some specific applications where high reliability is required.

3) High torque and flux ripple are the major drawbacks of a three-phase direct torque controlled system. The number of space voltage vectors directly influences the performance of DTC system. A five-phase drive, while benefiting from other advantages of high order phase drives, has inherently 32 space voltage vectors which permits better flexibility in selecting the switching states and finer adjustment of flux and torque. A sensorless direct torque control of five-phase permanent magnet motor is implemented. Speed information is obtained based on the position of stator flux linkages and load angle.

Experiments have been conducted on a 5kW five-phase surface mount permanent magnet motor and a 3kW five-phase interior permanent magnet motor by using TMS320C32 DSP. The results obtained are consistent with theoretical studies and simulation analysis, which further demonstrate the feasibility and practical significance of the five-phase permanent magnet motor drives.

To my dear parents

ACKNOWLEDGEMENTS

My deep appreciation goes to many people whose advice, assistance and encouragement have enabled me to get to this stage in my life. I am really fortunate to have known so many great people so far in my life that my limited memory cannot accomodate. To those who are missing in this brief list, and were supposed to be here, I sincerely apologize.

First, I wish to express my sincere thanks to my advisor, Prof. Hamid A. Toliyat. His knowledge, valuable guidance, and unlimited patience inspired the completion of this thesis. His encouragement, understanding and willingness to spend his precious time with me are beyond my appreciation.

I express my sincere gratitude to the members of my graduate study committee: Prof. Shankar Bhattacharyya, Prof. Mehrdad Ehsani, and Prof. Reza Langari for taking the time serving on my committee and for their valuable advice and help through the years I spent at Texas A&M University. I would like to thank Prof. Aniruddha Datta for graciously accepting to read my dissertation and attending my final exam.

I also acknowledge the Electrical Engineering Department of Texas A&M University for providing me with excellent academic circumstances that are essential to the accomplishment of my graduate study. Many thanks to Prof. Chanan Singh, Ms. Tammy Carda and Prof. Garng Huang for their help.

I would like to sincerely thank Dr. Farzad Rajaei Salmasi for many interesting and helpful discussions we had together. Also, I am grateful to Dr. Abbas Goodarzi of U.S. Hybrid for helping us with the experimental setup.

Many thanks to my colleagues and friends, past and present, including: Dr. Mehdi Abolhassani, Dr. Huansheng Xu, Peyman Niazi, Peyman Asadi, Dr. Sang-Shin Kwak, Steven Campbell, Baris Salih Ozturk, Dr. Namhun Kim, Salman Talebi, Dr. Ruhe Shi, Rahul Khopkar, Dr. Shailesh Waikar, Dr. Tilak Gopalarathnam and Dr. Mohammad Madani.

Finally, I do not have the words to express my gratitude to my parents and my sisters for their endless love, care, and support.

TABLE OF CONTENTS

Page

TABLE OF CONTENTS (Continued)

TABLE OF CONTENTS (Continued)

LIST OF FIGURES

LIST OF FIGURES (Continued)

LIST OF FIGURES (Continued)

LIST OF FIGURES (Continued)

LIST OF FIGURES (Continued)

LIST OF TABLES

CHAPTER I

INTRODUCTION

A. General

The advent of modern permanent magnets (PM) with significant amount of energy density led to the evolution of dc machines with PM field excitation in the 1950s. Replacing electromagnets with PM eliminated the need of using windings and external energy source. Therefore, compact dc machines were introduced. PM excitation also replaced the dc field excitation of the synchronous machines. In late 1950s, the availability of switching power devices led to the development of inverters. This achievement enabled the replacement of the mechanical commutator with an electronic commutator. Therefore permanent magnet synchronous and brushless dc machines were developed. By removing the mechanical commutator, the armature of the dc machine can be on the stator side. This enables better cooling and higher voltages to be achieved. In this configuration, PM poles used as excitation field are in the rotor side. From structural point of view, permanent magnet machines are the inside out of dc machines with the field and armature interchanged from the stator to the rotor and rotor to stator respectively.

This dissertation follows the style and format of *IEEE Transactions on Industry Applications.*

Permanent magnet machines present a unique set of opportunities to the drive designer. Combining high efficiency with high power density makes them widely appealing. Permanent magnet machines are synchronous machines without auxiliary rotor windings. Therefore accompanying power electronics drive is essential for their operation. These motors obtain life long field excitation from permanent magnets. The absence of rotor electrical circuit makes their analysis simple. Since there are no windings on the rotor, electrical losses in the rotor are minimal.

B. Classification of Permanent Magnet Motors

The permanent magnet (PM) synchronous machines can be widely classified based on the direction of field flux as Radial field, in which the flux direction is along the radius of the machine; and axial field, in which the flux direction is parallel to the rotor shaft. The radial-field PM machines are commonly used, however the axial filed machines are playing a significant role in a small number of applications because of their higher power density and acceleration.

The magnets are mounted either on the surface of the rotor, called surface mount permanent magnet motors or are placed insides the rotor, called interior permanent magnet motors (IPM). Interior permanent magnet motors have superior characteristics compared to surface mount permanent magnet motors. This is due to some of their inherent characteristics such as higher torque density and extended flux weakening region. These two advantages are because of their reluctance torque and ruggedness of the rotor structure. However, the IPM configuration produces considerable torque

pulsation.

In other classification, permanent magnet motors are divided into interior rotor and exterior rotor structures. If rapid acceleration and deceleration of the load is needed in a specific application, as is the case for servo systems, then torque/inertia ratio of the motor should be as high as possible. Therefore, permanent magnet motors with interior rotor and high energy density magnets are good candidates for this application. Exterior rotor configuration is usually being used in application requiring constant speed such as fans and blowers. The spindle motor used in computers is of this category as well. The high inertia of the exterior rotor is an advantage in achieving uniform and constant speed.

Based on the shape of back-EMF waveform, permanent magnet motors are classified into permanent magnet brushless dc motors (BLDC) and permanent magnet synchronous motors (PMSM) [1-3]. The stator winding of a BLDC motor is wound such that the induced back-EMF is quasi-rectangular and that of PMSM is wound such that the induced back-EMF is sinusoidal.

C. Property of Permanent Magnet

The property of permanent magnet and the selection of pertinent materials are crucial in the design of permanent magnet machine. Barium and strontium ferrites are broadly used as permanent magnets. Low cost and huge supply of raw material are two major advantages of ferrite. They can be easily produced and their process is adopted for high

volume as well as moderately high service temperature. The magnet has a practically linear demagnetization curve but has a low remnance. Therefore, the machine has a high volume as well as weight. The Cobalt-Samarium magnet is built of iron, Nickel, Cobalt, and rare-earth Samarium. High remnance, high energy density, and linear demagnetization characteristic are among its advantages. Although the material is quite expensive due to insufficient supply of Samarium, the service temperature can be as high as 300°C and the temperature stability is very satisfactory. The Neodymium-iron-boron (Nd-Fe-B) magnet has the highest energy density, highest remnance, and very good coercivity. The disadvantages are low service temperature, and susceptibility to oxidation if it is not protected by coating. In addition, the temperature stability is lower than that of a CoSm magnet. Although the material is expensive compared to ferrite, the machine weight is reduced due to its higher energy density magnets. Nowadays, Nd-Fe-B magnets are being used in different applications.

D. Multi-phase Machines

Power electronic converters are being utilized for variable speed drives. The power rating of the converter should meet the required level for the machine and driven load. However, the converter ratings can not be increased over a certain range due to the limitation on the power rating of semiconductor devices. One solution to this problem is using multi-level inverter where switches of reduced rating are employed to develop high power level converters. The advent of inverter-fed motor drives also removed the limits of the number of motor phases. This fact made it possible to design machine with

more than three phases and brought about the increasing investigation and applications of multi-phase motor drives.

Multi-phase machines can be used as an alternative to multi-level converters. In multi-phase machines, by dividing the required power between multiple phases, more than the conventional three, higher power levels can be obtained and power electronic converters with limited power range can be used to drive the multi-phase machine.

However whether it is better to use multi-phase machines vs. multi-level converters is debatable and in fact it is extremely application dependent. Insulation level is one of the limiting factors that can prohibit the use of high voltage systems. Therefore, multi-phase machines that employ converters operating at lower voltage level are preferred.

Multi-phase motor drives posses many advantages over the traditional three-phase motor drives such as reducing the amplitude and increasing the frequency of torque pulsation, reducing the stator current per phase without increasing the voltage per phase and increasing the reliability and power density.

E. Previous Research Work

In this section previous research work on multi-phase machine will be reviewed. Most of the previous studies are on multi-phase, split phase and dual stator induction machines. However, recently multi-phase permanent magnet machines have gained increasing attention as well. The purpose of using such systems is mainly achieving higher power level, reducing torque pulsation, increasing the torque density and

improving the reliability.

1. Multi-phase Induction Machines

In the study reported in [4] various current source inverter (CSI) systems were investigated. They had a phase number of two or three and the same number of capacitors as the standard single phase or three-phase CSI. It was concluded that increasing the phase number in multiples of three offers advantages such as reduction of commutation capacitor size and peak commutating voltages. It was also observed that the torque pulsations would be reduced while the number of pulses increases.

Application of inverters in ASD was investigated in [5]. It was shown that the number of phases is a free variable. One can change it based on specific application requirements. If number of phases is odd, the noise frequency of the dc link is in direct proportion to the number of phases. However, the noise amplitude and the torque harmonics are in inverse proportion to the number of phases. In this study the potential advantages in changing air-gap field spatial distribution were not factored in. Instead, harmonics in the supply, which are an essential part of rectangular field production, were considered undesirable. For the purpose of harmonic reduction, it was shown that windings connections should have the highest possible number of insulated star centers.

The behavior of a five-phase induction motor was investigated in [6]. It was concluded that the amplitude of torque pulsation could be reduced by increasing number of phases. However, the improvement was obtained at the expense of introducing strong third and higher orders of harmonic currents into the supply lines. This could result in stator losses in the motor.

Three different configurations of six phase induction motors were demonstrated in [7]. The authors showed that the sixth harmonic of torque pulsation can be eliminated in a motor with 30 degrees of phase belt. However, in their approach the amplitude of stator currents were increased.

The possibility of reducing torque pulsation in a six-phase induction motor was investigated in [8] and [9]. In this scheme, two sets of balanced three-phase windings, with a phase difference of 30 electrical degrees were used to form the six-phase motor. It was shown that the line-to-line voltage in the case of six-phase operation is almost half of that in the case of three-phase operation. For the 6-phase operation, the number of commutation transients on the line voltage is increased to 12 per cycle. The eddy current winding losses are reduced significantly as the torque pulsation reduces.

The steady state torque-speed characteristics of three, six, and nine-phase induction motors with n and n-1 phase sinusoidal excitation were analyzed in [10] and [11]. Windings with different coil pitch and their effect on the harmonic spectrum of the stator current were discussed. Similar other investigations on multi-phase motors were reported in [12] and [13].

In [14], it was suggested that the concentrated winding concept which was successfully applied to synchronous motors, might also be applicable to induction motors. It was shown that the losses of a nine phase induction motor can be reduced by almost 10% when operated near its rated condition. Induction motors with different numbers of phases were analyzed in [15]. It was concluded that for a given frame size, the torque of the six-phase motor can theoretically be increased by 17%. These two

studies showed the potential of improving the power density of multi-phase induction motors.

In split phase electric machines, two similar stator windings share the same magnetic circuit. In this scheme, because the total power is shared between the two drives, the power range of inverter based drives will be extended [16-17]. A split phase machine can be built by equally dividing the phase belt of a conventional three-phase machine into two parts with spatial phase separation of 30 electrical degrees. Due to lower number of turns per phase compared to a three-phase machine, the inverter dc bus voltage can be reduced to almost half of the previous value and still maintain the same airgap flux. The requirement of having two or more inverters in this system is its major drawback. Using split phase machine will also provide the advantage of harmonic cancellation. It has been previously shown that the sixth harmonic torque pulsation can be cancelled [7] and [18]. In [19], the authors investigated the reduction of harmonic content of airgap flux created by fifth and seventh harmonics currents of a six-step converter fed system in the split phase drives. However, the improvement was achieved at the expense of increased converter harmonic current. The harmonic currents can be cancelled by using some PWM techniques during modulation process. This task depends on the power ratings of the devices.

A split-wound induction motor was designed for improving the reliability of PWM inverter [20]. The machine has been designed such that it provides the inductor in series with two switches of the inverter leg and therefore providing fault tolerance to the drive.

Dual stator machines have been used in the literature for similar reasons as of split-

phase machines. In this topology, two independent stator windings share the same magnetic structure. However despite split phase machines, the two windings may have different number of poles, number of phases or ratings [16].

An induction generator with two independent stator windings was suggested in [21] and [22]. One of the stator windings is used for electromechanical power conversion and the other one for excitation. In this scheme, load is connected to power winding and PWM converter is connected to excitation winding. As a result, the converter does not need to meet the requirement for full load power delivery.

In [23], the authors applied the same concept for power factor correction of induction motor. In this approach, one set of windings is connected to the main power and is responsible for delivering active power, whereas the other set carries the reactive power. Sensorless control at low speeds can be improved if the number of poles in the two windings is different. Zero speed operation is achieved successfully by using combination of four poles and twelve poles three-phase windings.

From the above discussion, it is understood that the concept of dual stator machine is similar to that of multi-level converters. Instead of using multi levels in a three-phase converter system, the number of inverter legs is increased.

If third harmonic component is added to modulation signals of PWM inverters, the modulation index will reach beyond the unity without making the converter behavior nonlinear. Similar concept can be applied to electrical machines by considering the flux distribution. The flux level in a machine cannot be increased beyond a limit because the iron saturates. If a third harmonic component is added to the flux of the machine, the

resultant waveform for the airgap flux becomes flattened. Therefore the fundamental component can be increased without making the peak flux too high. Considering this fact, major contribution in design and performance improvement of five-phase machines was accomplished in [24]-[31]. A solution to harmonic problems of previous multi-phase motor drives was suggested and new criteria for designing five-phase motors were established. The proposed multi-phase motor in these studies had two major differences compared to the other multi-phase motors. First, the concentrated windings, instead of the conventional sinusoidal windings, were adopted in its structure design. Second, the third harmonic currents are incorporated into the motor currents. Therefore, this kind of five-phase induction motors while benefiting from all advantages of the previous multi-phase motors, make use of the third harmonic to alter the shape of the air-gap flux in the machine. As a result, better material utilization can be achieved and the torque producing capability of the machine can be significantly improved. The idea has been successfully implemented on five-phase induction and reluctance machines [32,33].

In [34], the third harmonic of current was used to increase the torque density of six-phase induction machine. In this scheme, the torque density improves due to two main reasons. In a six-phase machine, the third harmonic zero sequence components are in quadrature in each of the three-phase winding group. Therefore an additional rotating field is produced. Also, in this system the fundamental flux component is increased.

In a vector controlled drive, flux, and torque of the AC machine are being adjusted independently by using only the two stator d-q axis components of current. Therefore, additional degrees of freedom exist in any AC machine which has a phase number

greater than three. These additional degrees of freedom can be utilized in different ways. In one approach, as discussed earlier, the torque production capability of the motor can be improved by injecting higher order harmonics of the stator current. These additional degrees of freedom were used to independently control other AC machines in a multi motor drive system [42]. In this scheme, it was required that the stator windings of all the multi-phase machines be connected in series. However, proper phase transposition should be considered while connecting the phases. Vector control can be separately applied to each machine. The total inverter phase current references were found to be the sum of individual machine phase current references. A single current controlled voltage source inverter (VSI) provided the required supply to the stator windings of multi motor system.

2) Multi-phase Permanent Magnet Machines

A theory for multi-phase motors which considers all the time and space harmonics of the magnetomotive force (MMF) was developed in [35]. The fundamental component of voltage in converter with rectangular voltage is 27% more than the one with sinusoidal voltage. Therefore, in order to achieve the best performance of nearly all types of converters (except resonant converters), the output voltages, and currents should be rectangular. On the other hand, if a multi-phase machine is supplied with rectangular waveforms, the resultant flux is 20- 25% greater than that of a similar three-phase machine which is supplied with sinusoidal current and has the same air-gap flux density. Therefore, it was concluded that in order to achieve a better performance, a full pitch or nearly full pitch winding is required for multi-phase motors. Such Configurations will

result in a nearly rectangular space distribution of the phase MMF.

The design and performance evaluation of a polyphase brushless dc-machine direct drive system were investigated in [36]. The system was designed for applications where high performance and reliability are required such as in EV, HEV, and aerospace applications. The authors studied the design and analysis of this kind of drives and addressed the issues regarding the high level modeling including a transient model together with their corresponding experimental verification.

In [37], the rectangular waveform permanent magnet motor for propulsion application which is controlled by PWM chopper was studied. Fourier transformation was used to study the effect of low frequency chopping on armature current. Simulation and experimental results were provided to validate the theory. It was proved that in order to reduce the torque pulsation of PM motor the chopping frequency and the number of phases should be increased.

Electric motors are widely used for ship propulsion. Reference [38] discusses the advantages of PM propulsion system with respect to the dc motor propulsion system and suggests the high power multi-phase system for this application.

In [39], the design, modeling, and simulation of a high torque low speed permanent magnet motor for in-wheel electric vehicle application were discussed. In order to better approximate the behavior of the actual system, mutual inductance and armature reaction effect were considered in the modeling. Therefore, the dynamic simulation results are in good agreement with the experimental results.

P-pair poles n-phase sine wave permanent magnet synchronous motors were mathematically modeled in both the abc static reference frame and d-q rotating reference frame [40]. An expression for defining the maximum transient short circuit current in case of n phases symmetrical short circuit of the motor was derived. The analysis of maximum short circuit current provided the fundamental theory to specify the operating point of permanent magnet motor which is an important factor during design process.

In [41], the authors showed that by employing asymmetric distributed multi three-phase BLDC motors, the converter system can be simplified and torque pulsation can be reduced at low speed. For analyzing the behavior of multi-phase BLDC motors a mathematical model was developed. It was concluded that the torque ripple of six-phase BLDC can be reduced by up to 50% with respect to a similar three-phase BLDC motor running with same phase current and rotor speed. It was shown that the most significant component of torque ripple is the twelfth order harmonic component of the fundamental frequency. The frequency of the salient torque pulsation in multi-phase BLDC motor which is caused by variable inductances is twice the harmonic of fundamental frequency. Due to the complex coupling of magnetic circuits, the salient torque ripple in a six-phase BLDC motor is increased. However, the amplitude of the pulsation is less than 5% of the total output electromagnetic torque. It was also demonstrated that in a six-phase BLDC motor, the motor can continue operating safely if one three -phase group is inoperative.

3. Fault Tolerant Multi-phase Permanent Magnet Machines

In several applications, the failure of a drive has a serious effect on the operation of the system. In some cases, the failure results in lost production whereas in some others it

is very dangerous to human safety. Therefore, in life dependent application it is of major importance to use a drive which continues operating safely under occurrence of any fault.

The major faults which can occur within a machine or converter are considered as: winding open circuit, winding short circuit (phase-ground or within a phase), winding short circuit at the terminals, power device open circuit, power device short circuit and the DC link capacitor failure. In order to limit the short circuit current, the PM machine should have a sufficiently large phase inductance and in order to avoid loss of performance in healthy phases in faulty condition, mutual inductance between the phases should be small. These two points are required for the reliability of the system.

A fault tolerant multi-phase PMSM was studied in [43]. In order to increase the reliability of the system, each phase of the machine was separately excited by its own H-bridge voltage source inverter. The segmented structure made it possible to inject the defined current waveform correctly and achieve minimum torque ripple. For an n-phase non-sinusoidal surface mount permanent magnet synchronous motor an optimal current waveform was specified. Supplying the motor with the specified current allowed minimizing the copper losses in a constant torque under normal operating condition. In the presence of a fault, depending on the loss of the supply of one or more than one phase, an effective method to cancel torque pulsation, generated by faulty phases, was developed. For each faulty phase, the torque ripples were canceled by modifying the current waveform of one healthy phase.

In [44- 46], A multi-phase drive was designed in which each phase was considered

as a single module. The effect of each module on the others was minimized. Therefore, in case one module fails, the rest of the system maintains continuous operation. In was pointed out that the electrical, magnetic, thermal and physical interaction between the phases should be minimized. Being electrically isolated is an essential requirement in the event of short circuit in the power device or phase winding. Otherwise, the star point in a star connected system may increase to the DC link voltage. In that case, there will be no net torque capability. One solution is to supply each phase from a single phase bridge. However, in this case the number of switches will be doubled. Physical separation was guaranteed by placing each winding round a single tooth. Also to meet the requirement for magnetic isolation, using surface mount permanent magnet topology as well as having one winding per slot was proposed. By placing single phase winding in stator slot, thermal interaction between phases is reduced as well.

An optimal torque control strategy for five-phase fault-tolerant permanent magnet brushless ac drives was proposed in [47]. Both constant torque and constant power modes of operation were considered. By implementing the proposed optimal torque control strategy, the produced output torque is free from ripple and the copper losses will be minimized while maintaining the permissible current and voltage limit. The effect of the above mentioned optimal torque control on eddy current loss was investigated [48].

In [49], by studying a six-phase PM motor it was shown that the undetected turn to turn faults will result in currents many times larger than the rated current flowing in the faulted winding. The fault might distribute rapidly if no action is taken. Monitoring the sampled current in each PWM cycle allows detecting a single shorted turn. The fault

current will be limited to rated value by shorting the phase.

F. Research Objectives

In this research work, some unique properties of five-phase permanent magnet motor are studied.

First objective of this research work is to develop a system that has the same torque density of BLDC motor while overcoming its disadvantages and is benefiting from the controllability of PMSM. A five-phase permanent magnet motor with concentrated winding is proposed. This motor is supplied with combined fundamental and third harmonics of currents which replicates a rectangular waveform. Therefore, the back-EMF and current waveform of this motor is a good approximation of those in a BLDC drive. This motor is modeled in $d_1q_1d_3q_3n$ reference frame. This motor while having the high torque density, is compatible with vector control algorithm, therefore the motor is easily controllable over a wide speed range.

The second objective of this work is to improve the reliability of the five-phase system against open circuit fault. By modifying the control algorithm, the five-phase motor continues operating safely even if two phases are open circuited. For this purpose, it is important to keep the MMF produced by the stator unchanged in healthy and faulty conditions.

The third objective of this work is to implement sensorless direct torque control algorithm on five phase permanent magnet motor. High torque and flux ripple are the

major drawback of a DTC scheme. The reason is that the inverter keeps the same switching state as long as the outputs of flux and torque hysteresis controllers remain unchanged. The number of space voltage vectors directly influences the performance of DTC control system. A five-phase system, while benefiting from other advantages of high order phase systems, has inherently 32 space voltage vectors which permits better flexibility in selecting the switching states and finer adjustment of flux and torque.

Two five-phase permanent magnet motors were designed and built in the laboratory to obtain the experimental results.

G. Dissertation Organization

Chapter I covered the background information on permanent magnet AC motors, indicated the most important features of multi-phase AC machines, and presented a literature survey on the work accomplished in this area. Also research objectives of this dissertation were pointed out. In the rest of the dissertation, additional degrees of freedom in five-phase permanent magnet motors are employed to improve the overall performance of the system.

In chapter II, the additional degrees of freedom are used to supply the motor with combined fundamental and third harmonic of currents. Harmonic effect is studied in a five-phase machine with concentrated winding distribution. It is shown that the space and time harmonics of the same order will contribute positively to the output torque. The mathematical model of the machine supplied with quasi-rectangular current is derived in

$d_1q_1d_3q_3n$ frame of reference. The improvement in output torque and compatibility of the proposed motor with vector control are shown using the mathematical model. Simulation results from the finite element method and Matlab/Simulink are given to support the validity of the theoretical findings. Experimental results are presented to validate the effectiveness of the proposed approach.

In chapter III, a control scheme which provides fault tolerance to a five-phase permanent magnet motor under open phase condition will be presented. In this scheme, the five-phase PM motor continues operating safely under loss of up to two phases without any additional hardware and just by adjusting the current in the remaining healthy phases. Simulation and experimental results are provided to show the steady operation of the five-phase drive under open phase condition.

In chapter IV, the direct torque control (DTC) of five-phase motor is presented. Having a five-leg inverter, there exists 32 space voltage vectors which provides great flexibility in selecting the inverter switching states. Therefore, the stator flux and torque can be more precisely adjusted. Position information and speed are being estimated based on the position of the stator flux linkages. The mathematical model of the five-phase interior permanent magnet motor is first derived. Later, the speed sensorless direct torque control method of the five-phase IPM is introduced. Simulation and experimental results are provided to show that the DTC can be successfully implemented on the five-phase permanent magnet motor.

Chapter V concludes the work done in this dissertation and suggests some future research work in this area.

CHAPTER II

FIVE PHASE PERMANENT MAGNET MOTOR DRIVE WITH HIGH SPECIFIC TORQUE*

A. Introduction

Due to the additional degrees of freedom, multi-phase permanent magnet motors present some unique characteristics. One of them is providing the ability of injecting higher order harmonics of current and enhancing the torque producing capability of the motor. This chapter investigates the advantages of supplying the five-phase permanent magnet motor with combined fundamental and third harmonics of currents. This motor benefits from the high toque density of BLDC motor and better controllability of PMSM. First, the main advantages and drawbacks of BLDC motor and PMSM will be discussed. Then, the harmonic analysis of the motors with non sinusoidal winding functions will be presented. Later in this chapter, the mathematical model of the five-phase permanent magnet motor with quasi-rectangular back–EMF and supplied with fundamental and third harmonics of current is derived. Finally, the superior performance of the proposed motor will be validated through simulation and experiment.

B. Background

Based on the back-EMF waveform, permanent magnet AC motors are classified into permanent magnet brushless DC motors (BLDC) and permanent magnet synchronous motor. In BLDC motors, the stator windings is wound such that the produced back-EMF is trapezoidal. Therefore, supplying the motor with quasi rectangular current will produce almost constant torque. Figure 2-1 shows the back-EMF and current waveform of a three-phase BLDC motor. As it is seen from the figure only two phases are conducting at each instant of time and for the duration of 60 electrical degrees. Therefore, the exact position information is not needed in this kind of drive. The control of the motor is possible just by knowing the commutation instants. Low resolution position sensors such as hall sensors are capable of providing the information regarding the commutation instants.

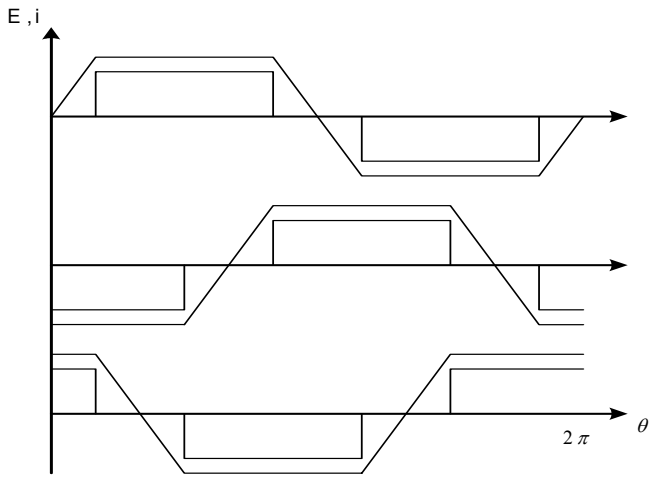

Figure 2-1 Current waveforms and back-EMF of a three-phase BLDC motor.

The stator voltage equation for a three-phase BLDC motor is given by,

$$\begin{bmatrix} v_a \\ v_b \\ v_c \end{bmatrix} = \begin{bmatrix} R & 0 & 0 \\ 0 & R & 0 \\ 0 & 0 & R \end{bmatrix} \begin{bmatrix} i_a \\ i_b \\ i_c \end{bmatrix} + \begin{bmatrix} L-M & 0 & 0 \\ 0 & L-M & 0 \\ 0 & 0 & L-M \end{bmatrix} \frac{d}{dt} \begin{bmatrix} i_a \\ i_b \\ i_c \end{bmatrix} + \begin{bmatrix} e_a \\ e_b \\ e_c \end{bmatrix} \tag{2-1}$$

Where R is the stator resistance per phase, L and M are the stator self and mutual inductances respectively, and e_a , e_b , e_c are the induced EMFs

The electromagnetic torque is defined as follows:

$$T_e = \frac{1}{\omega_r}(e_a i_a + e_b i_b + e_c i_c) \tag{2-2}$$

where ω_r is the motor speed.

The following equation determines how the motor speed builds up:

$$T_e = T_L + J\frac{d\omega_r}{dt} + B\omega_r \tag{2-3}$$

BLDC operation above rated speed is being performed by the advance angle technique. In this scheme, turning on each phase earlier will allow the current to build up in the winding before the back-EMF reaches its maximum value. However, there are two major problems with this scheme. First, at a given speed, the advance angle to be applied is not exactly known. Second, at high speeds, the phase inductance increases and therefore the phase current deviate significantly from ideal, in a sense that it is not possible to control the current as rectangular waveform. Therefore, the torque production capability of the motor decreases.

In PMSM, the stator is wound such that the produced back-Emf is sinusoidal and

therefore supplying the motor with sinusoidal currents will lead to producing constant torque. In this system, torque producing component and flux producing component of current has been decoupled and vector control is easily applicable to this kind of drive. This motor has better controllability over the whole speed range.

The stator voltage equations in d-q rotating frame of reference are:

$$v_{ds} = r_s i_{ds} - \omega L_{qs} i_{qs} + L_{ds} \frac{di_{ds}}{dt} \tag{2-4}$$

$$v_{qs} = r_s i_{qs} + \omega (L_{ds} i_{ds} + \psi_m) + L_{qs} \frac{di_{qs}}{dt} \tag{2-5}$$

where r_s is the stator resistance, L_{ds} and L_{qs} are the d- and q-axes inductances, ψ_m is the rotor permanent magnet flux, v_{ds} and v_{qs} are the d- and q-axes voltages, and i_{ds} and i_{qs} are the d and q-axes currents. The electromagnetic torque is given by,

$$T_e = \frac{3}{2}\frac{P}{2}\left[\psi_m i_{qs} + (L_{qs} - L_{ds}) i_{ds} i_{qs}\right] \tag{2-6}$$

where P is the number of poles. The second term in (2-6) is the reluctance torque. If there is no rotor saliency, i.e., L_{ds} equals L_{qs}, the reluctance torque would be zero and therefore the torque is just a function of q-axis current. The following equation determines how the motor speed builds up:

$$T_e = T_L + J \frac{d\omega_r}{dt} + B\omega_r \tag{2-7}$$

The input voltage and current of the motor are limited. Their maximum value is dictated by the upper limit of the available DC link voltage and the current rating of the

inverter. The voltage and current limits will affect the maximum speed attainable by the motor and also its torque producing capability. By imposing the upper limit of the current and voltage to the stator voltage and current equations and neglecting the ohmic drop the following equations will be obtained.

$$(i_{ds})^2 + (i_{qs})^2 = I_{rated}^2 \tag{2-8}$$

$$(\psi_m + L_d i_{ds})^2 + (L_q i_{qs})^2 = (\frac{V_{rated}}{\omega})^2 \tag{2-9}$$

From the above equation, it is clear that the required i_{ds} can be calculated for the speeds above the rated. Therefore, field weakening operation and running the motor at speeds higher than the rated speed can be easily implemented in this kind of drive. Figure 2-2 shows the torque-speed curve of the motor which has two intervals of constant torque region for the speeds below the rated speed and constant power region for speeds higher than the rated speed.

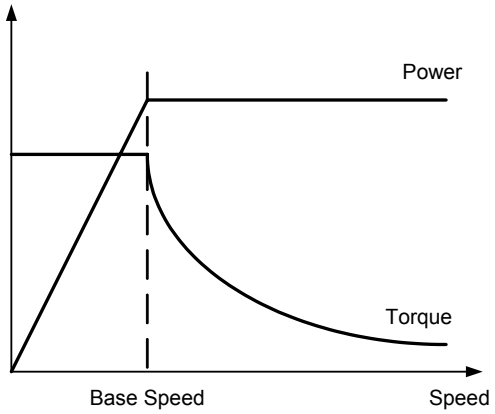

Figure 2-2 Torque speed characteristic of PM motor.

C. Comparing BLDC Motor and PMSM

It is known that permanent magnet brushless DC machines have higher torque density compared to permanent magnet synchronous machines [50]. The reason is that for the same peak values of flux, the rms value of the machine with trapezoidal back-EMF is higher than the one with sinusoidal waveform. Considering the same copper losses the ratio of the produced torque of the two machines will be obtained.

Assume I_{pmsm_peak} and I_{bldc_peak} are the peak values of the stator currents in the three-phase PMSM (supplied with sinusoidal current waveform) and BLDC (supplied with current pulses of 120 degrees) machines. The rms values of these currents are:

$$I_{pmsm\_rms} = \frac{I_{pmsm\_peak}}{\sqrt{2}} \tag{2-10}$$

and

$$I_{bldc\_rms} = I_{bldc\_peak}\sqrt{2/3} \tag{2-11}$$

Equating the copper losses and substituting for the currents in terms of their peak currents results in:

$$3I_{pmsm\_rms}^2 R_a = 3I_{bldc\_rms}^2 R_a \tag{2-12}$$

Therefore:

$$I_{bldc\_peak} = \frac{\sqrt{3}}{2}.I_{pmsm\_peak} \tag{2-13}$$

The ratio of output torque is obtained as follows:

$$\frac{BLDC\_Torque}{PMSM\_Torque} = \frac{(2xE_{peak}xI_{bldc\_peak})/\omega}{(3x\frac{E_{peak}}{\sqrt{2}}x\frac{I_{pmsm\_peak}}{\sqrt{2}})/\omega} = \frac{(2xE_{peak}x\frac{\sqrt{3}}{2}xI_{pmsm\_peak})/\omega}{(3x\frac{E_{peak}xI_{pmsm\_peak}}{2})/\omega} = 1.1547 \quad (2\text{-}14)$$

which shows that the BLDC motor is capable of producing 15% more torque compared to PMSM during the constant torque region. Therefore, it is useful to develop a motor which has almost the same torque density of BLDC and controllability of the PMSM.

Based on the above, a five-phase permanent magnet motor is introduced. The stator of the motor is wound such that the induced back-EMF is almost trapezoidal. The stator is supplied by combined sinusoidal and third harmonics of current. Figure 2-3 shows the back-EMF and current waveform of permanent magnet synchronous motor, permanent magnet brushless DC and the proposed motor, respectively.

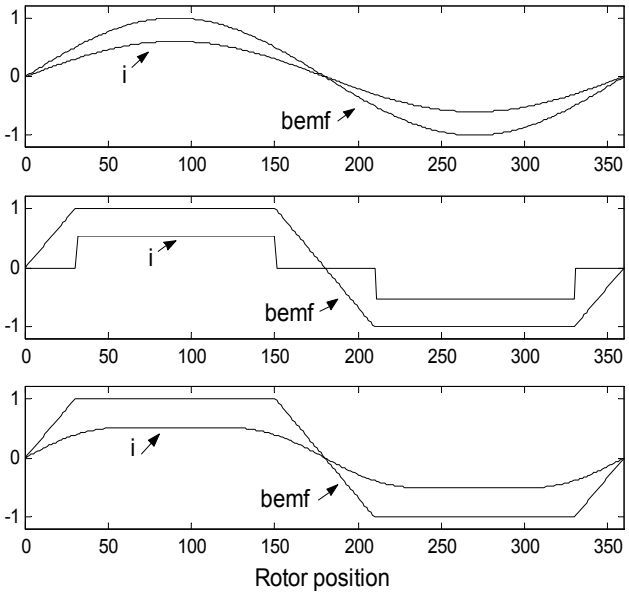

Figure 2-3 Top to bottom: PMSM, BLDC and the proposed five-phase motor current and back-EMF waveforms.

D. Harmonic Spectrum of MMF in Machines with Non-sinusoidal Winding Distribution

In this section, the effects of non-sinusoidal field spatial harmonics and current time harmonics on three-phase and five-phase permanent magnet motors are discussed. The motors have concentrated winding configuration and the study is based on the winding functions and Fourier analysis.

The following assumptions are made:

- Machines are considered to be operating at the steady state under no load conditions.
- Saturation effects are not included. Therefore, superposition of magnetic fields is possible.
- Skin effects in the stator conductors at the harmonic frequencies are neglected.

1. Harmonic Spectrum of MMF in Three-Phase Machines with the Concentrated Winding Distribution

Figure 2-4 shows the stator of a machine with two pole, 3-phase concentrated windings. The windings are 120^0 apart in space. The Fourier series of phase "a" winding function shown in figure 2-5 is as follows:

$$N_a(\phi) = \sum_{n=1}^{\infty} \frac{4}{n\pi} \frac{N}{2} \sin\frac{n\pi}{2} \cos n(\phi) \tag{2-15}$$

where ϕ is the spatial angle, and n is the harmonic order. Due to symmetry of winding functions, even order space harmonics do not exist. The winding functions of other

phases are similar to phase “a” winding function with proper phase shift.

In order to study a general case; we assume that this machine is being supplied from a current source inverter. Each coil carries current pulses of 120^0 as shown in figure 2-6. The Fourier series of phase “a” current waveforms are given by,

$$i_a(\theta) = \sum_{m=1}^{\infty} \frac{4}{m\pi} I_m \cos\frac{m\pi}{6} \sin m(\theta) \tag{2-16}$$

where θ is the rotor angle and is related to angular speed of ω by,

$$\theta = \omega t \tag{2-17}$$

The current waveforms of other phases are similar to phase “a” current waveform with proper phase displacement.Again, due to symmetry of current waveforms, it is clear that even harmonics cannot exist.

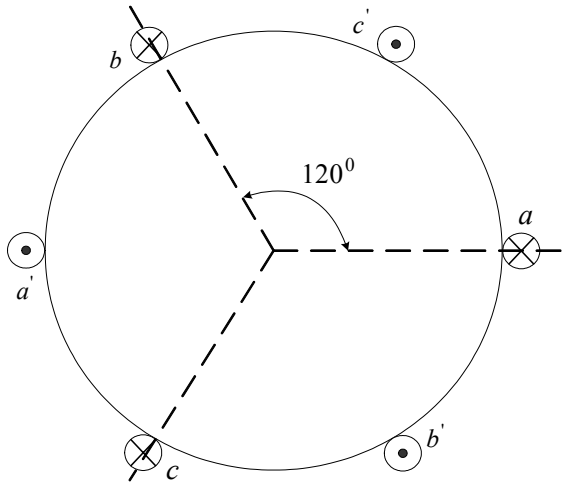

Figure 2-4 Two-pole, three-phase concentrated winding distribution.

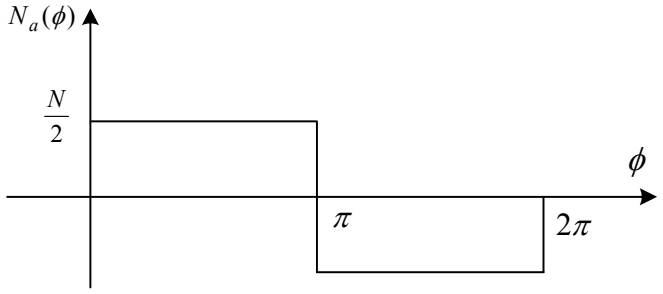

Figure 2-5 Winding function of phase "a" for the two-pole, three-phase concentrated winding motor.

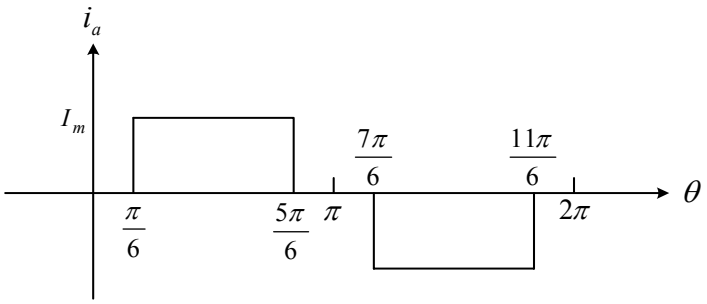

Figure 2-6 Phase "a" current waveform.

The instantaneous phase currents determine the spatial *MMF* pattern at any instant. Variation of these currents in time domain determines the rotational movement of the pattern. Let *F* be the total MMFs produced by coils a, b, c. Then

$$F = N_a i_a + N_b i_b + N_c i_c = \sum_{n=1}^{\infty}\sum_{m=1}^{\infty}\frac{1}{nm}\left(\frac{4}{\pi}\right)^2 \frac{NI_m}{2}\sin\frac{n\pi}{2}\cos\frac{m\pi}{6}$$
$$\left\{\sin(m\theta - n\phi)\left[\cos\frac{(m-n)2\pi}{3}+\frac{1}{2}\right]+\sin(m\theta + n\phi)\left[\cos\frac{(m+n)2\pi}{3}+\frac{1}{2}\right]\right\} \quad (2\text{-}18)$$

A pair of air-gap fields is defined in the above expression. The first component of the field is rotating forward and the second component is rotating backward. Table 2-1 shows the existing MMFs in the air gap of a 3-phase concentrated winding machine. In this table, the "F" sign indicates the MMFs which are rotating forward, while the "B" sign represents those rotating backward. A negative sign indicates the 180^{o} phase shift with respect to the fundamental harmonic. From the table it is understood that those MMFs, which are generated by the same order of space and time harmonics rotate forward at synchronous speed. Those generated by different order of time and space harmonic rotate at speeds equal to *n/m* times synchronous speed, some in the forward and some in the backward directions.

Table 2-1 Relationship between field space harmonics and current time harmonics for a concentrated, full pitch three-phase winding.

Space Harmonics

Time Harmonics	1	3	5	7	9	11	13	15
1	F 1.053		B .211	F -.15		B -.096	F .081	
3								
5	B -.211		F -.042	B .03		F .019	B -.016	
7	F -.15		B -.03	F .021		B .014	F -.012	
9								
11	B -.096		F .019	B -.014		F -.009	B .007	
13	F .081		B .016	F -.012		B -.007	F .006	
15								

Multiply all entries by NI

There are no multiples of third harmonic in the case of a three-phase Y connected without a neutral return. The effects of the higher harmonics are essentially to reduce the average torque. For instance, interaction of the fifth time harmonic with the fifth space harmonic produces a forward rotating MMF of 0.042 NI. However, the fifth harmonic in time combines with the first space harmonic will generate a backward rotating MMF with the amplitude of 0.211 NI. In addition, the fundamental time harmonic combines with the fifth space harmonic producing an additional backward rotating MMF with amplitude of 0.211 NI.

2. Harmonic Spectrum of MMF in Five-Phase Machines with the Concentrated Winding Distribution

Using the concepts developed in the previous section, the air-gap field for windings with different numbers of phases can be specified. In this section, a 5-phase machine is examined. The machine is supplied from an inverter supply where the electrical pulses can be adjusted to values greater than 120^0. The machine is assumed to be star connected with no neutral connection. Therefore the five currents should add up to zero. Figure 2-7 shows a two pole five-phase concentrated winding machine. The phases are 72^0 displaced with respect to each other and number of turns per phase is $3N/5$. Winding function of phase "a" is shown in figure 2-8. The Fourier series of phase "a" winding function can be written as follows:

$$N_a(\phi) = \sum_{n=1}^{\infty} \frac{4}{n\pi} \frac{3N}{10} \sin\frac{n\pi}{2} \cos n(\phi) \qquad (2\text{-}19)$$

The winding function of other phases is similar to that of phase "a" with proper phase

shift.

The stator is supplied with 144^0 pulses of current as shown in figure 2-9. Similar to the three-phase case the Fourier series of the phase "a" current waveform is:

$$i_a(\theta) = \sum_{m=1}^{\infty} \frac{4}{m\pi} I_m \cos\frac{m\pi}{10} \sin m(\theta) \tag{2-20}$$

The current waveforms of other phases are similar to phase "a" current waveform with proper phase displacement.

Assume F be the total MMFs produced by coils a, b, c, d and e. Then,

$$\begin{aligned} F &= N_a i_a + N_b i_b + N_c i_c + N_d i_d + N_e i_e \\ &= \sum_{n=1}^{\infty}\sum_{m=1}^{\infty}\left(\frac{1}{nm}\right)\left(\frac{4}{\pi}\right)^2 \frac{3NI_m}{10}\cos\frac{m\pi}{10}((\cos(m\theta - n\phi)(\cos\frac{(m-n)2\pi}{5} + \cos\frac{(m-n)4\pi}{5} \\ &\quad + \frac{1}{2}) + \cos(m\theta + n\phi)(\cos\frac{(m+n)2\pi}{5} + \cos\frac{(m+n)4\pi}{5} + \frac{1}{2})) \end{aligned} \tag{2-21}$$

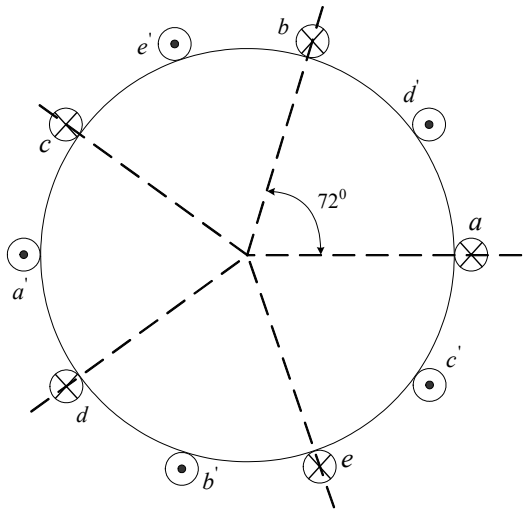

Figure 2-7 Five-phase concentrated winding distribution.

Table 2-2 shows the existing MMF for the five-phase case. It is obvious that in this case third harmonic of time flowing in third harmonic of space will generate a forward rotating MMF. In a five phase system the fifth harmonic of MMF does not exist.

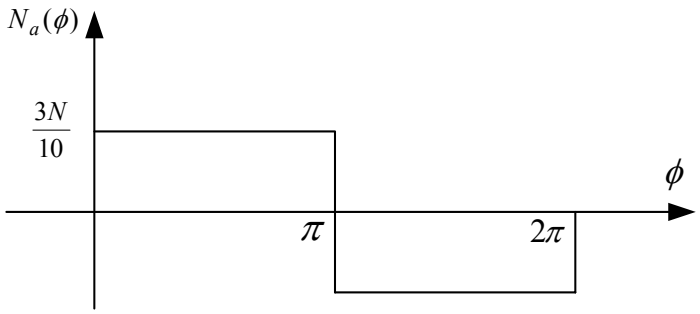

Figure 2-8 Winding function for phase "a" of five-phase motor.

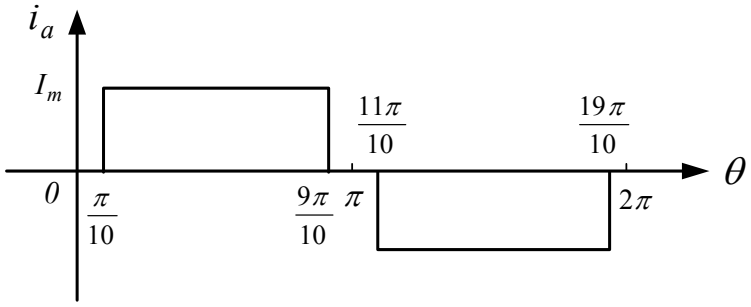

Figure 2-9 Phase "a" current waveform.

The operating region where the rotor rotates at synchronous speed is the useful region of PM machines. Therefore, only those fields rotating at synchronous speed will contribute positively to the output torque. Fields rotating at speeds higher than

synchronous speed will generate negligible torque, whereas those fields rotating at speeds lower than the synchronous speed, or those which are rotating backwards will have negative impact on the output torque. By increasing number of phases, the frequency of torque pulsation increases and its amplitude decreases.

Phase numbers of the order 3, 6 with currents in 2-, or 4-phase at any instant are all equivalent in terms of their fundamental flux producing capability. That is, for the same copper losses and the same copper weight the peak fundamental air gap MMF is 1.053 NI for all the three cases. However, for phase numbers of the order 5, 7, etc., 4-, 6-, etc. phases carry current at any instant. In this case, the fundamental MMF produced by the five-phase winding exceeds the usual three-phase winding by a small amount (1.056 NI). In addition, a useful MMF is produced by the third harmonic MMF, which rotates synchronously with the fundamental component (0.072 NI). The existence of the third harmonic in the air-gap alters the shape of the total air-gap MMF, and hence permits an increase in the output torque of the five-phase BLDC motor.

Therefore, instead of supplying the five-phase machine with 144^0 pulses of current, it is excited with the fundamental plus third harmonics of the current. In this case, harmonics shown in the first two rows of Table 2-2 are present. When a seven-phase winding is used, the fundamental MMF component actually decreases to 1.045 NI while the third harmonic component increases to 0.093 NI.It is interesting to note that with this basis for comparison the five-phase machine has the optimum torque per rms ampere.

Table 2-2 Relationship between field space harmonics and current time harmonics for a concentrated, full pitch five-phase winding.

Space Harmonics

Time Harmonics	1	3	5	7	9	11	13	15
1	F 1.056				B .117	F -.096		
3		F -.072		B -.031			F .017	
5								
7		B -.031		F .013			B -.007	
9	B -.117				F -.013	B .011		
11	F -.096				B -.011	F .009		
13		F .017		B .007			F -.004	
15								

Multiply all entries by NI

E. Mathematical Model of the Five-Phase BPM

In this section the mathematical model of the five-phase permanent magnet motor will be derived. The motor in this study has quasi-rectangular back-emf and is supplied with combined fundamental and third harmonic of current. The voltages, flux linkages and torque equations will be established in the $d_1q_1d_3q_3$ rotating frame of reference. It is shown the torque producing and flux producing component of current can be decoupled in the $d_1q_1d_3q_3$ frame of reference and vector control can be easily implemented for this drive.

1. Stator Voltage and Flux Equations

The stator voltage equations are given by,

$$V_s = R_s I_s + \frac{d\Lambda_s}{dt} \tag{2-22}$$

where the airgap flux linkages are presented by,

$$\Lambda_s = \Lambda_{ss} + \Lambda_m \tag{2-23}$$

or

$$\Lambda_s = L_{ss} I_s + \Lambda_m \tag{2-24}$$

R_s is given by,

$$R_s = \begin{bmatrix} r_s & & & & \\ & r_s & & & \\ & & r_s & & \\ & & & r_s & \\ & & & & r_s \end{bmatrix} \tag{2-25}$$

and L_{ss} is the stator inductance matrix which contains the self and mutual inductances of the stator phases:

$$L_{ss} = \begin{bmatrix} L_{ls} & & & & \\ & L_{ls} & & & \\ & & L_{ls} & & \\ & & & L_{ls} & \\ & & & & L_{ls} \end{bmatrix} + \begin{bmatrix} L_{asas} & L_{asbs} & L_{ascs} & L_{asds} & L_{ases} \\ L_{bsas} & L_{bsbs} & L_{bscs} & L_{bsds} & L_{bses} \\ L_{csas} & L_{csbs} & L_{cscs} & L_{csds} & L_{cses} \\ L_{dsas} & L_{dsbs} & L_{dscs} & L_{dsds} & L_{dses} \\ L_{esas} & L_{esbs} & L_{escs} & L_{esds} & L_{eses} \end{bmatrix} \tag{2-26}$$

L_{ls} is the stator leakage inductance.

V_s, Λ_s and I_s are the stator voltage, flux linkages and current matrices, respectively:

$$V_s = \begin{bmatrix} v_{as} & v_{bs} & v_{cs} & v_{ds} & v_{es} \end{bmatrix}^t \tag{2-27}$$

$$\Lambda_s = \begin{bmatrix} \lambda_{as} & \lambda_{bs} & \lambda_{cs} & \lambda_{ds} & \lambda_{es} \end{bmatrix}^t \tag{2-28}$$

$$I_s = \begin{bmatrix} I_{as} & I_{bs} & I_{cs} & I_{ds} & I_{es} \end{bmatrix}^t \tag{2-29}$$

Λ_m is the established flux linkage matrix due to the permanent magnets viewed from the stator phase windings. For simplifying the model, only the fundamental and third harmonic components of the permanent magnet flux linkage are taken into account. Considering the approximation Λ_m can be written as follows:

$$\Lambda_m = \lambda_{m1} \begin{bmatrix} \sin(\theta_r) \\ \sin(\theta_r - \frac{2\pi}{5}) \\ \sin(\theta_r - \frac{4\pi}{5}) \\ \sin(\theta_r + \frac{4\pi}{5}) \\ \sin(\theta_r + \frac{2\pi}{5}) \end{bmatrix} + \lambda_{m3} \begin{bmatrix} \sin(3\theta_r) \\ \sin 3(\theta_r - \frac{2\pi}{5}) \\ \sin 3(\theta_r - \frac{4\pi}{5}) \\ \sin 3(\theta_r + \frac{4\pi}{5}) \\ \sin 3(\theta_r + \frac{2\pi}{5}) \end{bmatrix} \tag{2-30}$$

λ_{m1} and λ_{m3} are the amplitude of fundamental and third harmonics components of the permanent magnet flux linkages and θ_r is the rotor position.

2. Inductance Matrix

As previously mentioned, this motor has concentrated windings, and the air gap is assumed to be uniform. The self and mutual inductances of the stator are constant values. In order to simplify the modeling, only the fundamental and the third harmonic components of the winding function are taken into account. Therefore, the Fourier series of winding function for each phase can be written as follows:

$$N_{as}(\phi) = \frac{4}{\pi}\frac{N_s}{P}\left[N_s \cos\phi - \frac{1}{3}N_s \cos 3\phi\right] \tag{2-31}$$

$$N_{bs}(\phi) = \frac{4}{\pi}\frac{N_s}{P}\left[N_s \cos(\phi - \frac{2\pi}{5}) - \frac{1}{3}N_s \cos 3(\phi - \frac{2\pi}{5})\right] \tag{2-32}$$

$$N_{cs}(\phi) = \frac{4}{\pi}\frac{N_s}{P}\left[N_s \cos(\phi - \frac{4\pi}{5}) - \frac{1}{3}N_s \cos 3(\phi - \frac{4\pi}{5})\right] \tag{2-33}$$

$$N_{ds}(\phi) = \frac{4}{\pi}\frac{N_s}{P}\left[N_s \cos(\phi + \frac{4\pi}{5}) - \frac{1}{3}N_s \cos 3(\phi + \frac{4\pi}{5})\right] \tag{2-34}$$

$$N_{es}(\phi) = \frac{4}{\pi}\frac{N_s}{P}\left[N_s \cos(\phi + \frac{2\pi}{5}) - \frac{1}{3}N_s \cos 3(\phi + \frac{2\pi}{5})\right] \tag{2-35}$$

where N_S is the total number of turns, P is the number of poles and φ is the spatial angle. The self and mutual inductances of the stator phases can be computed by using the corresponding winding functions. Self inductance is given by,

$$L_{asas} = \frac{\mu_0 rl}{g}\int_0^{2\pi} N_{as}^2(\phi)d\phi \tag{2-36}$$

And the mutual inductance is as follows:

$$L_{asbs} = \frac{\mu_0 rl}{g}\int_0^{2\pi} N_{as}(\phi)N_{bs}(\phi)d\phi \tag{2-37}$$

Considering:

$$\begin{aligned} N_{s1} &= \frac{4}{\pi}\frac{N_S}{P} \\ N_{s3} &= -\frac{1}{3}\frac{4}{\pi}\frac{N_S}{P} \end{aligned} \tag{2-38}$$

The self inductance of phase a can be written as:

$$
\begin{aligned}
L_{asas} &= \frac{\mu_0 rl}{g}\int_0^{2\pi}\left(N_{s1}^2\cos^2\phi + N_{s3}^2\cos^2 3\phi + 2N_{s1}N_{s3}\cos\phi\cos 3\phi\right)d\phi \\
&= \frac{\mu_0 rl}{g}\left(\frac{N_{s1}^2}{2}\left(\phi+\frac{1}{2}\sin 2\phi\right)_0^{2\pi} + \frac{N_{s3}^2}{2}\left(\phi+\frac{1}{6}\sin 6\phi\right)_0^{2\pi}\right) \\
&= \frac{\mu_0 rl\pi}{g}\left(N_{s1}^2 + N_{s3}^2\right) \\
&= L_{ms1} + L_{ms3}
\end{aligned}
\tag{2-39}
$$

and the mutual inductance between phase a and b will be:

$$
\begin{aligned}
L_{asbs} &= \frac{\mu_0 rl}{g}\int_0^{2\pi}\left(N_{s1}\cos\phi + N_{s3}\cos 3\phi\right)\left(N_{s1}\cos(\phi-\frac{2\pi}{5}) + N_{s3}\cos 3(\phi-\frac{2\pi}{5})\right)d\phi \\
&= \frac{\mu_0 rl}{g}\left(\int_0^{2\pi}\frac{N_{s1}^2}{2}\left(\cos\frac{2\pi}{5} + \cos(2\phi-\frac{2\pi}{5})\right)d\phi + \int_0^{2\pi}\frac{N_{s3}^2}{2}\left(\cos 3\frac{2\pi}{5} + \cos 3(2\phi-\frac{2\pi}{5})\right)d\phi\right) \\
&= \frac{\mu_0 rl\pi}{g}\left(N_{s1}^2\cos\frac{2\pi}{5} + N_{s3}^2\cos\frac{6\pi}{5}\right) \\
&= \cos\frac{2\pi}{5}L_{ms1} + \cos\frac{6\pi}{5}L_{ms3}
\end{aligned}
\tag{2-40}
$$

Similarly, the self and mutual inductances of other phases are given by,

$$
\begin{aligned}
&L_{bsbs} = L_{\csc s} = L_{dsds} = L_{eses} = L_{asas} = L_{ms1} + L_{ms3} \\
&L_{bscs} = L_{csds} = L_{dses} = L_{ases} = L_{asbs} = \cos\frac{2\pi}{5}L_{ms1} + \cos 3\frac{2\pi}{5}L_{ms3} \\
&L_{ascs} = L_{bsds} = L_{cses} = L_{dsas} = L_{esbs} = \cos\frac{4\pi}{5}L_{ms1} + \cos 3\frac{4\pi}{5}L_{ms3}
\end{aligned}
\tag{2-41}
$$

Therefore, the stator inductance matrix is written as:

$$L_{ss}=\begin{bmatrix} L_{ls} & & & & \\ & L_{ls} & & & \\ & & L_{ls} & & \\ & & & L_{ls} & \\ & & & & L_{ls} \end{bmatrix}+L_{ms1}\begin{bmatrix} 1 & \cos\frac{2\pi}{5} & \cos\frac{4\pi}{5} & \cos\frac{4\pi}{5} & \cos\frac{2\pi}{5} \\ \cos\frac{2\pi}{5} & 1 & \cos\frac{2\pi}{5} & \cos\frac{4\pi}{5} & \cos\frac{4\pi}{5} \\ \cos\frac{4\pi}{5} & \cos\frac{2\pi}{5} & 1 & \cos\frac{2\pi}{5} & \cos\frac{4\pi}{5} \\ \cos\frac{4\pi}{5} & \cos\frac{4\pi}{5} & \cos\frac{2\pi}{5} & 1 & \cos\frac{2\pi}{5} \\ \cos\frac{2\pi}{5} & \cos\frac{4\pi}{5} & \cos\frac{4\pi}{5} & \cos\frac{2\pi}{5} & 1 \end{bmatrix}$$

$$+L_{ms3}\begin{bmatrix} 1 & \cos 3\frac{2\pi}{5} & \cos 3\frac{4\pi}{5} & \cos 3\frac{4\pi}{5} & \cos 3\frac{2\pi}{5} \\ \cos 3\frac{2\pi}{5} & 1 & \cos 3\frac{2\pi}{5} & \cos 3\frac{4\pi}{5} & \cos 3\frac{4\pi}{5} \\ \cos 3\frac{4\pi}{5} & \cos 3\frac{2\pi}{5} & 1 & \cos 3\frac{2\pi}{5} & \cos 3\frac{4\pi}{5} \\ \cos 3\frac{4\pi}{5} & \cos 3\frac{4\pi}{5} & \cos 3\frac{2\pi}{5} & 1 & \cos 3\frac{2\pi}{5} \\ \cos 3\frac{2\pi}{5} & \cos 3\frac{4\pi}{5} & \cos 3\frac{4\pi}{5} & \cos 3\frac{2\pi}{5} & 1 \end{bmatrix} \quad (2\text{-}42)$$

3. Transformation Matrix

For simplifying the model, an arbitrary coordinate transformation is introduced, which transfers the variables of the five-phase motor into a reference frame rotating at an arbitrary angular velocity. Including the effect of third harmonic, a d_1-q_1-d_3-q_3-n transformation can be applied, where the d_1-q_1 coordinate is rotating at synchronous speed and the d_3-q_3 coordinate is rotating at three times the synchronous speed as shown in figure 2-10.

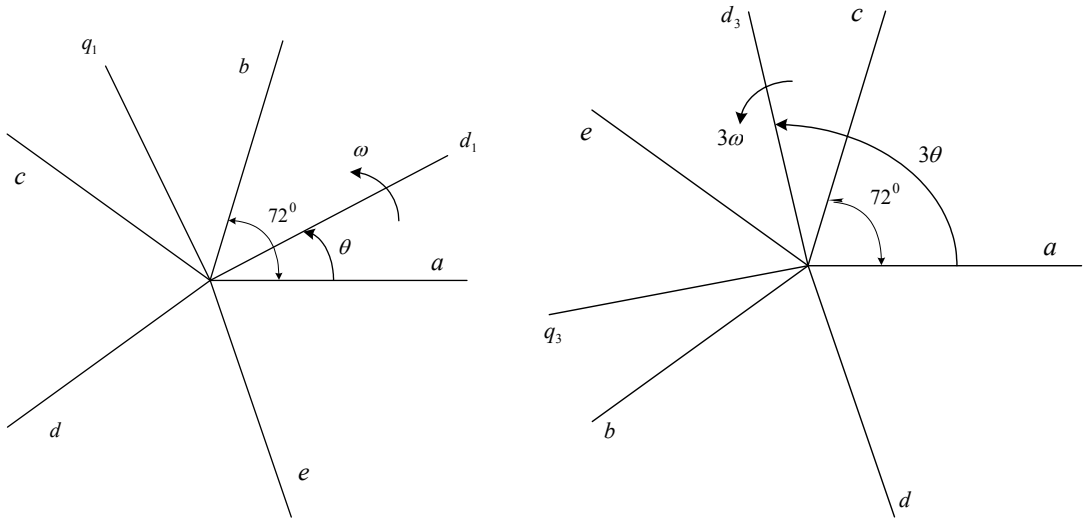

Figure 2-10 d_1q_1 and d_3q_3 space.

The transformation matrix for this system is considered as:

$$T(\theta_r)=\frac{2}{5}\begin{bmatrix} \sin\theta_r & \sin(\theta_r-\frac{2\pi}{5}) & \sin(\theta_r-\frac{4\pi}{5}) & \sin(\theta_r+\frac{4\pi}{5}) & \sin(\theta_r+\frac{2\pi}{5}) \\ \cos\theta_r & \cos(\theta_r-\frac{2\pi}{5}) & \cos(\theta_r-\frac{4\pi}{5}) & \cos(\theta_r+\frac{4\pi}{5}) & \cos(\theta_r+\frac{2\pi}{5}) \\ \sin 3\theta_r & \sin 3(\theta_r-\frac{2\pi}{5}) & \sin 3(\theta_r-\frac{4\pi}{5}) & \sin 3(\theta_r+\frac{4\pi}{5}) & \sin 3(\theta_r+\frac{2\pi}{5}) \\ \cos 3\theta_r & \cos 3(\theta_r-\frac{2\pi}{5}) & \cos 3(\theta_r-\frac{4\pi}{5}) & \cos 3(\theta_r+\frac{4\pi}{5}) & \cos 3(\theta_r+\frac{2\pi}{5}) \\ \frac{1}{\sqrt{2}} & \frac{1}{\sqrt{2}} & \frac{1}{\sqrt{2}} & \frac{1}{\sqrt{2}} & \frac{1}{\sqrt{2}} \end{bmatrix} \tag{2-43}$$

The inverse transformation matrix is defined by:

$$T^{-1}(\theta_r)=\begin{bmatrix} \sin\theta_r & \cos\theta_r & \sin 3\theta_r & \cos 3\theta_r & \frac{1}{\sqrt{2}} \\ \sin(\theta_r-\frac{2\pi}{5}) & \cos(\theta_r-\frac{2\pi}{5}) & \sin 3(\theta_r-\frac{2\pi}{5}) & \cos 3(\theta_r-\frac{2\pi}{5}) & \frac{1}{\sqrt{2}} \\ \sin(\theta_r-\frac{4\pi}{5}) & \cos(\theta_r-\frac{4\pi}{5}) & \sin 3(\theta_r-\frac{4\pi}{5}) & \cos 3(\theta_r-\frac{4\pi}{5}) & \frac{1}{\sqrt{2}} \\ \sin(\theta_r+\frac{4\pi}{5}) & \cos(\theta_r+\frac{4\pi}{5}) & \sin 3(\theta_r+\frac{4\pi}{5}) & \cos 3(\theta_r+\frac{4\pi}{5}) & \frac{1}{\sqrt{2}} \\ \sin(\theta_r+\frac{2\pi}{5}) & \cos(\theta_r+\frac{2\pi}{5}) & \sin 3(\theta_r+\frac{2\pi}{5}) & \cos 3(\theta_r+\frac{2\pi}{5}) & \frac{1}{\sqrt{2}} \end{bmatrix} \tag{2-44}$$

4. Stator Voltage and Flux Equations in the Rotating Frame of Reference

By applying the above transformation to the stator voltages equations, the following will be obtained:

$$T(\theta_r)V_s = R_s T(\theta_r)I_s + T(\theta_r)\frac{d\lambda_s}{dt} \tag{2-45}$$

Equation (2-45) can be rewritten as:

$$T(\theta_r)V_s = R_s T(\theta_r)I_s + T(\theta_r)\frac{d}{dt}T^{-1}(\theta_r)T(\theta_r)\lambda_s \tag{2-46}$$

where:

$$T(\theta_r)\frac{dT^{-1}(\theta_r)}{dt} = \omega\begin{bmatrix} 0 & -1 & 0 & 0 & 0 \\ 1 & 0 & 0 & 0 & 0 \\ 0 & 0 & 0 & -3 & 0 \\ 0 & 0 & 3 & 0 & 0 \\ 0 & 0 & 0 & 0 & 0 \end{bmatrix} = \omega\times \tag{2-47}$$

The stator voltage equation can be expressed as:

$$V_{d_1q_1d_3q_3s} = R_s I_{d_1q_1d_3q_3s} + \frac{d\lambda_{d_1q_1d_3q_3s}}{dt} + \omega\times\lambda_{d_1q_1d_3q_3s} \tag{2-48}$$

Therefore:

$$V_{ds1} = r_s i_{ds1} - \omega\lambda_{qs1} + \frac{d\lambda_{ds1}}{dt} \tag{2-49}$$

$$V_{qs1} = r_s i_{qs1} + \omega\lambda_{ds1} + \frac{d\lambda_{qs1}}{dt} \tag{2-50}$$

$$V_{ds3} = r_s i_{ds3} - 3\omega\lambda_{qs3} + \frac{d\lambda_{ds3}}{dt} \tag{2-51}$$

$$V_{qs3} = r_s i_{qs3} + 3\omega\lambda_{ds3} + \frac{d\lambda_{qs3}}{dt} \tag{2-52}$$

By applying the transformation matrix to stator flux linkages equations, the following will be obtained:

$$T(\theta_r)\lambda_s = T(\theta_r)L_{ss}T^{-1}(\theta_r)T(\theta_r)I_s + T(\theta_r)\Lambda_m \tag{2-53}$$

where

$$T(\theta_r)L_{ss}T^{-1}(\theta_r) = \begin{bmatrix} L_{ls}+\frac{5}{2}L_{ms1} & & & & & \\ & L_{ls}+\frac{5}{2}L_{ms1} & & & & \\ & & L_{ls}+\frac{5}{2}L_{ms3} & & & \\ & & & L_{ls}+\frac{5}{2}L_{ms3} & & \\ & & & & L_{ls} & \end{bmatrix} \tag{2-54}$$

and

$$T(\theta_r)\Lambda_m = \begin{bmatrix} \lambda_{m1} \\ 0 \\ \lambda_{m3} \\ 0 \\ 0 \end{bmatrix} \tag{2-55}$$

Therefore, the stator flux equations in the new frame of reference are as follows:

$$\lambda_{ds1} = (L_{ls} + \frac{5}{2}L_{ms1})i_{ds1} + \lambda_{m1} \tag{2-56}$$

$$\lambda_{qs1} = (L_{ls} + \frac{5}{2}L_{ms1})\, i_{qs1} \tag{2-57}$$

$$\lambda_{ds3} = (L_{ls} + \frac{5}{2} L_{ms3}) i_{ds3} + \lambda_{m3} \tag{2-58}$$

$$\lambda_{qs3} = (L_{ls} + \frac{5}{2} L_{ms3}) i_{qs3} \tag{2-59}$$

5. Electromagnetic Torque

The electromagnetic torque is determined by:

$$T_e = \frac{\partial W_{co}}{\partial \theta_{rm}} \tag{2-60}$$

where W_{co} is the co-energy and θ_{rm} is the mechanical rotor angle. Co-energy is defined as follows:

$$W_{co} = \frac{1}{2} I_s^T L_s I_s + I_s^T \Lambda_m \tag{2-61}$$

Taking the partial derivative with respect to θ_{rm} and considering that there is no saliency on the rotor yields:

$$T_e = \frac{P}{2} I_s^T \frac{\partial \Lambda_m}{\partial \theta_r} \tag{2-62}$$

or

$$T_e = \frac{P}{2} (T(\theta_r)^{-1} i_{d1q1d3q30s})^t \frac{\partial \Lambda_m}{\partial \theta_r} \tag{2-63}$$

The transformation matrix has the following pseudo-orthogonal property:

$$T^{-1}(\theta_r) = \frac{5}{2} T^t(\theta_r) \tag{2-64}$$

Therefore:

$$T_e = \frac{5}{2}\frac{P}{2} i_{d1q1d3q30s}{}^{t} T(\theta_r) \frac{\partial \Lambda_m}{\partial \theta_r} \tag{2-65}$$

and finally:

$$T_e = \frac{5}{2}\frac{P}{2}\left[\lambda_{m1} i_{qs1} + 3\lambda_{m3} i_{qs3}\right] \tag{2-66}$$

Substituting from (2-56)-(2-59):

$$T_e = \frac{5}{2}\frac{P}{2}\left\{\left[\left[\lambda_{ds1} - (L_{ls} + \frac{5}{2}L_{ms1}) i_{ds1}\right] i_{qs1}\right] + \left[3\left[\lambda_{ds3} - (L_{ls} + \frac{5}{2}L_{ms3}) i_{ds3}\right] i_{qs3}\right]\right\} \tag{2-67}$$

The electromagnetic torque can be written as:

$$T = 5/2 \cdot P/2 \,(\lambda_{ds1} \cdot i_{qs1} - \lambda_{qs1} i_{ds1} + 3\lambda_{ds3} i_{qs3} - 3\lambda_{qs3} i_{ds3}) \tag{2-68}$$

where λ_{ds1}, λ_{qs1}, λ_{ds3}, λ_{qs3} are the stator fluxes in d1, q1, d3, q3 axes, respectively. i_{ds1}, i_{qs1}, i_{ds3}, i_{qs3} are the transformed stator currents in these rotating axes. The improvement in the developed torque due to the third harmonic can be noticed from (2-68).

Mechanical motion equations are given by,

$$T_e - T_L = J_m \frac{d\omega_r}{dt} \tag{2-69}$$

Equations (2-49) to (2-69) can be used to model the five-phase permanent magnet motor with the combined fundamental and third harmonic currents in the $d_1q_1d_3q_3n$ reference frame. As it can be understood from the equations, the so-called vector control is easily applicable to this kind of motor.

The equivalent circuits of the five-phase PM motor are given in figure 2-11. In this figure, i_{m1} and i_{m3} are being used to represent the fundamental and third harmonic component of permanent magnet flux. Figure 2-12 shows the control block diagram of the proposed system where the difference between the reference speed and the actual speed determines the reference stator currents in the rotating reference frame. The reference stator voltages in the $d_1q_1d_3q_3n$ reference frame are generated by the associated PI current regulator based on the difference between the commanded currents and the transformed sensed currents. Sinusoidal PWM technique has been used to drive the inverter.

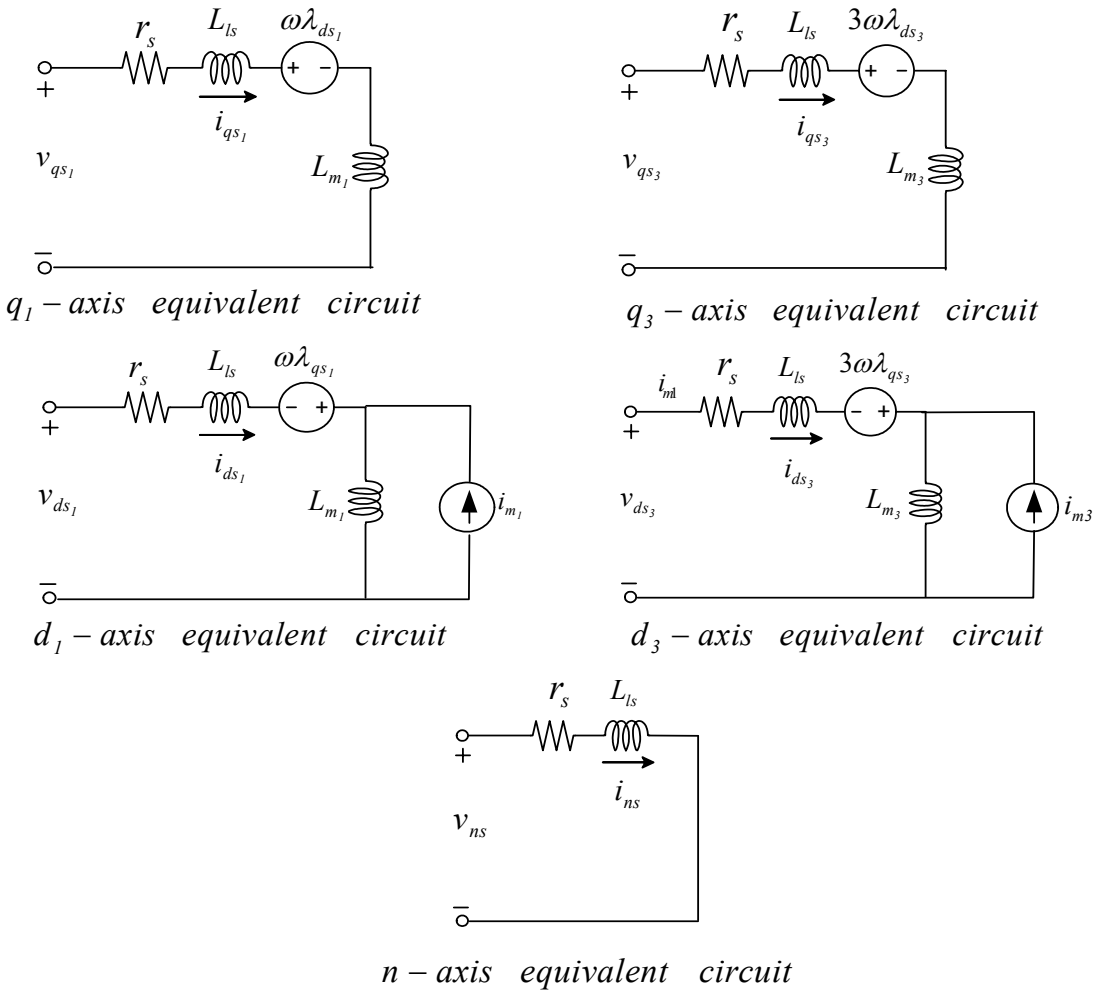

Figure 2-11 Equivalent circuits of the five-phase permanent magnet motor in the arbitrary frame of reference.

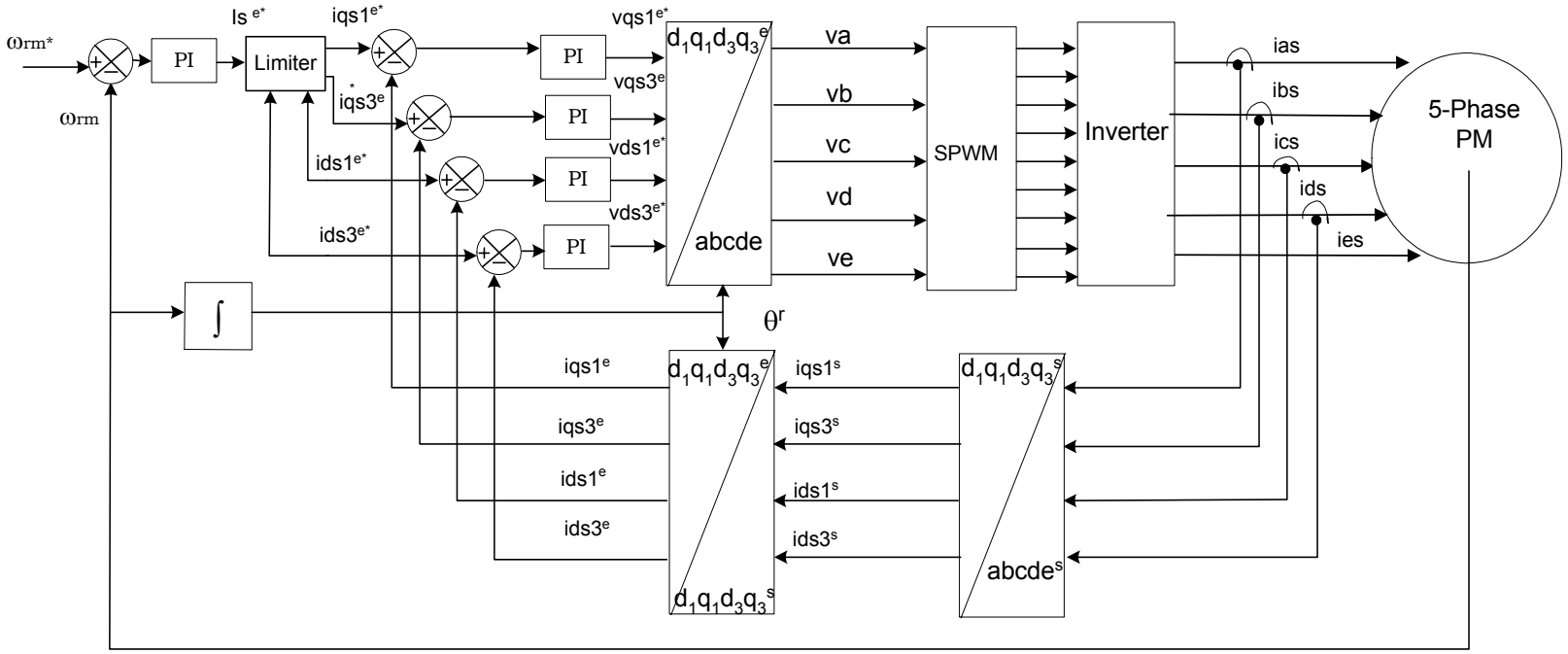

Figure 2-12 Control block diagram.

F. Simulation Results

Simulations have been performed using both finite element method and Matlab/Simulink to verify the superior performance of the proposed motor. A three-phase 7.5 hp, 4-pole, 230 V, 20 A, 36 slots off-the-shelf induction motor is used for this study. The rotor of this motor has been replaced with a permanent magnet rotor shown in figure 2-13a. In each pole, 12 pieces of magnets are used. Figure 2-13b illustrates the cross section of the PMSM motor which was built on the same stator frame as the induction motor, and is used as our reference motor.

The magnets are Nd-Fe-Br of type 35EH with B_r=1.21 Tesla. The stator coil pitch is 7/9, and the number of turns per coil is 30. The stator outer diameter, inner diameter, rotor outer diameter, shaft outer diameter and stack length are 228.6mm, 127mm, 124mm, 40mm and 101.6mm, respectively.

The induced back-EMF of coil A which is calculated from the flux linking coil A using the Ansoft finite element package is shown in figure 2-14. The package uses virtual work principles to compute the torque on an object:

$$T = \frac{\partial W_{co}}{\partial \theta_{rm}} = \frac{\partial}{\partial \theta_{rm}} \left[\int_V \left(\int_0^H B.dH \right) dV \right] \tag{2-70}$$

This motor has sinusoidal back-EMF and is supplied with sinusoidal currents . The developed static torque obtained from the finite element package is shown in figure 2-15. The average torque in this case is 42.62 N.m. The torque pulsations due to the slots openings are clear.

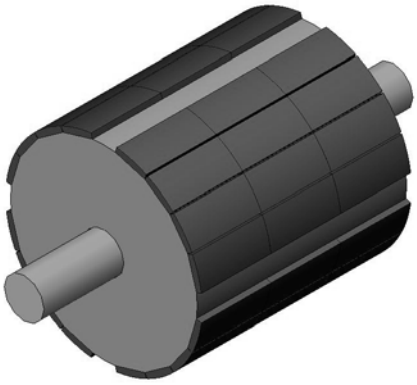

(a)

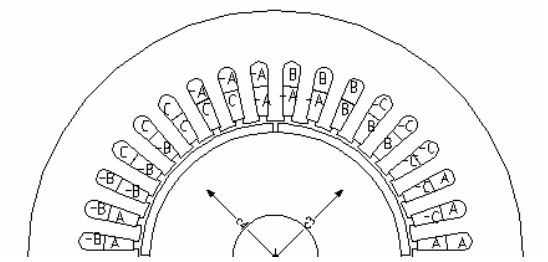

(b)

Figure 2-13 Three-phase PMSM motor, (a) permanent magnet rotor, (b) permanent magnet motor cross section.

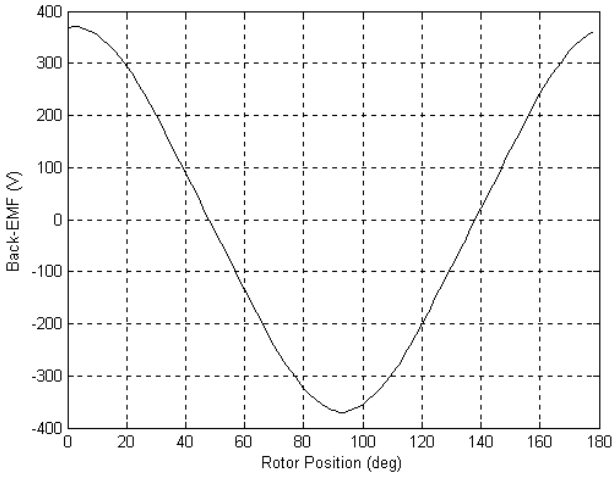

Figure 2-14 Back-EMF of 36-slot, three-phase PMSM motor.

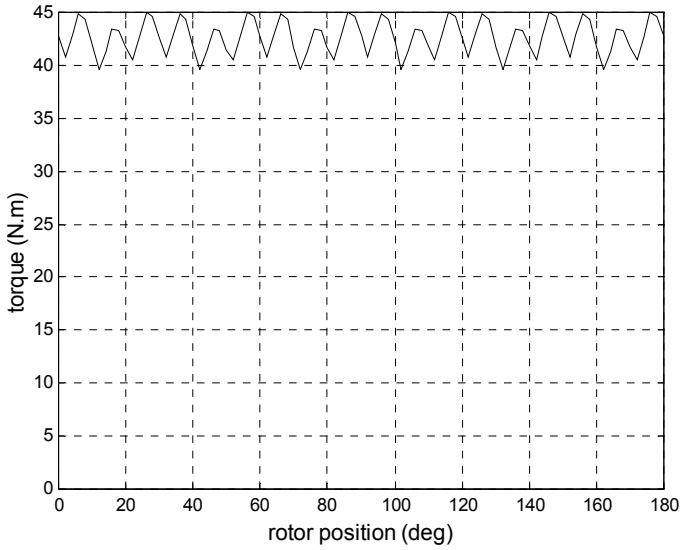

Figure 2-15 Torque of the 36 slots PMSM motor.

With a 12-slot stator, the back-EMF is quasi-rectangular and the motor can be supplied with current pulses of 120 degrees to produce almost constant torque. The developed torque using finite element is 46.9 Nm in this case. The torque is 10% higher than the 36-slot PMSM motor. The five-phase 20-slot, the 40-slot, single layer which is used for experimental verifications, and the 40-slot double layer motors have been designed using the same frame size as the original three-phase motor. The number of turns and slots width have been adjusted to maintain almost the same amount of copper and iron, and therefore almost equal copper and core losses are maintained. The performance of five-phase 20-slot, 40-slot single layer, and 40-slot double layer PM motors are compared. In this study, the motors with quasi rectangular back-EMF are supplied with both combined fundamental and third harmonics of current and current pulses of 144 degrees with 4 phases conducting at each instant of time. In this way, it

can be shown that both kind of excitation will generate almost the same output torque while those supplied with combined fundamental and third harmonic of current have better controllability due to vector control.

The 40-slot double layer motor has been considered as the reference for comparing the five-phase conventional sinusoidally-fed PMSM with the motors supplied with fundamental and third harmonic of currents. Figure 2-16 shows the cross section and winding distribution of all the three motors. Figure 2-17 shows the back-EMF waveforms of these motors. The back-EMF of the 20-slot motor is trapezoidal. It progresses toward sinusoidal waveform as the number of stator slots increases to 40 slots, and the number of layers changes from single to double layer.

The developed torque of all the motors supplied with different current waveforms have been obtained using the finite element method. In each case, the peak values of the current has been adjusted so that the rms current for all the cases is kept the same as shown in figure 2-18. The amount of the the injected third harmonic of current is 15% of the fundamental frequency current. From figure 2-18, it is clear that the 144 degree pulse of current has the lowest peak value among all the three types of currents. The 20-slot and the 40-slot single layer motors with quasi-rectangular back-EMF have been supplied with both the 144^0 current pulses, and the combined fundamental and third harmonic of currents. The double layer 40-slot motor has been supplied with sinusoidal current. The static torque of the motors with different excitation currents under rated condition are shown in figure 2-19.

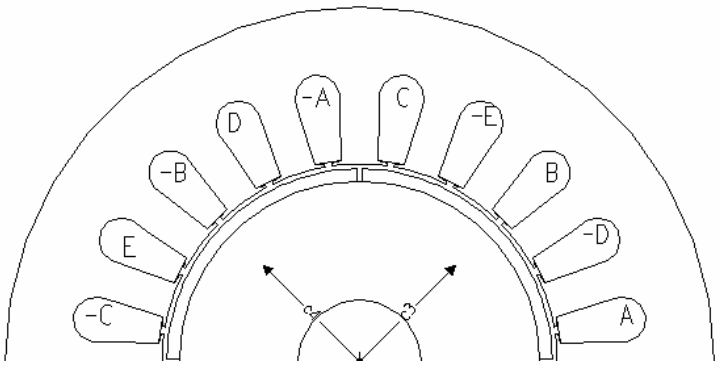

(a)

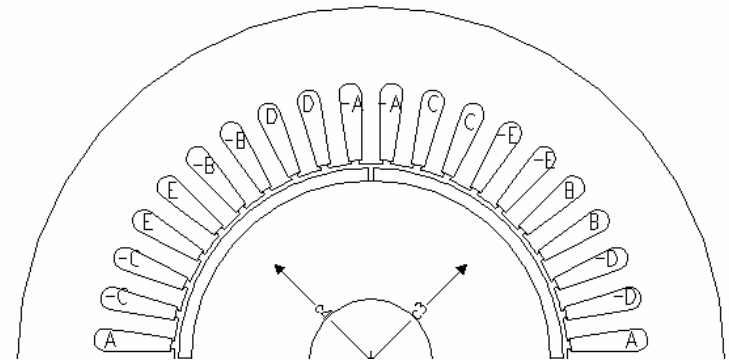

(b)

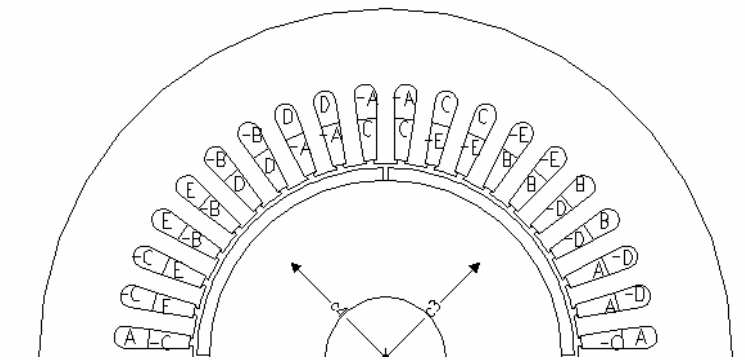

(c)

Figure 2-16 Cross section of five-phase, (a) 20-slot, (b) 40-slot single layer, (c) 40-slot double layer.

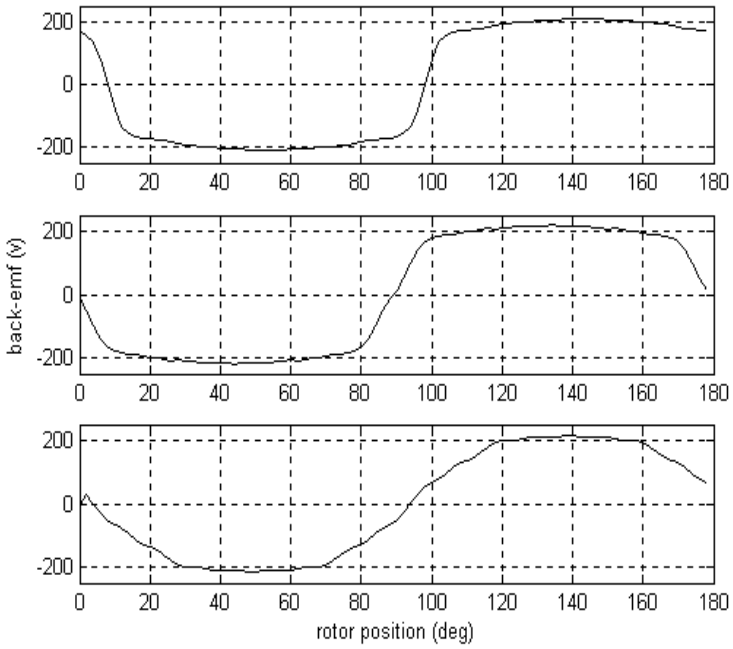

Figure 2-17 Back-EMF of, (a) 20-slot, (b) 40-slot, single layer, (c) 40-slot, double layer, five-phase machines.

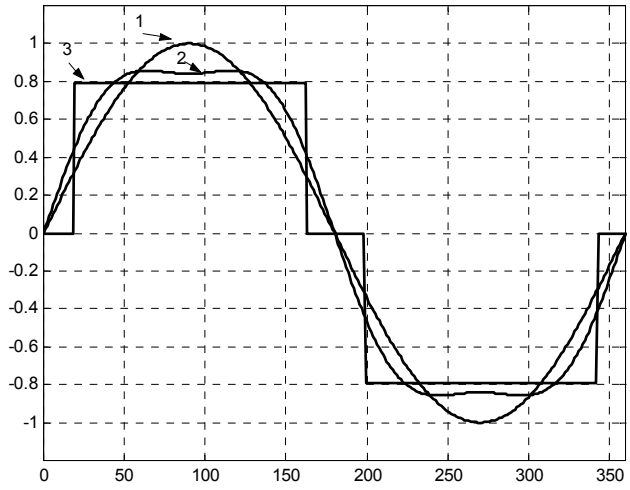

Figure 2-18 (1) Sinusoidal, (2) combined sinusoidal and third harmonic, (3) 144^0 pulses of current with the same rms values.

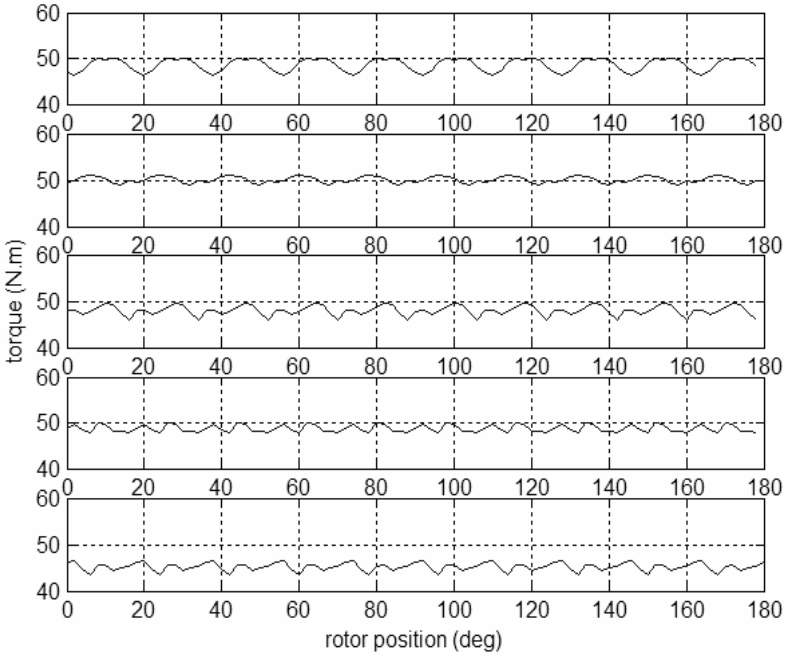

Figure 2-19 Torque of (a) 20 stator slots motor supplied as BLDC, (b) 20-slot motor supplied with combined sinusoidal and third harmonic, (c) 40-slot single layer motor supplied as BLDC, (d) 40 slots single layer motor supplied with combined fundamental and third harmonic, (e) 40-slot double layer motor supplied with sine currents.

From figures 2-15 and 2-19, the developed torque by five-phase 20-slot and 40-slot single layer motors are higher than that of the three-phase 36-slot and five-phase double layer 40-slot PMSM motors.

Figure 2-20 shows the torque-angle curve for 40-slot single layer motor when supplied with combined fundamental and third harmonic of rated and 50% of the rated current. Figure 2-21 presents the flux densities in the stator tooth and the stator back iron for the proposed 5-phase, 40-slot, single layer PM motor supplied with combined fundamental and third harmonic of currents. The tooth and back iron flux densities of other motors have been calculated and presented in Table 2-3 together with the average

torque and torque ripple of all the motors.

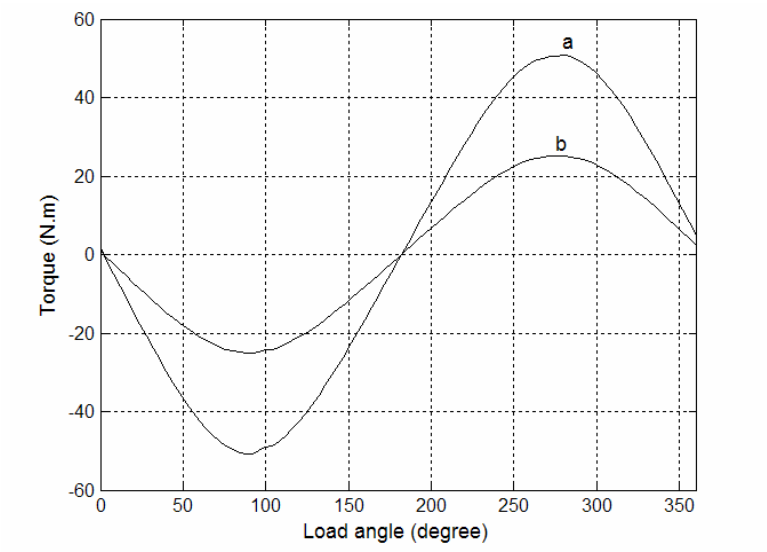

Figure 2-20 Torque versus load angle curves for rated and 50% of the rated currents.

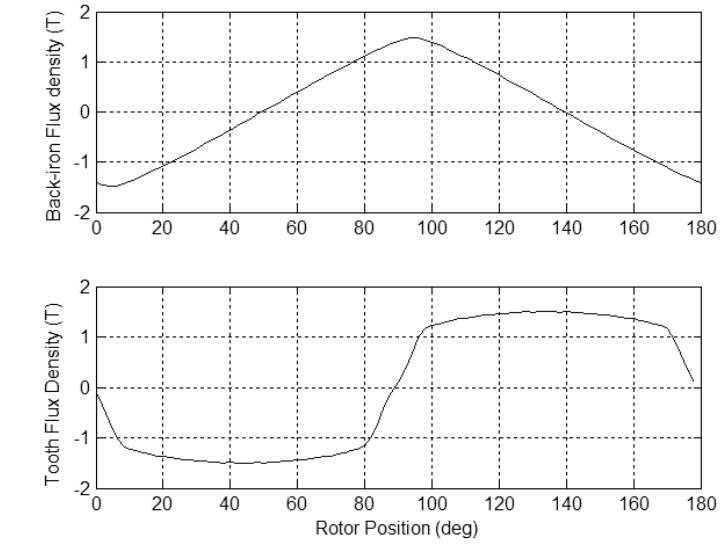

Figure 2-21 (a) Tooth flux density, and (b) back iron flux density of 40 slots motor supplied with combined fundamental plus third harmonic of currents.

The developed torque can be computed using d-q transformation as explained in Section II. The results of digital computer simulations have been summerized in Table 2-3 as well. As can be seen from the table, the five-phase 20-slot motor supplied with the combined fundamental plus third harmonic of currents produce about 17.3 % more torque with respect to the original three-phase PMSM motor.

The proposed five-phase, 40-slot motor supplied with the fundamental plus third harmonic of currents produces about 14.5% more torque than the original three-phase motor. The proposed five-phase motor (supplied with combined fundamental plus third harmonic of currents) have 10% more torque than the five-phase PMSM motor . The five-phase 20-slot and 40-slot single layer motors generate almost the same output torque when supplied with combined fundamental and third harmonic of current and current pulses of 144 degrees. However those supplied with combined fundamental and third harmonic of current have better controllability due to vector control.

Also, it is noted that the tooth and the back iron flux densities in the proposed motor are lower than the PMSM counterpart. In all cases, the flux densities in the tooth and back iron are within the acceptable range. The table also shows the torque ripple for all the motors. As expected, the torque ripple of the five-phase motors are lower than that of the three-phase and have higher frequencies. The last column of the table shows the torque computed using the d-q model. From the table, it can be realized that the torque values agree well with those calculated using the finite element package.

It should be mentioned that the percentages of torque improvement of five-phase 20-slot and 40-slot motor with respect to that of the three-phase 36-slot motor is in fact a

few percent lower than those numbers calculated above since the effect of end windings lengths has been neglected. Considering the effect of end windings on the number of turns, the torque improvement of the proposed five-phase 40-slot motor with respect to the three-phase motor decreases from 14.5% to 12.4%. It is expected that the torque improvement of the five-phase, 20-slot motor compared to the 36-slot motor which initially was calculated to be 17.3% should also drop by a few percent after considering the end windings effect.

Figure 2-22 shows the result from dynamic simulation in Matlab/Simulink when the motor speeds up, reaches to steady states and slows down. Vector control in d_1-q_1-d_3-q_3-n frame of reference was applied to the motor. As it is clear from the figure, the proposed algorithm is implemented successfully.

Table 2-3 Summary of simulation results

Motor type	Current type	Ave. torque from FE	Torque ripple	Tooth flux density	Back-iron flux density	Ave. torque from d-q model
3 phase 36 slots	Sine	42.62	6.37%	1.54	1.57	43.31
3. phase12 slots	120° pulses	46.9	8.5%	1.53	1.567	47.1
5 phase 20 slots	144° pulses	49.6	4%	1.551	1.492	50.12
5 phase 20 slots	Sine+3rd h	50	3.86%	1.558	1.498	50.9
5 phase 40 slots single layer	144° pulses	48	4.3%	1.545	1.484	48.7
5 phase 40 slots single layer	Sine+3rd h	48.8	3.72%	1.55	1.49	49.5
5 phase 40 slot double layers	Sine	44.2	3.4%	1.56	1.5070	44.6

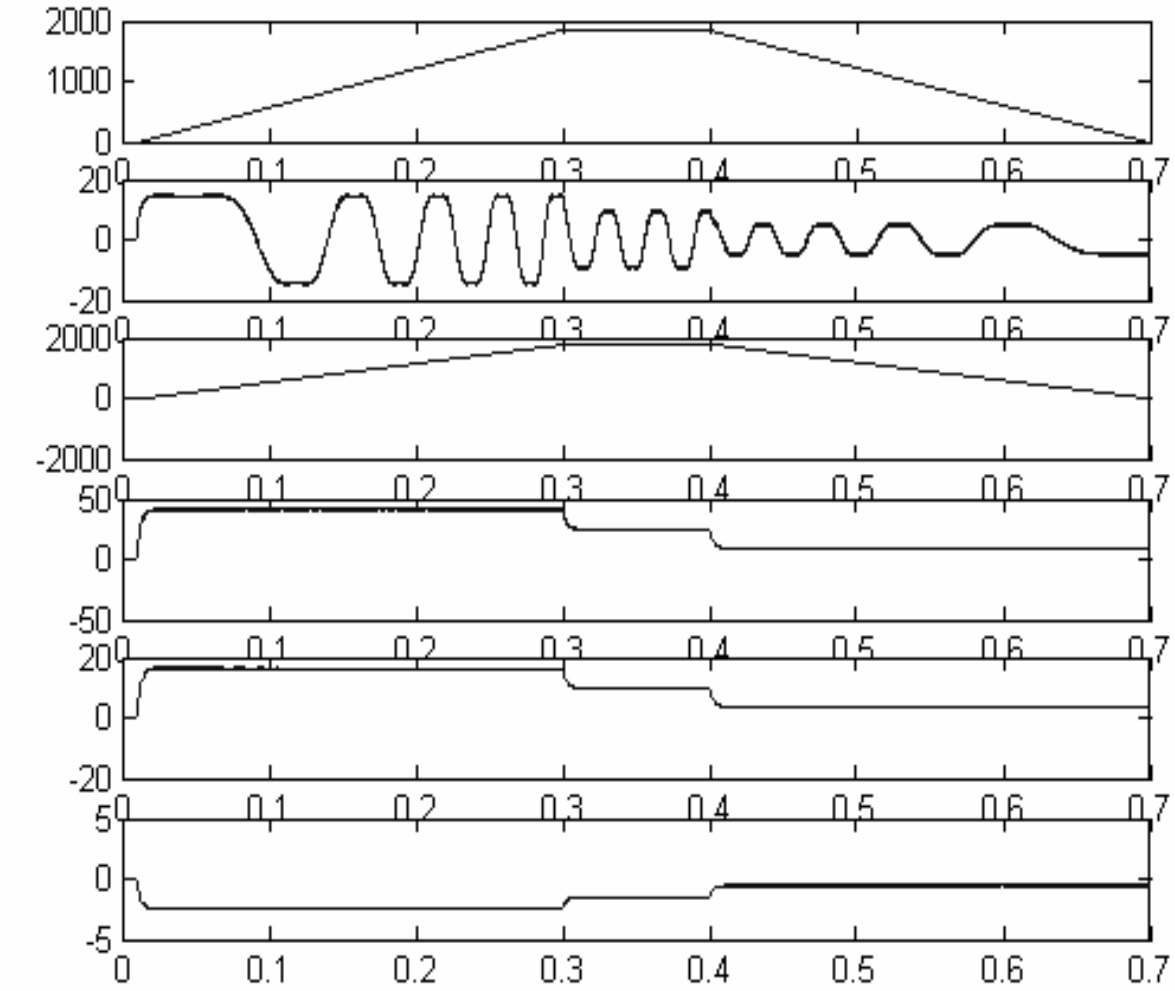

Figure 2-22 From top to bottom, reference speed, phase current, actual speed, output torque, i_{q1} and i_{q3}.

G. Experimental Results

The five-phase permanent magnet motor has been fabricated in the laboratory. Figure 2-23 shows the rotor made from small pieces of loaf magnets and the five-phase stator. The motor is 4-pole, 7.5 hp, 230 V, 20 A. The magnet type is Nd-Fe-Br of type

35EH with B_r=1.21 Tesla. The stator has 40 slots. Five-leg IGBT-based inverter has also been fabricated in the laboratory. The TMS320C32 floating point digital signal processor (DSP) is used to implement the digital control. Phase currents are being sensed through four current sensors. An encoder provides the position information and a DC generator is being used as a load. Figure 2-24 shows the hardware diagram. The control algorithm is based on figure 2-12.

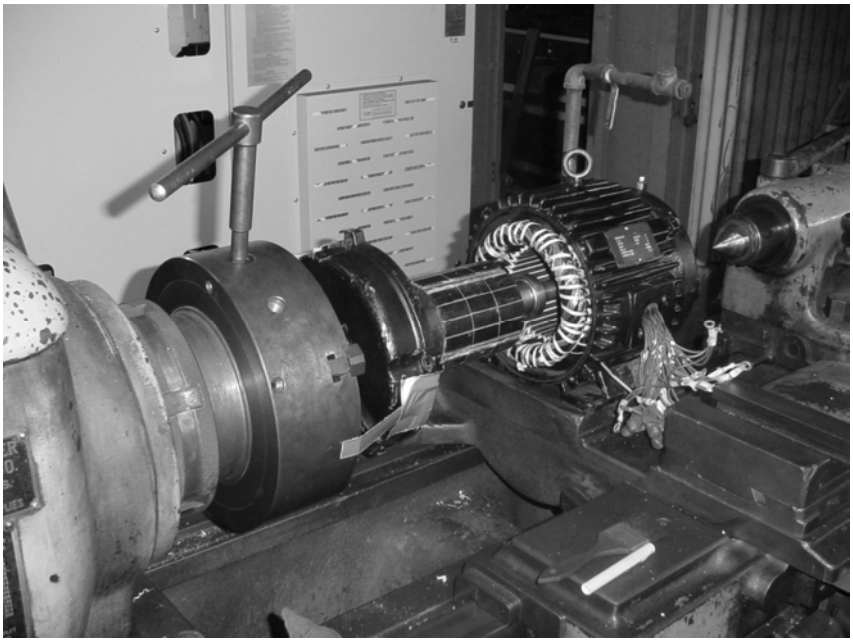

Figure 2-23 Rotor and stator of the 5BPM during assembly.

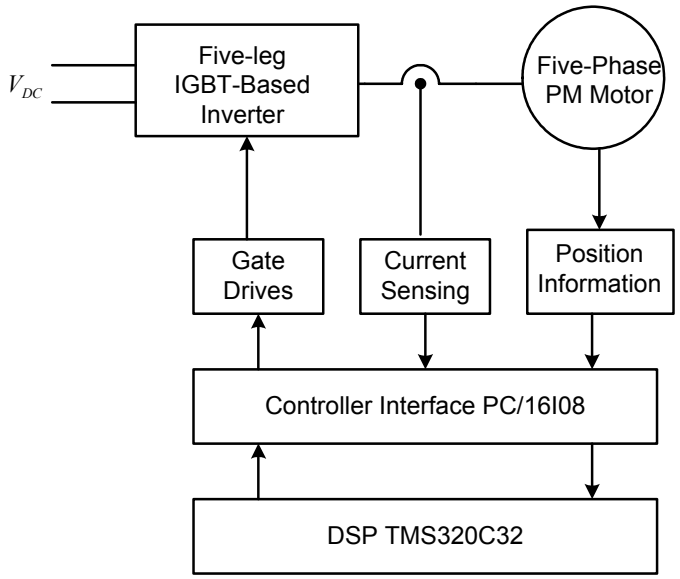

Figure 2-24 Hardware diagram

This motor is supplied with combined sinusoidal and third harmonic of currents. Figure. 2-25 shows the current waveform and the produced output torque of the motor. The rms value of the current in this case is 1.4 A, and the developed torque is 7 Nm. The torque obtained from the finite element package under the same condition is 6.84 Nm. Figure 2-26 shows the torque-angle curve of the motor under rated and 50% of the rated current. This figure is in good agreement with figure 2-20 which has been obtained from the finite element study. For the rated current, the peak torque from finite element is 50.6 Nm and from experiment is 51.1 Nm. For 50% of the rated current, the peak torque from finite element is 25.1 Nm and from experiment is 25.4 Nm. The tooth flux density and the back iron flux densities have also been monitored and are shown in figure 2-27. It is clear from these figures that these two waveforms are in good agreement with those obtained from the finite element shown in Figures (2-21-a) and (2-21-b).

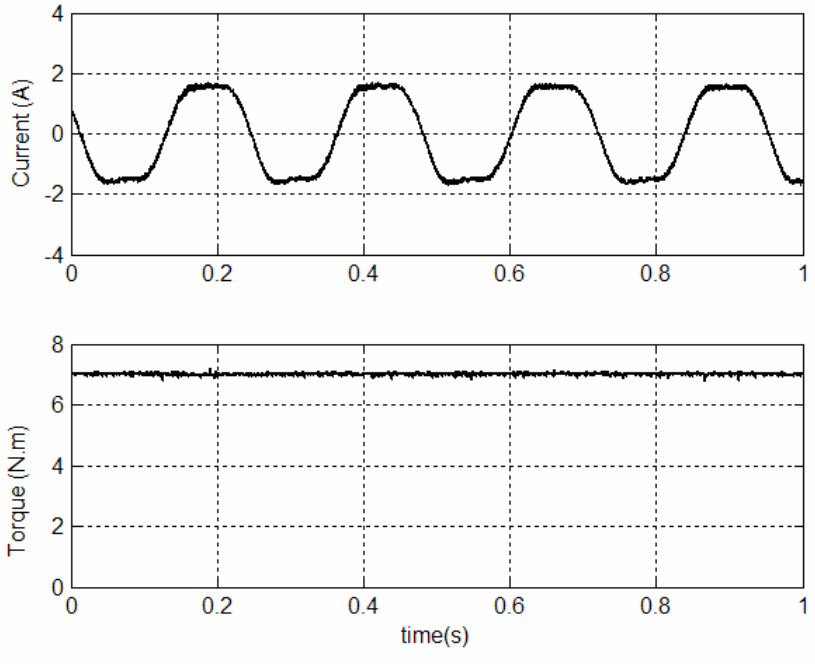

Figure 2-25 From top to bottom: Stator phase current and output torque.

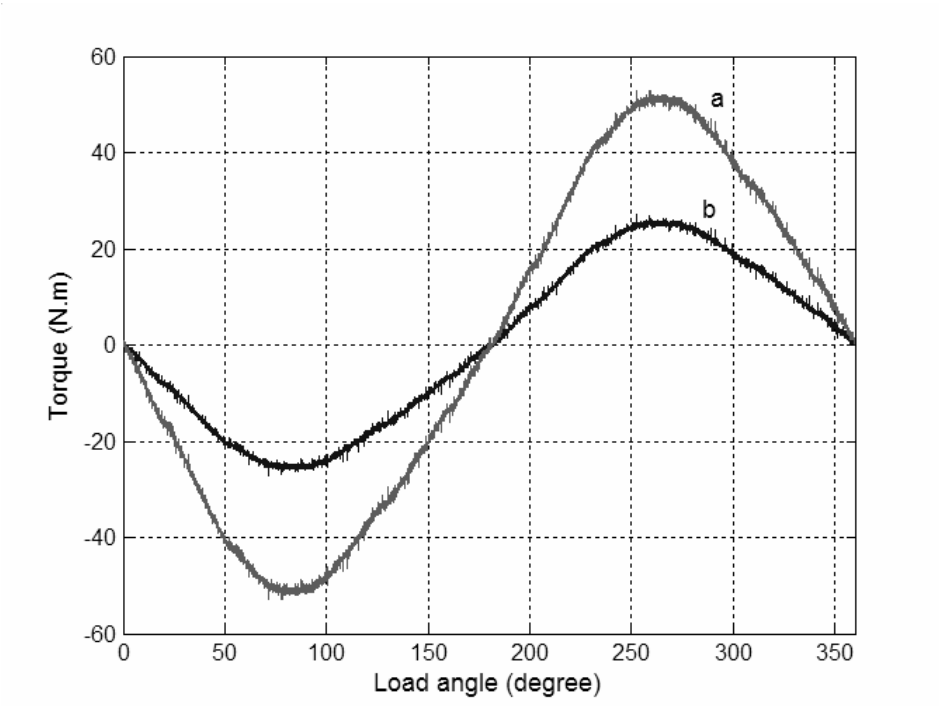

Figure 2-26 Torque versus load angle curve.

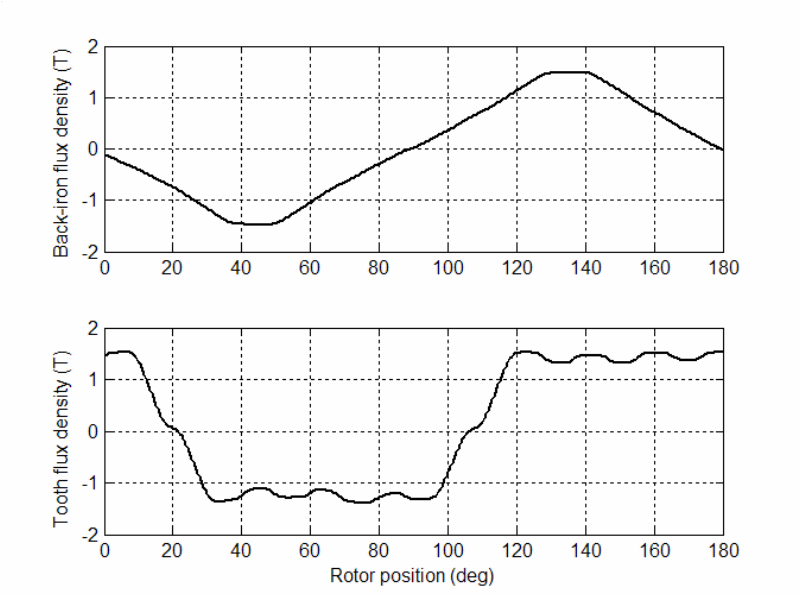

Figure 2-27 Top to bottom: Back iron and tooth flux densities.

To show the efficient performance of synchronous frame current regulators, frequent changing the command current from +5A to -5A has been considered. Switching interval from +5A to –5A is about 1sec. As shown in figures 2-28 to 2-31, all synchronous frame current components, $I_{d1}, I_{q1}, I_{d3}, I_{q3}$, can be regulated as ripple-free dc components in the steady state.

Figures 2-32 to 2-37 show the performance of the motor under closed loop speed control during 2 seconds and while the motor is operating below the rated speed. The speed change is from 300 rpm to -300 rpm at 1 second. Figure 2-32 shows the reference speed and actual speed for forward and backward operations. Figures 2-33 to 2-37 show the reference values of $I_{d1}, I_{q1}, I_{d3}, I_{q3}$ which are the output of the speed controllers and their actual values. Figure 2-37 shows the phase a and phase b currents.

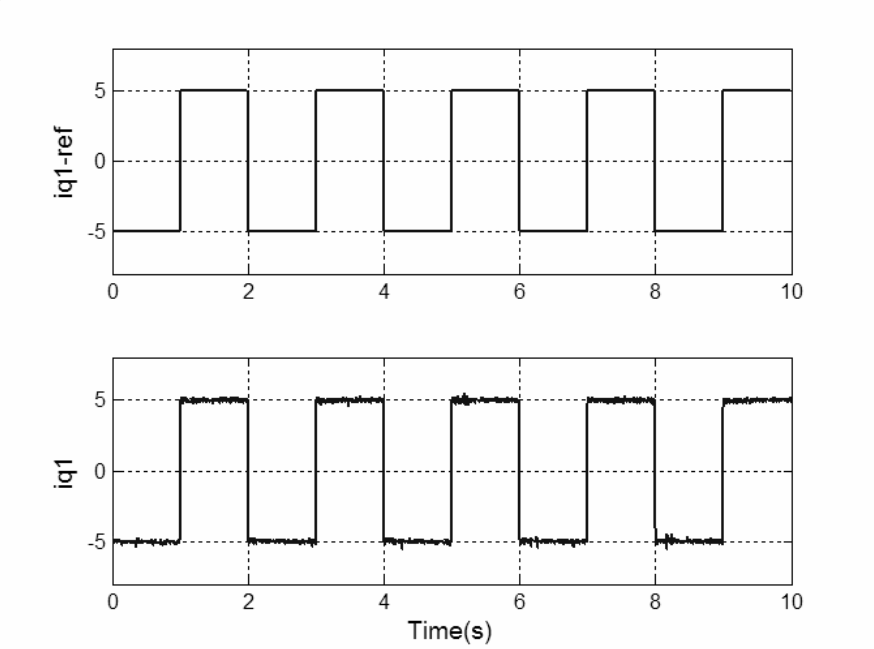

Figure 2-28 Reference and actual i_{q1} when speed loop is open.

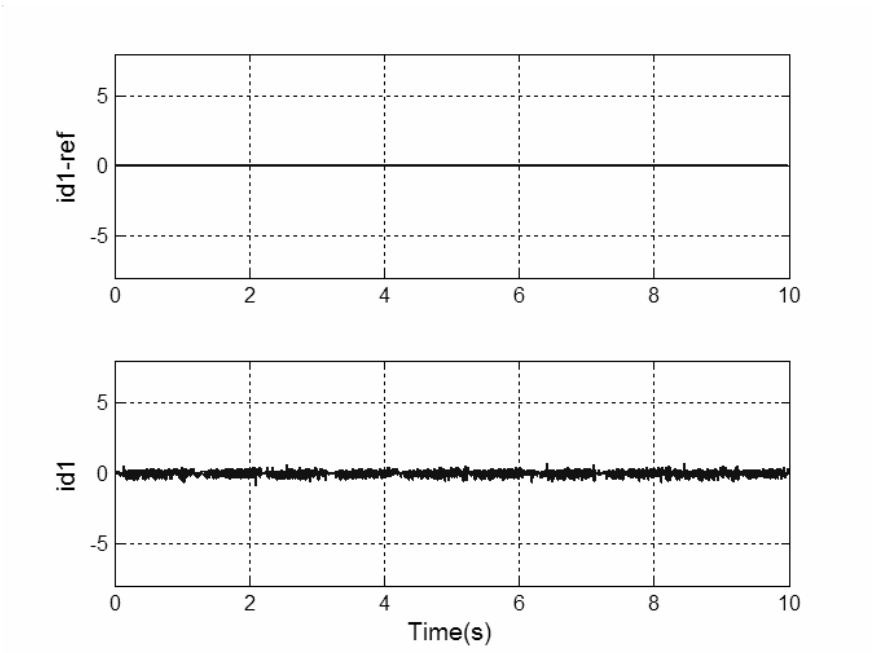

Figure 2-29 Reference and actual i_{d1} when speed loop is open.

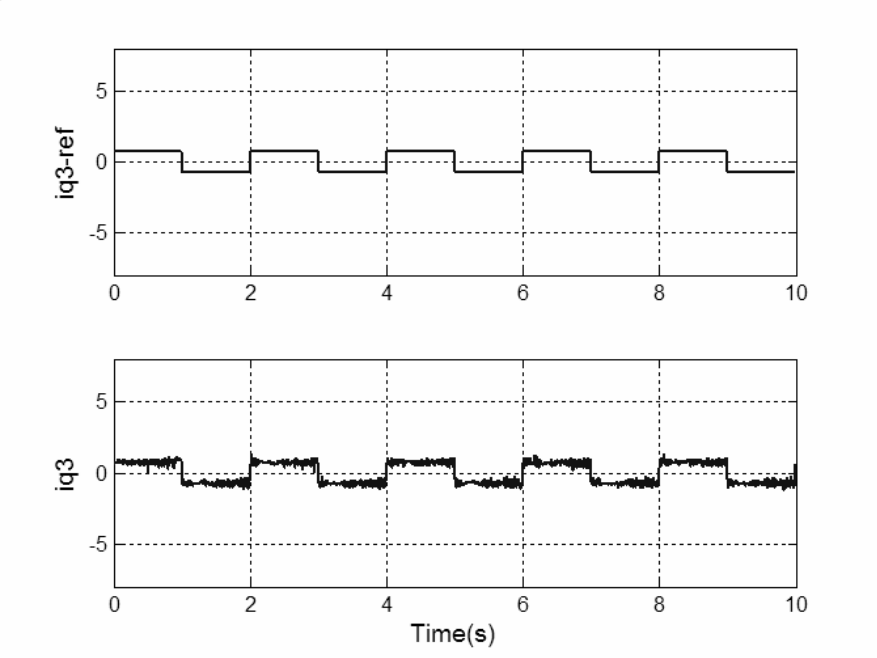

Figure 2-30 Reference and actual i_{q3} when speed loop is open.

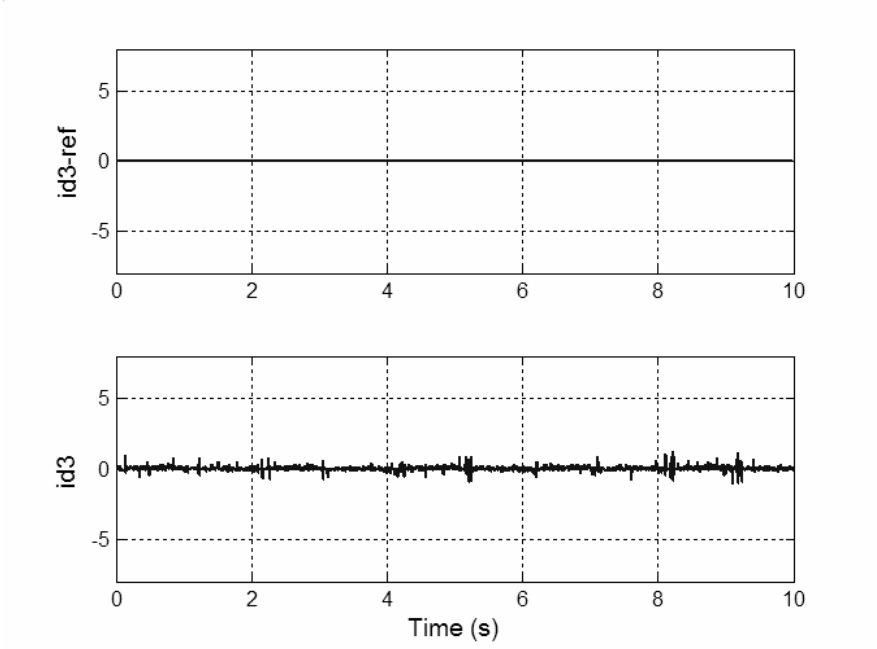

Figure 2-31 Reference and actual i_{d3} when speed loop is open.

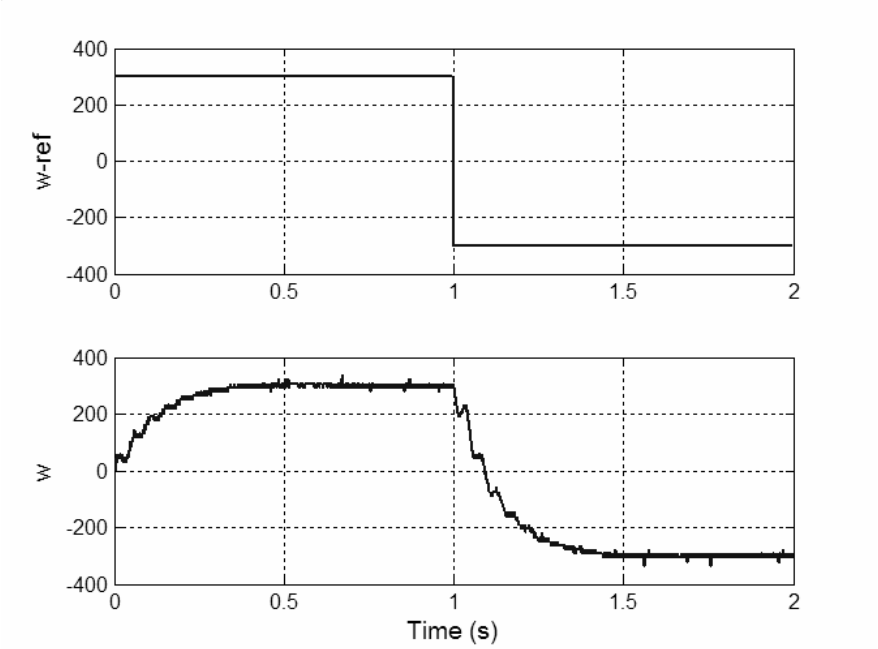

Figure 2-32 Reference speed and actual speed.

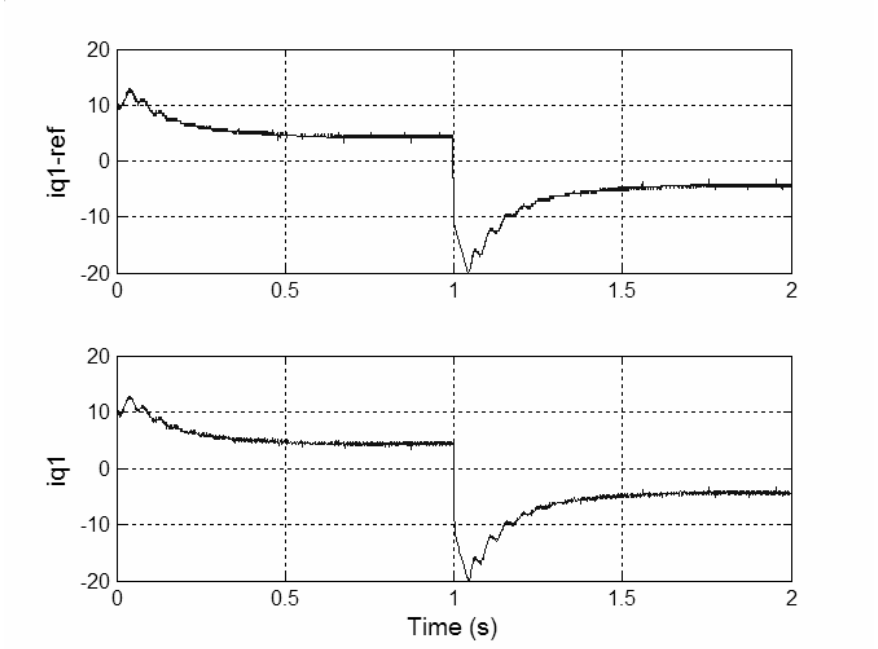

Figure 2-33 Reference and actual i_{q1} under closed speed loop control.

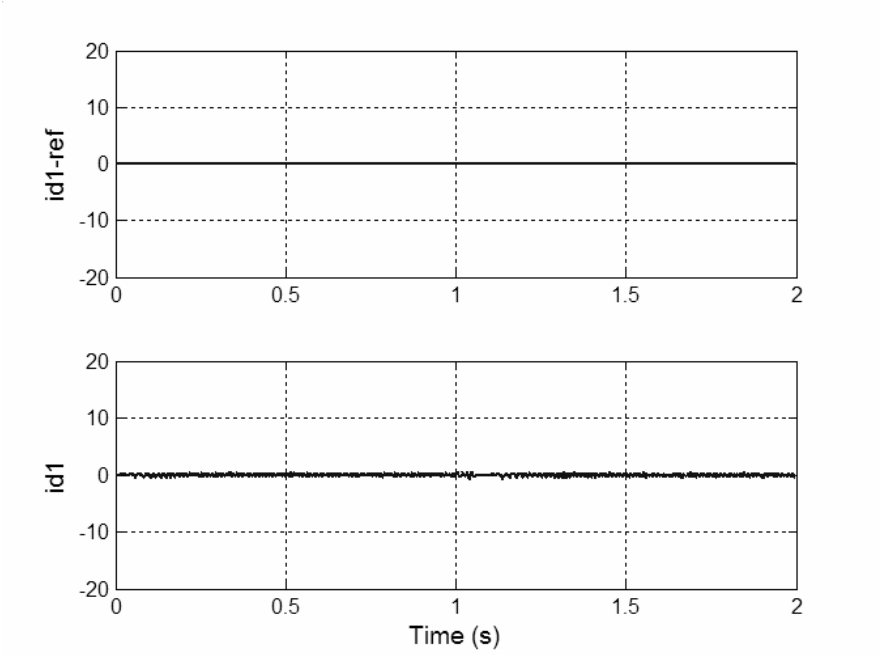

Figure 2-34 Reference and actual i_{d1} under closed speed loop control.

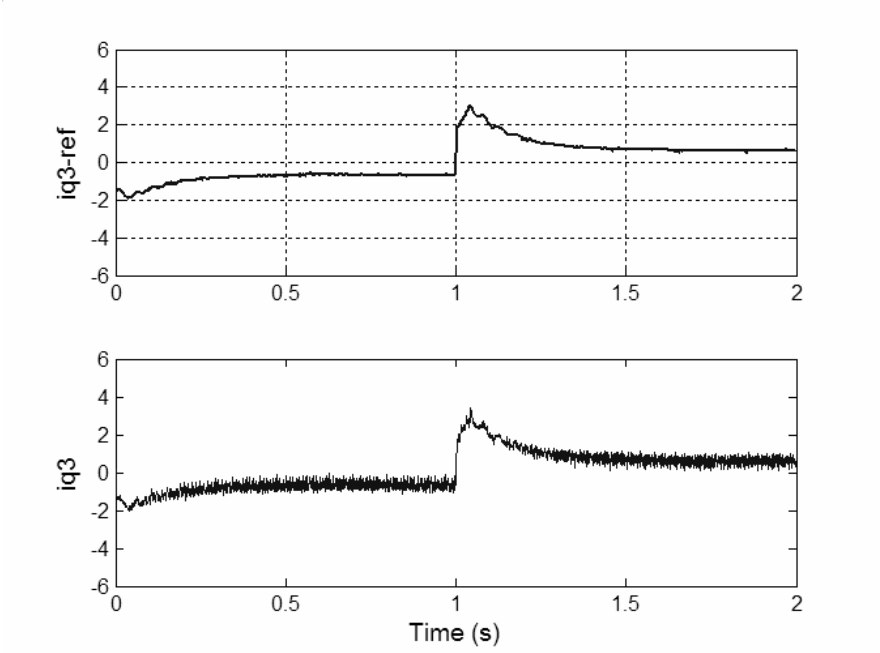

Figure 2-35 Reference and actual i_{q3} under closed speed loop control.

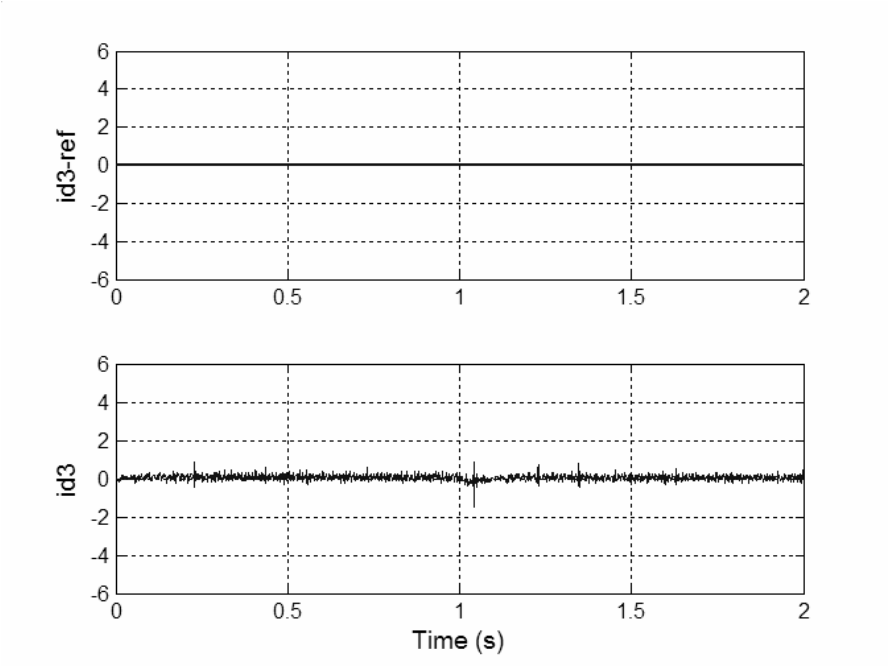

Figure 2-36 Reference and actual i_{d3} under closed speed loop control.

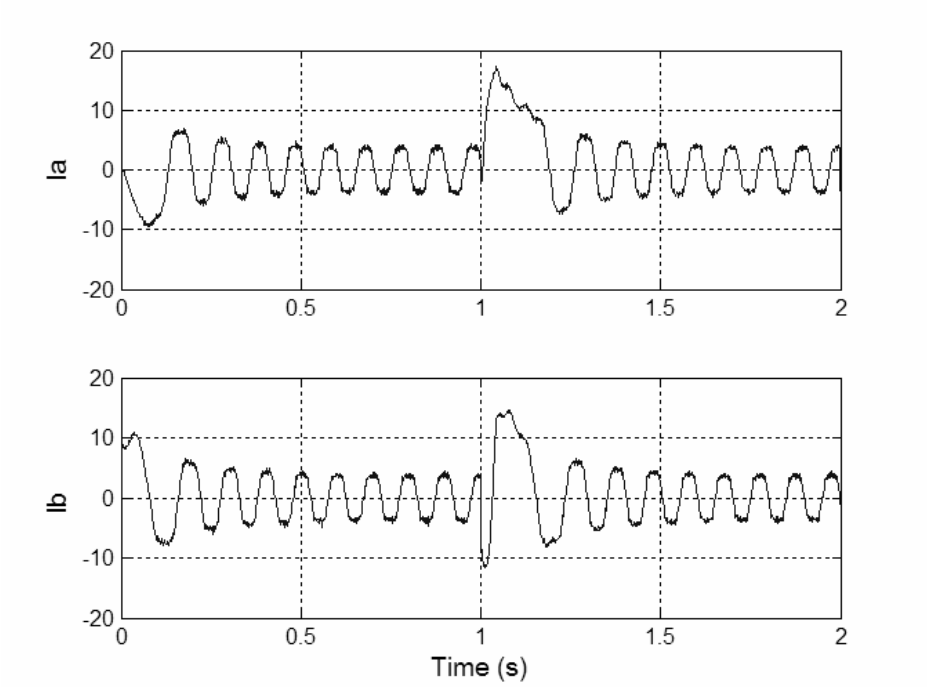

Figure 2-37 Phase a and b currents.

H. Conclusion

This chapter analyzed a new five-phase permanent magnet motor, which has near trapezoidal back-EMF and is supplied with the combined fundamental plus third harmonic of currents. The mathematical model of the motor has been derived in $d_1q_1d_3q_3n$ frame of reference. From the mathematical model it was understood that vector control algorithm can be easily implemented and the output torque of the motor is increased. Through simulation, it was shown that this motor while having almost the same torque density of a BLDC motor, benefits from controllability of a PMSM due to its compatibility with vector control technique. Experimental results are provided to validate the theoretical findings.

CHAPTER III

FAULT TOLERANT OPERATION OF PERMANENT MAGNET MOTOR DRIVES*

A. Introduction

Due to additional degrees of freedom, five-phase motors have better reliability compared to conventional three-phase motors. In this chapter, a control strategy that provides fault tolerance to five-phase permanent magnet motors is introduced. In this scheme, the five-phase permanent magnet (PM) motor continues operating safely under loss of up to two phases without any additional hardware connections and just by modifying the control algorithm. This feature is very important in traction and propulsion applications where high reliability is of major importance. The five-phase PM motors with sinusoidal and quasi-rectangular back-EMFs have been considered. To obtain the new set of phase currents to be applied to the motor during fault in stator phases or inverter legs, the produced MMF by the stator is kept constant under healthy and faulty conditions for both cases. Simulation and experimental results are provided to verify that the five-phase motor continues operating continuously and steadily under faulty conditions. It is worth mentioning that for a three-phase motor to continue

operating under loss of one phase, a divided dc bus and neutral connection are required. In other words, a zero sequence component is necessary to provide an undisturbed rotating MMF after one phase is lost. In five-phase motor drives, the zero-sequence current is no longer a necessary component under the fault conditions. From a reliability standpoint, the zero sequence currents have been shown to have detrimental effects on motor bearing failure, reduce the reliability and increase the maintenance cost of the motor. The developed current control strategy in this chapter eliminates the use of a neutral line and provides the same rotating MMF to ensure that the motor is running as smoothly as it was during the normal operations. Load adjustment is needed to avoid over currents especially in case of loss of two phases. Simulation and experimental results will be presented to support the validity of the proposed fault tolerant scheme.

B. Fault Tolerant Operation of Five-Phase PMSM

In this part, fault tolerant operation of PM motor with sinusoidal winding distribution and sinusoidal phase currents is discussed. The space phasors of the five-phase currents in healthy condition is shown in figure 3-1. The stator phases MMFs are as follows:

$$
\begin{aligned}
MMF_a(\phi,\theta) &= \frac{N_s}{2} I_m \cos(\phi)\cos(\theta) \\
MMF_b(\phi,\theta) &= \frac{N_s}{2} I_m \cos(\phi-\frac{2\pi}{5})\cos(\theta-\frac{2\pi}{5}) \\
MMF_c(\phi,\theta) &= \frac{N_s}{2} I_m \cos(\phi-\frac{4\pi}{5})\cos(\theta-\frac{4\pi}{5}) \\
MMF_d(\phi,\theta) &= \frac{N_s}{2} I_m \cos(\phi+\frac{4\pi}{5})\cos(\theta+\frac{4\pi}{5}) \\
MMF_e(\phi,\theta) &= \frac{N_s}{2} I_m \cos(\phi+\frac{2\pi}{5})\cos(\theta+\frac{2\pi}{5})
\end{aligned}
\qquad (3\text{-}1)
$$

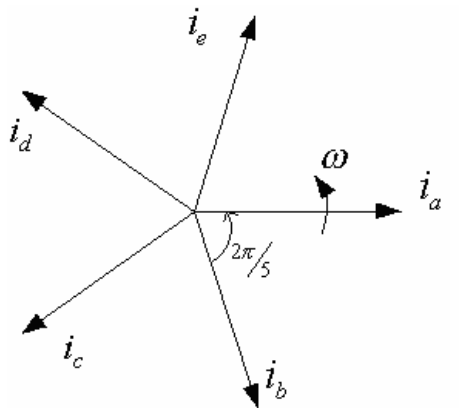

Figure 3-1 Space vector of the currents in healthy condition.

N_s is the total number of turns for each phase, ϕ is the spatial angle and $\theta=\omega t$. I_m is the amplitude of phase current. The stator total MMF is the sum of MMFs of all the phases:

$$MMF_t(\phi,\theta) = MMF_a(\phi+\theta) + MMF_b(\phi,\theta) + MMF_c(\phi,\theta) + MMF_d(\phi,\theta) + MMF_e(\phi,\theta) \quad (3\text{-}2)$$

which is given as:

$$MMF_t(\phi,\theta) = \frac{5}{4}(N_s I_m \cos(\theta-\phi)) \quad (3\text{-}3)$$

The above equation can be rewritten as:

$$MMF_t(\phi,\theta) = \frac{5}{8}(N_s I_m (e^{j\theta}e^{-j\phi} + e^{-j\theta}e^{j\phi})) \quad (3\text{-}4)$$

The total MMF can be also written as:

$$\begin{aligned} MMF_t = \frac{1}{4}\{N_s[(i_a + e^{-j\frac{2\pi}{5}} i_b + e^{-j\frac{4\pi}{5}} i_c + e^{j\frac{4\pi}{5}} i_d + e^{j\frac{2\pi}{5}} i_e)e^{j\phi} \\ + (i_a + e^{j\frac{2\pi}{5}} i_b + e^{j\frac{4\pi}{5}} i_c + e^{-j\frac{4\pi}{5}} i_d + e^{-j\frac{2\pi}{5}} i_e)e^{-j\phi}\} \end{aligned} \quad (3\text{-}5)$$

Based on (3-4) and (3-5), the following can be obtained:

$$\frac{5}{2} I_m e^{j\theta} = i_a + e^{j\frac{2\pi}{5}} i_b + e^{j\frac{4\pi}{5}} i_c + e^{-j\frac{4\pi}{5}} i_d + e^{-j\frac{2\pi}{5}} i_e \tag{3-6}$$

If phase "a" is open as a result of a device failure or a fault in the phase windings , a forward rotating field can be still obtained by setting i_a to zero in (3-6) and keeping the MMF unchanged. Assume:

$$i_b^{'} = -i_d^{'}; \qquad i_c^{'} = -i_e^{'} \tag{3-7}$$

The currents in the remaining phases are found to be:

$$i_b^{'} = -i_d^{'} = \frac{5I_m}{4(\sin\frac{2\pi}{5})^2} \cos(\theta - \frac{\pi}{5}) = 1.38\cos(\theta - \frac{\pi}{5}) \tag{3-8}$$

$$i_c^{'} = -i_e^{'} = \frac{5I_m}{4(\sin\frac{2\pi}{5})^2} \cos(\theta - \frac{4\pi}{5}) = 1.38\cos(\theta - \frac{4\pi}{5}) \tag{3-9}$$

Figure 3-2 shows the phasor diagram of the desired currents.

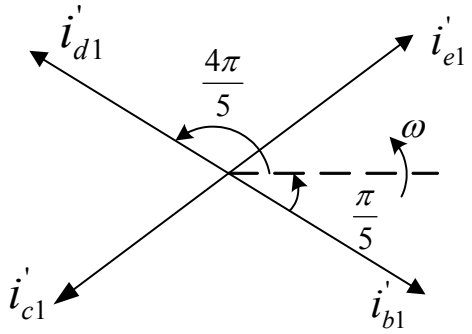

Figure 3-2 Phasor diagram of the desired currents for the remaining four healthy phases when phase "A" is open.

In this case, the fundamental current amplitude of the healthy phases needs to be increased up to 1.382 time of the initial value when all the five phases are functional.

Similar to the previous case, if both phase-a and phase-b are simultaneously lost, then considering that the sum of currents should be zero, the remaining three-phase currents are calculated as:

$$i_c^{"} = \frac{5I_m \cos(\frac{\pi}{5})}{2(\sin\frac{2\pi}{5})^2}\cos(\theta - \frac{2\pi}{5}) = 2.2361 I_m \cos(\theta - \frac{2\pi}{5}) \tag{3-10}$$

$$i_d^{"} = \frac{5I_m \cos(\frac{\pi}{5})^2}{(\sin\frac{2\pi}{5})^2}\cos(\theta + \frac{4\pi}{5}) == 3.618 I_m \cos(\theta + \frac{4\pi}{5}) \tag{3-11}$$

$$i_e^{"} = \frac{5I_m \cos(\frac{\pi}{5})}{2(\sin\frac{2\pi}{5})^2}\cos\theta == 2.2361 I_m \cos\theta \tag{3-12}$$

Figure 3-3 shows the phasor diagram of the desired currents.

MMF distributions in time and space for the healthy condition is shown in figure 3-4a. Figure 3-4b shows the MMF distribution in time and space when phase “a” is lost and no current control has been performed, and figure 3-4c shows the MMF distribution when the newly obtained currents have been applied to the motor. It is clear from the figure 3-4c that the MMF distribution is exactly the same as the MMF in the healthy condition of Figure 3-4a. Figures 3-4d and 3-4e show the MMF distribution before and after applying the new set of currents when both phases “a” and “b” are lost. Again it is clear from the figure 3-4e that the MMF distribution is exactly the same as the MMF in the healthy condition of Figure 3-4a. Therefore, if one or two phases are open-circuited, fault-free control is possible.

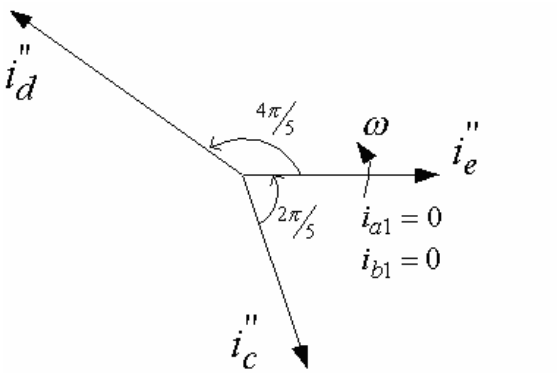

Figure 3-3 Phasor diagram of the desired currents for the remaining three healthy phases when phase "A" and "B" are open.

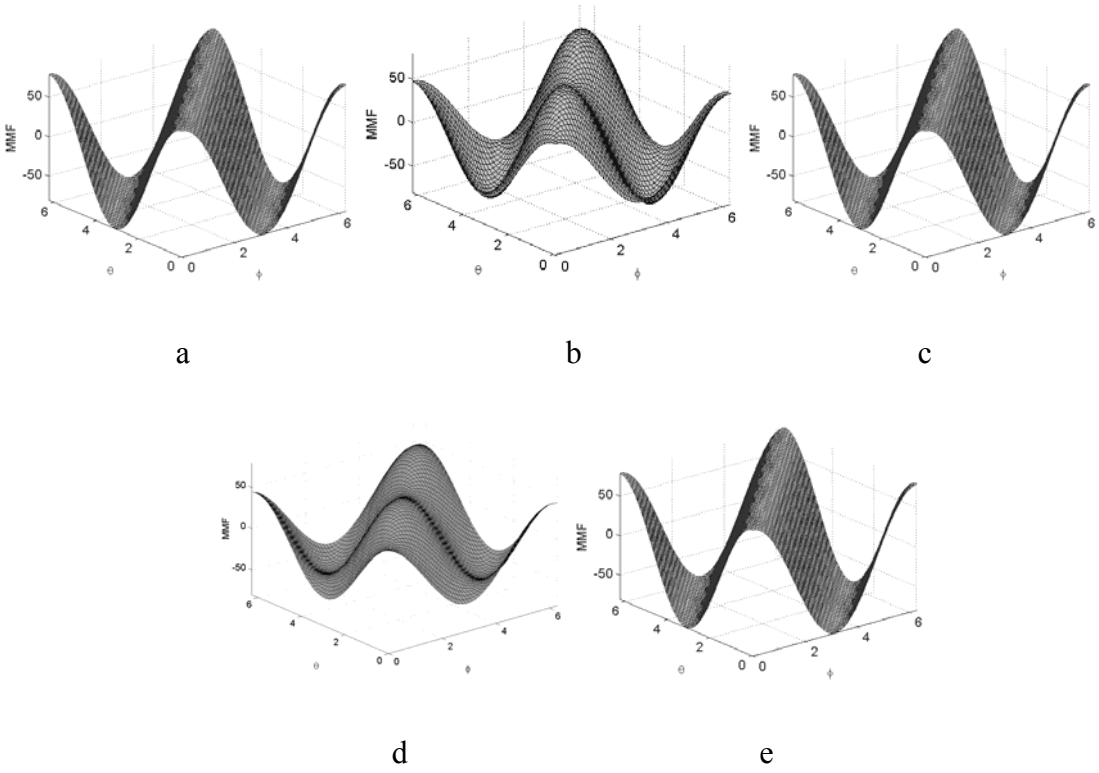

Figure 3-4 MMF distribution of, (a) healthy condition, (b) phase a is lost without current control, (c) phase a is lost with current control, (d) phase a and b are lost without current control, (e) phase a and b are lost with current control.

To have a fault tolerant drive, the control software should be adopted to implement the fault tolerant algorithm without adding any additional hardware. Open circuit fault of each phase can be detected through the associated current sensor then the control scheme should switch to fault tolerant control algorithm. Figure 3-5 shows the control block diagram of the fault tolerant five-phase motor. Consider I_{qs}^{*} and I_{ds}^{*} correspond to torque and flux producing current commands. Now, if phase-a is open, the remaining current commands i_{bs}^{*}, i_{cs}^{*}, i_{ds}^{*} and i_{es}^{*} are given by,

$$i_{bs}^{*} = 1.382(I_{qs}^{*}\cos(\theta - \frac{\pi}{5}) + I_{ds}^{*}\sin(\theta - \frac{\pi}{5})) \tag{3-13}$$

$$i_{cs}^{*} = 1.382(I_{qs}^{*}\cos(\theta - \frac{4\pi}{5}) + I_{ds}^{*}\sin(\theta - \frac{4\pi}{5})) \tag{3-14}$$

$$i_{ds}^{*} = 1.382(I_{qs}^{*}\cos(\theta + \frac{4\pi}{5}) + I_{ds}^{*}\sin(\theta + \frac{4\pi}{5})) \tag{3-15}$$

$$i_{es}^{*} = 1.382(I_{qs}^{*}\cos(\theta + \frac{\pi}{5}) + I_{ds}^{*}\sin(\theta + \frac{\pi}{5})) \tag{3-16}$$

If phase-a and -b are both open, the remaining reference currents will be:

$$i_{cs}^{*} = 2.2361(I_{qs}^{*}\cos(\theta - \frac{2\pi}{5}) + I_{ds}^{*}\sin(\theta - \frac{2\pi}{5})) \tag{3-17}$$

$$i_{ds}^{*} = 3.618(I_{qs}^{*}\cos(\theta + \frac{4\pi}{5}) + I_{ds}^{*}\sin(\theta + \frac{4\pi}{5})) \tag{3-18}$$

$$i_{es}^{*} = 2.2361(I_{qs}^{*}\cos\theta + I_{ds}^{*}\sin\theta) \tag{3-19}$$

Similar procedure should be followed when any other of phases are open.

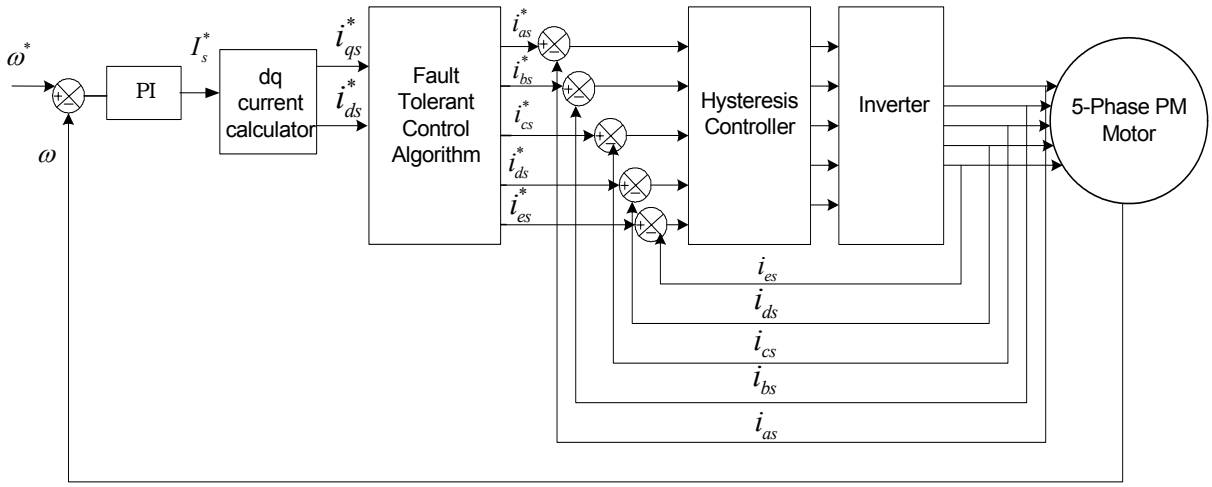

Figure 3-5 Control block diagram of fault tolerant system.

C. Fault Tolerant Operation of Five-Phase Permanent Magnet Motor Supplied with Combined Fundamental Plus Third Harmonic of Currents

As previously mentioned, this motor has concentrated windings. In order to simplify the modeling, only the fundamental and the third harmonic components of the winding function are taken into account. This motor is supplied with combined fundamental and third harmonic of the current. The phasor diagram of the phase currents in healthy condition is shown in figure 3-6.

The MMFs in the five-phase permanent magnet motor supplied with the fundamental plus third harmonic of currents are as follows:

$$\begin{aligned} MMF_a(\phi,\theta) = {} & \frac{N_{s1}}{2} I_{m1} \cos(\phi)\cos(\theta) + \frac{N_{s3}}{2} I_{m3} \cos 3(\phi)\cos 3(\theta) \\ & + \frac{N_{s1}}{2} I_{m3} \cos(\phi)\cos 3(\theta) + \frac{N_{s3}}{2} I_{m1} \cos 3(\phi)\cos(\theta) \end{aligned} \tag{3-20}$$

$$MMF_b(\phi,\theta)=\frac{N_{s1}}{2}I_{m1}\cos(\phi-\frac{2\pi}{5})\cos(\theta-\frac{2\pi}{5})+\frac{N_{s3}}{2}I_{m3}\cos 3(\phi-\frac{2\pi}{5})\cos 3(\theta-\frac{2\pi}{5})$$
$$+\frac{N_{s1}}{2}I_{m3}\cos(\phi-\frac{2\pi}{5})\cos 3(\theta-\frac{2\pi}{5})+\frac{N_{s3}}{2}I_{m1}\cos 3(\phi-\frac{2\pi}{5})\cos(\theta-\frac{2\pi}{5}) \quad (3\text{-}21)$$

$$MMF_c(\phi,\theta)=\frac{N_{s1}}{2}I_{m1}\cos(\phi-\frac{4\pi}{5})\cos(\theta-\frac{4\pi}{5})+\frac{N_{s3}}{2}I_{m3}\cos 3(\phi-\frac{4\pi}{5})\cos 3(\theta-\frac{4\pi}{5})$$
$$+\frac{N_{s1}}{2}I_{m3}\cos(\phi-\frac{4\pi}{5})\cos 3(\theta-\frac{4\pi}{5})+\frac{N_{s3}}{2}I_{m1}\cos 3(\phi-\frac{4\pi}{5})\cos(\theta-\frac{4\pi}{5}) \quad (3\text{-}22)$$

$$MMF_d(\phi,\theta)=\frac{N_{s1}}{2}I_{m1}\cos(\phi+\frac{4\pi}{5})\cos(\theta+\frac{4\pi}{5})+\frac{N_{s3}}{2}I_{m3}\cos 3(\phi+\frac{4\pi}{5})\cos 3(\theta+\frac{4\pi}{5})$$
$$+\frac{N_{s1}}{2}I_{m3}\cos(\phi+\frac{4\pi}{5})\cos 3(\theta+\frac{4\pi}{5})+\frac{N_{s3}}{2}I_{m1}\cos 3(\phi+\frac{4\pi}{5})\cos(\theta+\frac{4\pi}{5}) \quad (3\text{-}23)$$

$$MMF_e(\phi,\theta)=\frac{N_{s1}}{2}I_{m1}\cos(\phi+\frac{2\pi}{5})\cos(\theta+\frac{2\pi}{5})+\frac{N_{s3}}{2}I_{m3}\cos 3(\phi+\frac{2\pi}{5})\cos 3(\theta+\frac{2\pi}{5})$$
$$+\frac{N_{s1}}{2}I_{m3}\cos(\phi+\frac{2\pi}{5})\cos 3(\theta+\frac{2\pi}{5})+\frac{N_{s3}}{2}I_{m1}\cos 3(\phi+\frac{2\pi}{5})\cos(\theta+\frac{2\pi}{5}) \quad (3\text{-}24)$$

N_s is the total number of turns for each phase, ϕ is the spatial angle and $\theta=\omega t$. I_{m1} and I_{m3} are the amplitudes of fundamental and third harmonic of current. The amplitude of third harmonic of current in this study is considered to be 15% of the fundamental component.

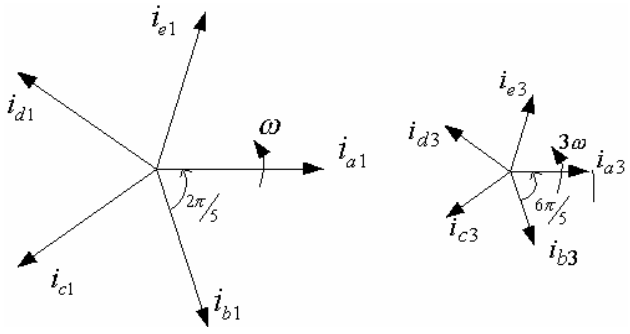

Figure 3-6 Space vector diagram of the fundamental and the third harmonic currents.

The stator total MMF will be:

$$MMF_t(\phi,\theta) = MMF_a(\phi+\theta) + MMF_b(\phi,\theta) + MMF_c(\phi,\theta) + MMF_d(\phi,\theta) + MMF_e(\phi,\theta) \quad (3\text{-}25)$$

and finally,

$$MMF_t(\phi,\theta) = \frac{5}{4}(N_{s1}I_{m1}\cos(\theta-\phi) + N_{s3}I_{m3}\cos 3(\theta-\phi)) \quad (3\text{-}26)$$

or,

$$\begin{aligned} MMF_t(\phi,\theta) &= \frac{5}{8}(N_{s1}I_{m1}(e^{j\theta}e^{-j\phi} + e^{-j\theta}e^{j\phi}) + N_{s3}I_{m3}(e^{j3\theta}e^{-j3\phi} + e^{-j3\theta}e^{j3\phi})) \\ &= MMF_{t1} + MMF_{t3} \end{aligned} \quad (3\text{-}27)$$

As it is clear from the equations, the total MMF is the result of fundamental component of time flowing in the fundamental component of space and third harmonic component of time flowing in the third harmonic component of space. The interaction of fundamental component of time flowing in the third harmonic component of space and vice versa does not appear in the total MMF when the motor is operating under healthy condition. It should be noted that in general, only same order harmonics of time and space contribute to torque production and space and time harmonics of different order produce pulsating torque. The total torque producing MMF can also be written as:

$$\begin{aligned} MMF_t = \frac{1}{4}\{&N_{s1}[(i_{a1} + e^{-j\frac{2\pi}{5}}i_{b1} + e^{-j\frac{4\pi}{5}}i_{c1} + e^{j\frac{4\pi}{5}}i_{d1} + e^{j\frac{2\pi}{5}}i_{e1})e^{j\phi} \\ &+ (i_{a1} + e^{j\frac{2\pi}{5}}i_{b1} + e^{j\frac{4\pi}{5}}i_{c1} + e^{-j\frac{4\pi}{5}}i_{d1} + e^{-j\frac{2\pi}{5}}i_{e1})e^{-j\phi}] + N_{s3}[(i_{a3} + e^{j\frac{4\pi}{5}}i_{b3} + e^{-j\frac{2\pi}{5}}i_{c3} + e^{j\frac{2\pi}{5}}i_{d3} + e^{-j\frac{4\pi}{5}}i_{e3})e^{j3\phi} \\ &+ (i_{a3} + e^{-j\frac{4\pi}{5}}i_{b3} + e^{j\frac{2\pi}{5}}i_{c3} + e^{-j\frac{2\pi}{5}}i_{d3} + e^{j\frac{4\pi}{5}}i_{e3})e^{-j3\phi}]\} = MMF_{t1} + MMF_{t3} \end{aligned} \quad (3\text{-}28)$$

Based on (3-27) and (3-28), the following can be obtained:

$$\frac{5}{2} I_{m1} e^{j\theta} = i_{a1} + e^{j\frac{2\pi}{5}} i_{b1} + e^{j\frac{4\pi}{5}} i_{c1} + e^{-j\frac{4\pi}{5}} i_{d1} + e^{-j\frac{2\pi}{5}} i_{e1} \tag{3-29}$$

$$\frac{5}{2} I_{m3} e^{j3\theta t} = i_{a3} + e^{-j\frac{4\pi}{5}} i_{b3} + e^{j\frac{2\pi}{5}} i_{c3} + e^{-j\frac{2\pi}{5}} i_{d3} + e^{j\frac{4\pi}{5}} i_{e3} \tag{3-30}$$

Figure 3-7 shows the fundamental and third harmonic MMF distributions in time and space for the healthy condition. If phase "a" is open resulting from power electronic device failures or motor windings, a rotating field can still be obtained by setting i_{a1} and i_{a3} equal to zero and keeping the torque producing MMF unchanged. Assuming:

$$i'_{b1} = -i'_{d1}; \qquad i'_{c1} = -i'_{e1}$$

$$i'_{b3} = -i'_{d3}; \qquad i'_{c3} = -i'_{e3} \tag{3-31}$$

The currents in the remaining phases are:

$$\begin{aligned} i'_b = -i'_d &= \frac{5I_{m1}}{4(\sin\frac{2\pi}{5})^2}\cos(\theta - \frac{\pi}{5}) - \frac{5I_{m3}}{4(\sin\frac{\pi}{5})^2}\cos 3(\theta - \frac{\pi}{5}) \\ &= 1.382 I_{m1}\cos(\theta - \frac{\pi}{5}) - 3.618 I_{m3}\cos(3\theta - \frac{3\pi}{5}) \end{aligned} \tag{3-32}$$

$$\begin{aligned} i'_c = -i'_e &= \frac{5I_{m1}}{4(\sin\frac{2\pi}{5})^2}\cos(\theta - \frac{4\pi}{5}) - \frac{5I_{m3}}{4(\sin\frac{\pi}{5})^2}\cos 3(\theta - \frac{4\pi}{5}) \\ &= 1.382 I_{m1}\cos(\theta - \frac{4\pi}{5}) - 3.618 I_{m3}\cos(3\theta - \frac{12\pi}{5}) \end{aligned} \tag{3-33}$$

Figure 3-8 shows the phasor diagram of the desired currents.

Figure 3-9a shows the MMF distribution in time and space when phase "a" is lost and no current control has been performed, and figure 3-9b shows the MMF distribution when the newly obtained currents have been applied to the motor. It is clear from the figure in the second case that the fudamental and third harmonic MMF distribution are

exactly the same as the fundamental and third harmonic MMF in the healthy condition of Figure 3-7.

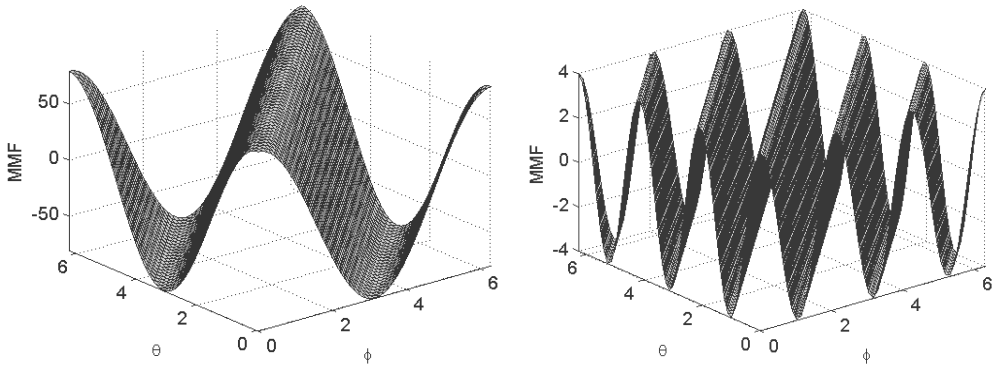

Figure 3-7 Fundamental and third harmonic of MMF in healthy condition.

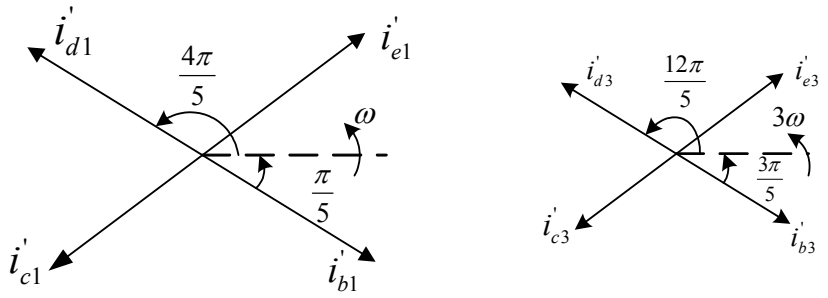

Figure 3-8 Phasor diagram of the currents for the remaining four healthy phases when phase "A" is open.

Therefore, if in a five-phase permanent magnet motor, one phase is opened, the currents in the remaining four phases is still able to maintain an undisturbed torque

producing MMF, which can be used to control the electromagnetic torque of the motor. The fundamental and third harmonic current amplitudes of the healthy phases should be adjusted to 1.382 and 3.618 times of the initial values under healthy condition.

Similar to the previous case, if both phase-a and phase-b are simultaneously lost, the remaining reference currents will be:

$$i_c^{"} = \frac{5I_{m1}\cos(\frac{\pi}{5})}{2(\sin\frac{2\pi}{5})^2}\cos(\theta-\frac{2\pi}{5}) + \frac{5I_{m3}\cos(\frac{3\pi}{5})}{2(\sin\frac{6\pi}{5})^2}\cos 3(\theta-\frac{2\pi}{5}) \tag{3-34}$$
$$= 2.2361I_{m1}\cos(\theta-\frac{2\pi}{5}) - 2.2361I_{m3}\cos(3\theta-\frac{6\pi}{5})$$

$$i_d^{"} = \frac{5I_{m1}\cos(\frac{\pi}{5})^2}{(\sin\frac{2\pi}{5})^2}\cos(\theta+\frac{4\pi}{5}) - \frac{5I_{m3}\cos(\frac{3\pi}{5})^2}{(\sin\frac{6\pi}{5})^2}\cos 3(\theta+\frac{4\pi}{5}) \tag{3-35}$$
$$= 3.618I_{m1}\cos(\theta+\frac{4\pi}{5}) - 1.382I_{m3}\cos(3\theta+\frac{12\pi}{5})$$

$$i_e^{"} = \frac{5I_{m1}\cos(\frac{\pi}{5})}{2(\sin\frac{2\pi}{5})^2}\cos\theta - \frac{5I_{m3}\cos(\frac{3\pi}{5})}{2(\sin\frac{6\pi}{5})^2}\cos 3\theta \tag{3-36}$$
$$= 2.2361I_{m1}\cos\theta + 2.2361I_{m3}\cos\theta$$

Phasor diagram of the desired currents are shown in figure 3-10. In this case, if we draw the MMF distribution before and after applying the new set of currents similar results will be observed.

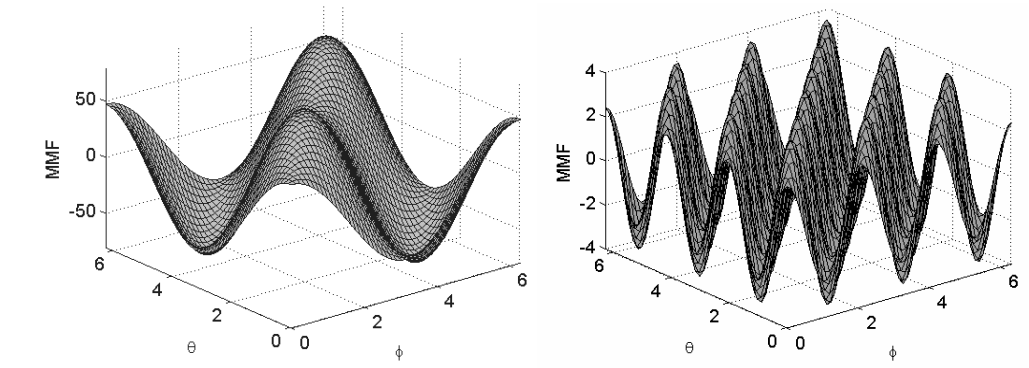

a

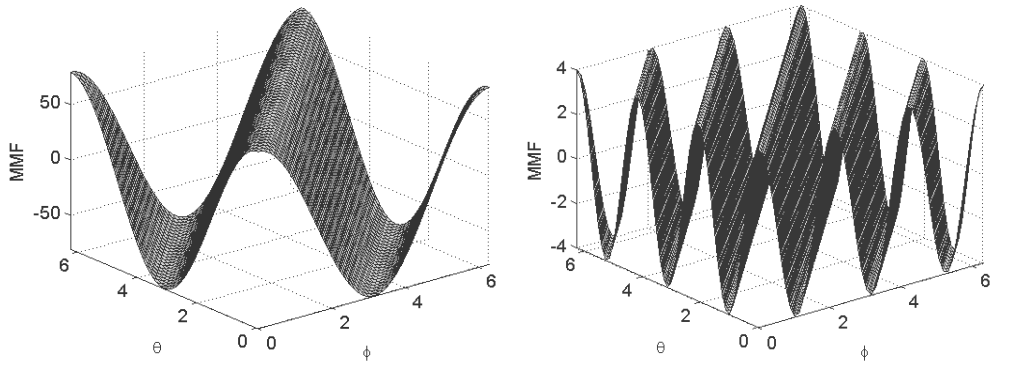

b

Figure 3-9 Fundamental and third harmonic MMF when phase-a is lost, (a) without any current control, (b) with applying the obtained currents.

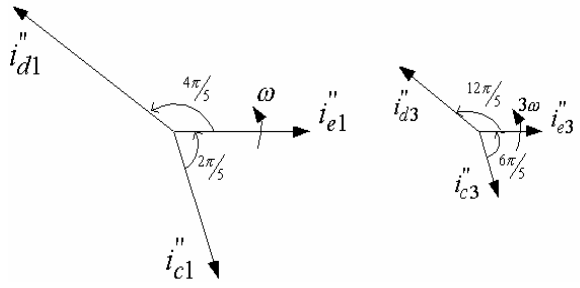

Figure 3-10 Phasor diagram of the desired currents for the remaining three healthy phases when both phases "A" & "B" are open.

In this case, again the control software should switch to fault tolerant algorithm in case of failure. The control process is similar to the one shown in Figure 3-5 but current calculator block should compute $I_{qs1}^*, I_{ds1}^*, I_{qs3}^*$ and I_{ds3}^*. Consider I_{qs1}^*, I_{qs3}^* and I_{ds1}^*, I_{ds3}^* correspond to torque and flux producing current commands, now if phase-a is open, the remaining current commands i_{bs}^*, i_{cs}^*, i_{ds}^* and i_{es}^* are given by,

$$i_{bs}^* = 1.382(I_{qs1}^* \cos(\theta - \frac{\pi}{5}) + I_{ds1}^* \sin(\theta - \frac{\pi}{5})) + 3.618(I_{qs3}^* \cos 3(\theta - \frac{\pi}{5}) + I_{ds3}^* \sin 3(\theta - \frac{\pi}{5})) \quad (3\text{-}37)$$

$$i_{cs}^* = 1.382(I_{qs1}^* \cos(\theta - \frac{4\pi}{5}) + I_{ds1}^* \sin(\theta - \frac{4\pi}{5})) + 3.618(I_{qs3}^* \cos 3(\theta - \frac{4\pi}{5}) + I_{ds3}^* \sin 3(\theta - \frac{4\pi}{5})) \quad (3\text{-}38)$$

$$i_{ds}^* = 1.382(I_{qs1}^* \cos(\theta + \frac{4\pi}{5}) + I_{ds1}^* \sin(\theta + \frac{4\pi}{5})) + 3.618(I_{qs3}^* \cos 3(\theta + \frac{4\pi}{5}) + I_{ds3}^* \sin 3(\theta + \frac{4\pi}{5})) \quad (3\text{-}39)$$

$$i_{es}^* = 1.382(I_{qs1}^* \cos(\theta + \frac{\pi}{5}) + I_{ds1}^* \sin(\theta + \frac{\pi}{5})) + 3.618(I_{qs3}^* \cos 3(\theta + \frac{\pi}{5}) + I_{ds3}^* \sin 3(\theta + \frac{\pi}{5})) \quad (3\text{-}40)$$

In the case that both phase-a and phase-b are open, the reference currents, i_{cs}^*, i_{ds}^* and i_{es}^*, are redefined as:

$$i_{cs}^* = 2.2361(I_{qs1}^* \cos(\theta - \frac{2\pi}{5}) + I_{ds1}^* \sin(\theta - \frac{2\pi}{5}) + I_{qs3}^* \cos 3(\theta - \frac{2\pi}{5}) + I_{ds3}^* \sin 3(\theta - \frac{2\pi}{5})) \quad (3\text{-}41)$$

$$i_{ds}^* = 3.618(I_{qs1}^* \cos(\theta + \frac{4\pi}{5}) + I_{ds1}^* \sin(\theta + \frac{4\pi}{5})) + 1.382(I_{qs3}^* \cos 3(\theta + \frac{4\pi}{5}) + I_{ds3}^* \sin 3(\theta + \frac{4\pi}{5})) \quad (3\text{-}42)$$

$$i_{es}^* = 2.2361(I_{qs1}^* \cos\theta + I_{ds1}^* \sin\theta + I_{qs3}^* \cos 3\theta + I_{ds3}^* \sin 3\theta) \quad (3\text{-}43)$$

D. Results

Experiments were done on the five-phase permanent magnet motors fabricated in our laboratory and the TMS320C32 DSP was used to implement the digital control. Figures 3-11 and 3-12 show the experimental results related to the five phase permanent magnet

motor which has sinusoidal back-EMF and is supplied with sinusoidal current. Figure 3-11 shows the motor speed, phase-a, and phase-b and c currents when phase-a is open circuited. As it is clear from the figure, the speed remains unchanged. Figure 3-12 shows the motor speed, phase-b, and phase-c and d currents when both phase-a and phase-b are open circuited. Like the previous case, the speed remains unchanged. It can be easily noticed that the amplitude of phase-d current is relatively high. Practically, it is impossible for the motor to run for a long time under such high current circumstances. Therefore, proper adjustment of the speed and load must be made so that the stator currents do not overtake the rated currents. However, in this experiment the motor is lightly loaded and therefore no adjustment of speed and load has been done. Figures 3-13 and 3-14 show the experimental results related to a five-phase permanent magnet motor which has quasi-rectangular back-EMF and is supplied with combined sinusoidal and third harmonic of currents. Figure 3-13 shows the motor speed, phase-a, and phase-b and c currents when phase-a is open circuited. As it is clear from the figure, the speed remains unchanged. Figure 3-14 shows the motor speed, phase-b, and phase-d currents when both phase-a and phase-b are open circuited. Like the previous case, the speed remains unchanged. It can easily be noticed that again the amplitude of phase-d current is relatively high.

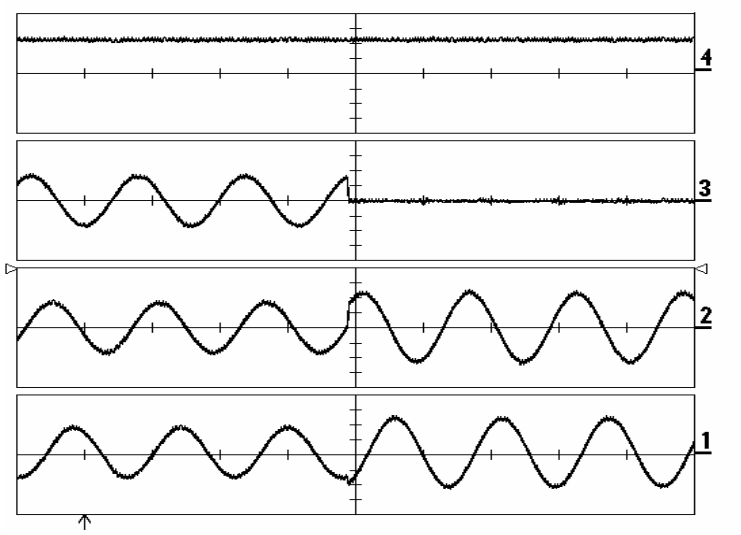

Figure 3-11 Motor speed, phase-a and phase-b and c currents phase-a is opened after a while (3A/div).

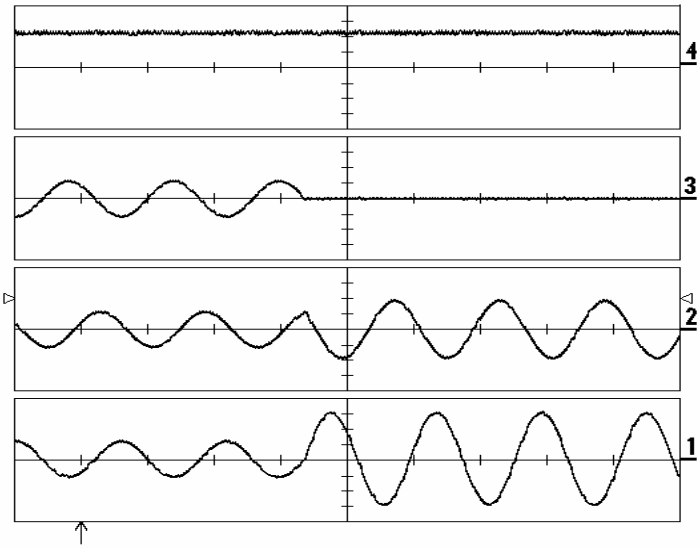

Figure 3-12 Motor speed, phase-b and phase-c and d currents, phase-b is opened after a while (6A/div).

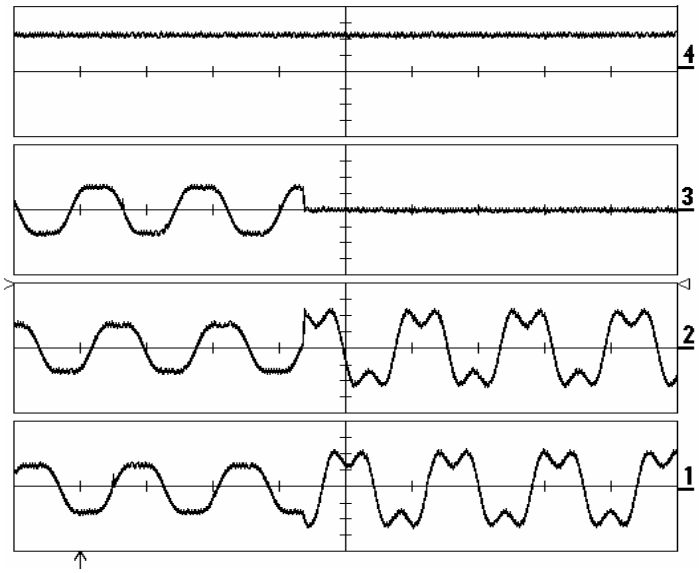

Figure 3-13 Motor speed, phase-a and phase-b and c currents phase-a is opened after a while (5A/div).

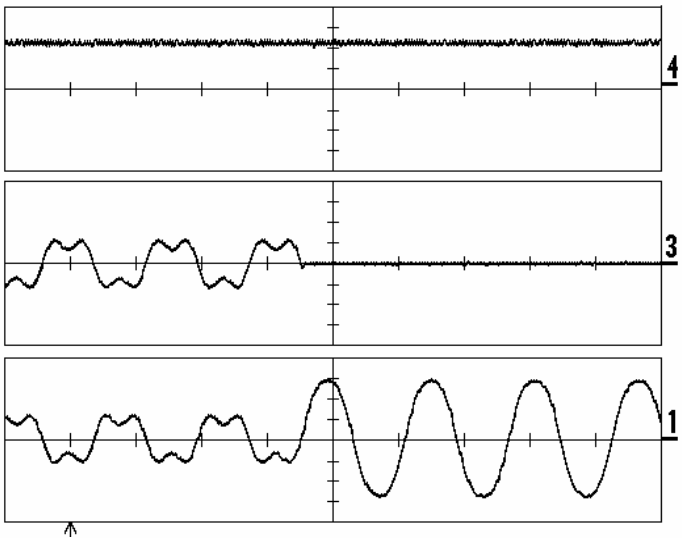

Figure 3-14 Motor speed, phase-b and phase-d currents, phase-b is opened after a while (10A/div).

E. Conclusion

In this chapter, the fault tolerant operation of five-phase permanent magnet motors was studied. The permanent magnet motors in this study had either sinusoidal back-EMF and were supplied with sinusoidal current or had quasi-rectangular back-EMF and were supplied with combined fundamental and third harmonic of currents. The new sets of stator currents to keep the total MMF unchanged were introduced in case of loss of one or two phases. The proposed control scheme eliminates the need for a neutral line which is a requirement for fault tolerant operation of three-phase motors. It can be simply implemented by adjusting the control scheme through software modifications without any requirement for additional hardware when the faults occur. The motor speed and average torque are almost unaffected. In case that the two phases are open, the shaft speed and load need to be adjusted in order to reduce the stator currents to ensure that the stator currents do not exceed their rated values. Simulation and experimental results have been included to verify the possibility of the control scheme.

CHAPTER IV

SPEED SENSORLESS DIRECT TORQUE CONTROL OF FIVE-PHASE INTERIOR PERMANENT MAGNET MOTOR*

A. Introduction

Direct torque control scheme has been first proposed and implemented for induction machines [52, 53]. The same concept has been extended to synchronous machines. Direct torque control of three-phase permanent magnet motor, which has been developed in the recent decade [54-57], is a powerful control method for motor drives. Featuring direct control of the stator flux and torque instead of the conventional current control technique, it provides a systematic solution to improving operating characteristics of not only the motor but also the voltage source inverter. Basically, the DTC method is based on the instantaneous space vector theory. By optimal selection of the space voltage vectors in each sampling period, the DTC achieves effective control of the stator flux and torque.

In this chapter, after pointing out the main advantages and drawbacks of DTC system, the mathematical model governing the five-phase interior permanent magnet motor will be introduced. Next, the speed sensorless direct torque control method of the five-phase interior permanent magnet motor and the associated switching vectors will be discussed. A five-phase interior permanent magnet motor and five-leg IGBT-based

inverter were designed and fabricated in the laboratory. The control method is implemented on a TMS320C32 digital signal processor board. Simulation and experimental results have been included to show the effectiveness of the five-phase DTC system.

B. Advantages and Drawbacks of the DTC System

DTC scheme has some potential advantages such as lesser parameter dependency and easier implementation of field weakening regime. The latter is because the stator flux linkages are being controlled directly in a DTC system.

Another main feature of DTC scheme is that current controllers are not being employed to control the motor torque and fluxes. The absence of the d-q axes current controllers eliminates the need for coordinate transformation. Therefore using a position sensor in a DTC controlled drive is not crucial either. Whereas, in a vector controlled drive the position information is required in each instant of time. However, speed information is required in existence of a speed loop in the direct torque controlled drive.

High torque and flux ripples are the major drawbacks of a DTC scheme. The reason is that the inverter keeps the same switching state as long as the outputs of flux and torque hysteresis controllers remain unchanged. Variable switching frequency is also another disadvantage. In a direct torque controlled drive, the switching frequency varies with speed, load torque, and bandwidth of flux and torque hysteresis controllers. The number of space voltage vectors and the switching frequency directly influence the performance of DTC control system. Recently, research has been done on reducing the

flux and torque ripple of DTC scheme by employing multi-level inverter which provides more voltage space vectors for controlling the flux and torque [58,59].

A five-phase system, while benefiting from other advantages of high order phase systems, has inherently 32 space voltage vectors. Therefore, in a five-phase system the existence of 32 possible space voltage vectors; permits better flexibility in selecting the switching states and finer adjustment of flux and torque. Whereas, in a three-phase drive the control is being implemented by just 8 possible switching states.

C. Mathematical Model of Five-Phase Interior Permanent Magnet Motor

In this section, the mathematical model of the five-phase IPM in rotating (dq) and stationary (αβ) reference frames will be derived.

1. Stator Voltages and Flux Linkages Equations

The stator voltage equations are given by,

$$V_S = R_S I_S + \frac{d\Lambda_S}{dt} \tag{4-1}$$

where the airgap flux linkages are presented by,

$$\Lambda_s = \Lambda_{ss} + \Lambda_m \tag{4-2}$$

or

$$\Lambda_S = L_{SS} I_S + \Lambda_m \tag{4-3}$$

R_s, I_s and Λ_s are the stator resistances, currents and flux linkages matrices, respectively.

Λ_m is the flux linking the stator due to the permanent magnet and considering sinusoidal distribution is defined by:

$$\Lambda_m = \lambda_m \begin{bmatrix} \sin(\theta_r) \\ \sin(\theta_r - \frac{2\pi}{5}) \\ \sin(\theta_r - \frac{4\pi}{5}) \\ \sin(\theta_r + \frac{4\pi}{5}) \\ \sin(\theta_r + \frac{2\pi}{5}) \end{bmatrix} \tag{4-4}$$

2. Stator Self and Mutual Inductances

L_{ss} in (4-3) is the stator inductance matrix which contains the self and mutual inductances of the stator phases and varies with the rotor position due to the salient structure of the rotor.

Using the winding functions method, windings inductance matrices can be obtained which are positions dependent. Considering sinusoidal distribution, winding functions of the five phases can be expressed as:

$$N_a(\phi) = \frac{4}{\pi}\frac{N}{2}[\cos\phi] \tag{4-5}$$

$$N_b(\phi) = \frac{4}{\pi}\frac{N}{2}[\cos(\phi - \frac{2}{5}\pi)] \tag{4-6}$$

$$N_c(\phi) = \frac{4}{\pi}\frac{N}{2}[\cos(\phi - \frac{4}{5}\pi)] \tag{4-7}$$

$$N_d(\phi) = \frac{4}{\pi}\frac{N}{2}[\cos(\phi + \frac{4}{5}\pi)] \tag{4-8}$$

$$N_e(\phi) = \frac{4}{\pi}\frac{N}{2}[\cos(\phi + \frac{2}{5}\pi)] \tag{4-9}$$

Figure 4-1 represents the generalized type of a two-pole, five-phase synchronous motor which has both permanent magnet and magnetic saliency in the rotor.

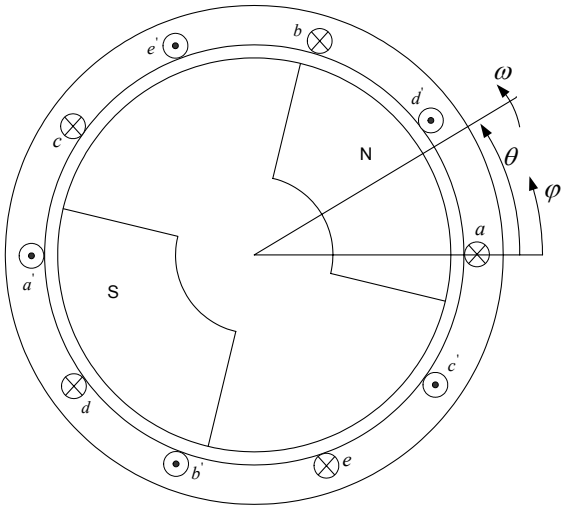

Figure 4-1 Generalized plan of a two-pole, five-phase IPM motor

For the ideal model of a two-pole five-phase IPM motor with salient pole rotor, the inverse of air gap function is also shown in Figure 4-2. θ is the rotor position.

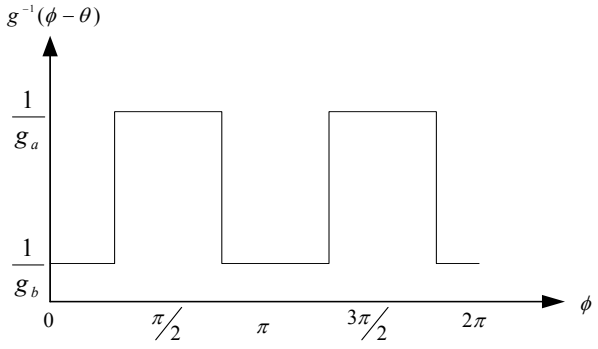

Figure 4-2 Inverse air gap function.

The Fourier's series of the inverse air gap function can be defined as:

$$g^{-1}(\phi-\theta)=c_1-c_2\cos 2(\phi-\theta) \tag{4-10}$$

where the constants are:

$$c_1=\frac{1}{2}(\frac{1}{g_a}+\frac{1}{g_b}) \tag{4-11}$$

$$c_2=\frac{2}{\pi}(\frac{1}{g_a}-\frac{1}{g_b}) \tag{4-12}$$

By employing the winding function method, phase "A" self inductance can be calculated as:

$$L_{AA}=\mu_0 rl\int_0^{2\pi}N_a^2(\phi)g^{-1}(\phi-\theta)d\phi+\mu_0 rl<n_a>\int_0^{2\pi}N_a(\phi)g^{-1}(\phi-\theta)d\phi \tag{4-13}$$

where μ_0 is the peameability of air, r is the inner radius of stator, and l is the stack length of rotor. Also:

$$<n_a>=N/2$$

where N is the number of turns per coil.

The five-phase self inductances are calculated as:

$$L_{AA}=K\{c_1-\frac{c_2}{2}[\cos 2\theta]\} \tag{4-14}$$

$$L_{BB}=K\{c_1-\frac{c_2}{2}[\cos 2(\theta-\frac{2\pi}{5})]\} \tag{4-15}$$

$$L_{CC}=K\{c_1-\frac{c_2}{2}[\cos 2(\theta-\frac{4\pi}{5})]\} \tag{4-16}$$

$$L_{DD} = K\{c_1 - \frac{c_2}{2}[\cos 2(\theta + \frac{4\pi}{5})]\} \tag{4-17}$$

$$L_{EE} = K\{c_1 - \frac{c_2}{2}[\cos 2(\theta + \frac{2\pi}{5})]\} \tag{4-18}$$

Here,

$$K = \mu_0 rl 4 * N^2 / \pi \tag{4-19}$$

Similarly, winding function is also employed to calculate the mutual inductances. Mutual inductance of phases "A" and "B" are calculated as:

$$L_{AB} = \mu_0 rl \int_0^{2\pi} N_A(\phi) N_B(\phi) g^{-1}(\phi - \theta) d\phi + \mu_0 rl < n_a > \int_0^{2\pi} N_B(\phi) g^{-1}(\phi - \theta) d\phi \tag{4-20}$$

$$L_{AB} = K\{c_1[\cos\frac{2\pi}{5}] - \frac{c_2}{2}[\cos 2(\theta + \frac{4\pi}{5})]\} \tag{4-21}$$

Similarly, all the other mutual inductances are:

$$L_{AC} = K\{c_1[\cos\frac{4\pi}{5}] - \frac{c_2}{2}[\cos 2(\theta - \frac{2\pi}{5})]\} \tag{4-22}$$

$$L_{AD} = K\{c_1[\cos\frac{6\pi}{5}] - \frac{c_2}{2}[\cos 2(\theta + \frac{2\pi}{5})]\} \tag{4-23}$$

$$L_{AE} = K\{c_1[\cos\frac{2\pi}{5}] - \frac{c_2}{2}[\cos 2(\theta - \frac{4\pi}{5})]\} \tag{4-24}$$

$$L_{BC} = K\{c_1[\cos\frac{2\pi}{5}] - \frac{c_2}{2}[\cos 2(\theta + \frac{2\pi}{5})]\} \tag{4-25}$$

$$L_{BD} = K\{c_1[\cos\frac{4\pi}{5}] - \frac{c_2}{2}[\cos 2(\theta - \frac{4\pi}{5})]\} \tag{4-26}$$

$$L_{BE} = K\{c_1[\cos\frac{4\pi}{5}] - \frac{c_2}{2}[\cos 2\theta]\} \tag{4-27}$$

$$L_{CD} = K\{c_1[\cos\frac{2\pi}{5}] - \frac{c_2}{2}[\cos 2\theta]\} \tag{4-28}$$

$$L_{CE} = K\{c_1[\cos\frac{4\pi}{5}] - \frac{c_2}{2}[\cos 2(\theta + \frac{4\pi}{5})]\} \tag{4-29}$$

$$L_{DE} = K\{c_1[\cos\frac{2\pi}{5}] - \frac{c_2}{2}[\cos 2(\theta - \frac{2\pi}{5})]\} \tag{4-30}$$

The self and mutual inductance matrix can be written as:

$$L(\theta) = \begin{bmatrix} L_{AA} & L_{AB} & L_{AC} & L_{AD} & L_{AE} \\ L_{AB} & L_{BB} & L_{BC} & L_{BD} & L_{BE} \\ L_{AC} & L_{BC} & L_{CC} & L_{CD} & L_{CE} \\ L_{AD} & L_{BD} & L_{CD} & L_{DD} & L_{DE} \\ L_{AE} & L_{BE} & L_{CE} & L_{DE} & L_{EE} \end{bmatrix}$$

$$Kc_1 \begin{bmatrix} 1 & \cos\frac{2\pi}{5} & \cos\frac{4\pi}{5} & \cos\frac{4\pi}{5} & \cos\frac{2\pi}{5} \\ \cos\frac{2\pi}{5} & 1 & \cos\frac{2\pi}{5} & \cos\frac{4\pi}{5} & \cos\frac{4\pi}{5} \\ \cos\frac{4\pi}{5} & \cos\frac{2\pi}{5} & 1 & \cos\frac{2\pi}{5} & \cos\frac{4\pi}{5} \\ \cos\frac{4\pi}{5} & \cos\frac{4\pi}{5} & \cos\frac{2\pi}{5} & 1 & \cos\frac{2\pi}{5} \\ \cos\frac{2\pi}{5} & \cos\frac{4\pi}{5} & \cos\frac{4\pi}{5} & \cos\frac{2\pi}{5} & 1 \end{bmatrix}$$

$$-\frac{Kc_2}{2} \begin{bmatrix} \cos 2\theta & 0 & 0 & 0 & 0 \\ 0 & \cos 2(\theta - \frac{2\pi}{5}) & 0 & 0 & 0 \\ & 0 & \cos 2(\theta - \frac{4\pi}{5}) & 0 & 0 \\ 0 & 0 & 0 & \cos 2(\theta + \frac{4\pi}{5}) & 0 \\ 0 & 0 & 0 & 0 & \cos 2(\theta + \frac{2\pi}{5}) \end{bmatrix}$$

$$-\frac{Kc_2}{2}\begin{bmatrix} 0 & \cos 2(\theta+\frac{4\pi}{5}) & \cos 2(\theta-\frac{2\pi}{5}) & \cos 2(\theta+\frac{2\pi}{5}) & \cos 2(\theta-\frac{4\pi}{5}) \\ \cos 2(\theta+\frac{4\pi}{5}) & 0 & \cos 2(\theta+\frac{2\pi}{5}) & \cos 2(\theta-\frac{4\pi}{5}) & \cos 2\theta \\ \cos 2(\theta-\frac{2\pi}{5}) & \cos 2(\theta+\frac{2\pi}{5}) & 0 & \cos 2\theta & \cos 2(\theta+\frac{4\pi}{5}) \\ \cos 2(\theta+\frac{2\pi}{5}) & \cos 2(\theta-\frac{4\pi}{5}) & \cos 2\theta & 0 & \cos 2(\theta-\frac{2\pi}{5}) \\ \cos 2(\theta-\frac{4\pi}{5}) & \cos 2\theta & \cos 2(\theta+\frac{4\pi}{5}) & \cos 2(\theta-\frac{2\pi}{5}) & 0 \end{bmatrix} \tag{4-31}$$

3. Stator Voltage and Flux Linkages in the Rotating Frame of Reference

For simplifying the model, an arbitrary coordinate transformation is introduced, that transfers the variables of the five-phase motor into a reference frame rotating at an arbitrary angular velocity. The transformation matrix for this system can be written as:

$$T(\theta)=\frac{2}{5}\begin{bmatrix} \cos\theta & \cos(\theta-\frac{2\pi}{5}) & \cos(\theta-\frac{4\pi}{5}) & \cos(\theta+\frac{4\pi}{5}) & \cos(\theta+\frac{2\pi}{5}) \\ \sin\theta & \sin(\theta-\frac{2\pi}{5}) & \sin(\theta-\frac{4\pi}{5}) & \sin(\theta+\frac{4\pi}{5}) & \sin(\theta+\frac{2\pi}{5}) \\ \cos\theta & \cos(\theta+\frac{4\pi}{5}) & \cos(\theta-\frac{2\pi}{5}) & \cos(\theta+\frac{2\pi}{5}) & \cos(\theta-\frac{4\pi}{5}) \\ \sin\theta & \sin(\theta+\frac{4\pi}{5}) & \sin(\theta-\frac{2\pi}{5}) & \sin(\theta+\frac{2\pi}{5}) & \sin(\theta-\frac{4\pi}{5}) \\ \frac{1}{\sqrt{2}} & \frac{1}{\sqrt{2}} & \frac{1}{\sqrt{2}} & \frac{1}{\sqrt{2}} & \frac{1}{\sqrt{2}} \end{bmatrix} \tag{4-32}$$

This transformation matrix has the following pseudo-orthogonal property:

$$T^{-1}(\theta)=\frac{5}{2}T^{t}(\theta) \tag{4-33}$$

where $T^{-1}(\theta)$ and $T^{t}(\theta)$ are the inverse and transpose matrices of $T(\theta)$, respectively.

Therefore, the inverse transformation matrix is:

$$T^{-1}(\theta)=\begin{bmatrix} \cos\theta & \sin\theta & \cos\theta & \sin\theta & \frac{1}{\sqrt{2}} \\ \cos(\theta-\frac{2\pi}{5}) & \sin(\theta-\frac{2\pi}{5}) & \cos(\theta+\frac{4\pi}{5}) & \sin(\theta+\frac{4\pi}{5}) & \frac{1}{\sqrt{2}} \\ \cos(\theta-\frac{4\pi}{5}) & \sin(\theta-\frac{4\pi}{5}) & \cos(\theta-\frac{2\pi}{5}) & \sin(\theta-\frac{2\pi}{5}) & \frac{1}{\sqrt{2}} \\ \cos(\theta+\frac{4\pi}{5}) & \sin(\theta+\frac{4\pi}{5}) & \cos(\theta+\frac{2\pi}{5}) & \sin(\theta+\frac{2\pi}{5}) & \frac{1}{\sqrt{2}} \\ \cos(\theta+\frac{2\pi}{5}) & \sin(\theta+\frac{2\pi}{5}) & \cos(\theta-\frac{4\pi}{5}) & \sin(\theta-\frac{4\pi}{5}) & \frac{1}{\sqrt{2}} \end{bmatrix} \tag{4-34}$$

Figure 4-3 shows the coordinate systems used for this study. (αβ) is the stationary two-phase reference frame. (dq) is the rotor flux reference frame and (xy) is the stator flux reference frame. Load angle δ is the angle between the stator and rotor flux linkages. During the steady states, δ is constant for a specific load torque. During transients δ varies and the rotational speed of the stator and rotor fluxes are different. By applying the above transformation to the stator inductance, voltages and flux linkages equations and torque, the following equations will be obtained in the synchronous rotating (q-d-z1-z2-z3) reference frame.

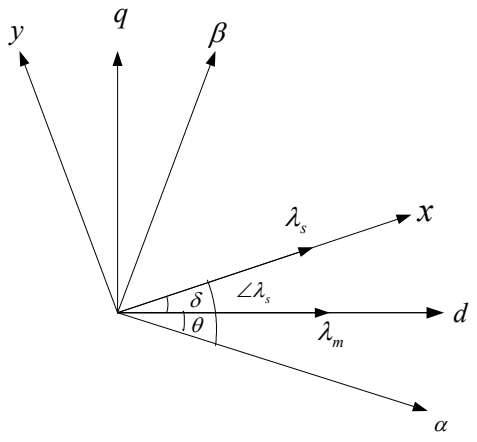

Figure 4-3 Stator and rotor flux linkages and different reference frames.

The stator inductance matrix is given by,

$$L_{qdz1z2z3} = \begin{bmatrix} L_q & 0 & 0 & 0 & 0 \\ 0 & L_d & 0 & 0 & 0 \\ 0 & 0 & L_{ls} & 0 & 0 \\ 0 & 0 & 0 & L_{ls} & 0 \\ 0 & 0 & 0 & 0 & L_{ls} \end{bmatrix} \tag{4-35}$$

The stator flux linkages equations are given by,

$$\lambda_{qs} = L_q i_{qs}$$

$$\lambda_{ds} = L_d\, i_{ds} + \lambda_m$$

$$\lambda_{z1s} = L_{ls}\, i_{z1s} \tag{4-36}$$

$$\lambda_{z2s} = L_{ls}\, i_{z2s}$$

$$\lambda_{z3s} = L_{ls}\, i_{z3s}$$

The stator terminal voltage equations are,

$$\begin{aligned} V_{qs} &= r_s i_{qs} + \omega\lambda_{ds} + \frac{d\lambda_{qs}}{dt} \\ V_{ds} &= r_s i_{ds} - \omega\lambda_{qs} + \frac{d\lambda_{ds}}{dt} \\ V_{z1s} &= r_s i_{z1s} + \frac{d\lambda_{z1s}}{dt} \\ V_{z2s} &= r_s i_{z2s} + \frac{d\lambda_{z2s}}{dt} \\ V_{z3s} &= r_s i_{z3s} + \frac{d\lambda_{z3s}}{dt} \end{aligned} \tag{4-37}$$

4. Electromagnetic Torque

The electromagnetic torque can be found using the well-known magnetic co-energy method as follows:

$$T_{em} = \frac{\partial W_{co}}{\partial \theta_r} \tag{4-38}$$

Therefore,

$$T_e = \frac{P}{4} I_S{}^t \frac{\partial L_{SS}}{\partial \theta} I_S + \frac{P}{2} I_s^T \frac{\partial \Lambda_m}{\partial \theta_r} \tag{4-39}$$

The above equation can be re-written as:

$$T_e = \frac{P}{4}[T(\theta) I_S]^t \frac{5}{2} T(\theta) \frac{\partial L_{SS}}{\partial \theta} T(\theta)^{-1} [T(\theta) I_S] + \frac{P}{2} (T(\theta_r)^{-1} i_{d1q1d3q30s})^t \frac{\partial \Lambda_m}{\partial \theta_r} \tag{4-40}$$

Based on the above two equations and the transformation matrix the electromagnetic torque can be obtained from,

$$T_{em} = \frac{P}{2}\frac{5}{2}(\lambda_m i_{qs} + (L_d - L_q) i_{ds} i_{qs}) \tag{4-41}$$

or,

$$T_{em} = \frac{5}{2}\frac{P}{2}[\frac{\lambda_m |\lambda_s| \sin\delta}{L_d} - \frac{|\lambda_s|^2 (L_d - L_q) \sin 2\delta}{2 L_d L_q}] \tag{4-42}$$

or,

$$T_{em} = \frac{5}{2}\frac{P}{2}\left(\lambda_{ds} i_{qs} - \lambda_{qs} i_{ds}\right) \tag{4-43}$$

where P is the number of poles and δ is the load angle.

The stator voltage and torque equations of the five-phase IPM can also be obtained in the stationary reference frame and are as follows:

$$\begin{aligned} v_\alpha &= r_s i_\alpha + \frac{d\lambda_\alpha}{dt} \\ v_\beta &= r_s i_\beta + \frac{d\lambda_\beta}{dt} \end{aligned} \tag{4-44}$$

where,

$$\lambda_{\alpha} = L_{\alpha}(\theta) i_{\alpha} + \lambda_m \cos(\theta)$$
$$\lambda_{\beta} = L_{\beta}(\theta) i_{\beta} + \lambda_m \sin(\theta) \quad (4\text{-}45)$$

Therefore, the torque equation will be:

$$T_{em} = \frac{5}{2}\frac{P}{2}(\lambda_{\alpha} i_{\beta} - \lambda_{\beta} i_{\alpha}) \quad (4\text{-}46)$$

D. Speed Sensorless Direct Torque Control of Five-Phase IPM Motor Drives

In this part speed sensorless direct torque control of five-phase IPM motor drives is discussed. As mentioned earlier, high torque and flux ripple are major drawbacks of DTC system. A five phase system has more space voltage vectors compared to a three-phase system. Therefore better adjustment of flux and torque is possible.

1. Switching States

In the five-phase inverter shown in Figure 4-4, each leg switching function, that is called S_a, S_b, S_c, S_d, S_e, can take either 1 or 0 value based on the state of the upper or lower switch. If the upper switch is on then the switching function assumes a value of 1, else 0.

Thirty-two switching combinations can be considered for a five-phase inverter with different amplitudes as shown in Table 4-1 and 4-2. They consist of two zero voltage vectors and thirty non-zero space voltage vectors as shown in figure 4-5.

The 32 space voltage vectors are composed of three sets of different amplitude vectors, and divide the switching plane pattern into 10 sectors as shown in Figure 4-6. Each sector is $\pi/5$ radian. The ratio of the amplitudes of the voltage vectors is

$1:1.618:1.618^2$ from the smallest one to the largest one, respectively. However, it is clear that only one switching is needed from one vector to either of the two nearby vectors for the largest decagon, as shown in Figure 4-5. Therefore, for minimizing the switching loss it is better to use this decagon. The other two decagons are being used when finer adjustment of the stator flux and torque are needed.

Position information of the stator flux linkages space vector is needed to define the required sector. The proper voltage vector should be applied based on the stator flux and torque errors with respect to their reference values.

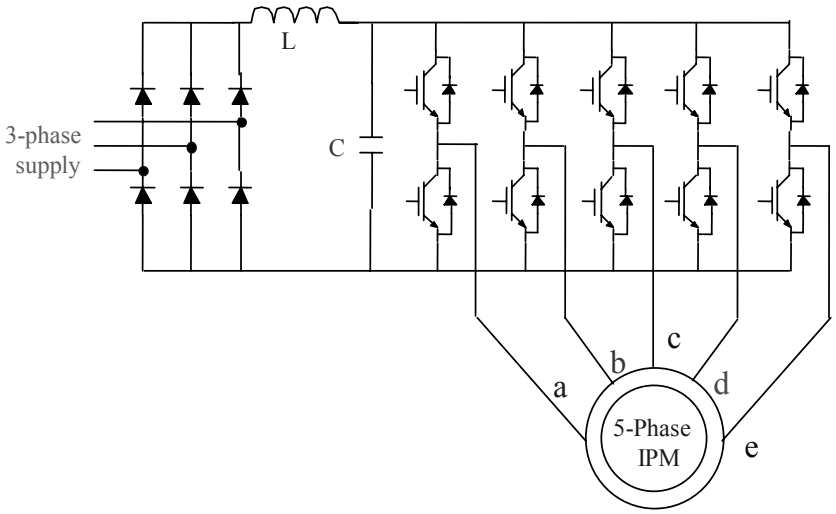

Figure 4-4 Five-phase PWM inverter.

Table 4-1. Switching states

	S_e	S_d	S_c	S_b	S_a
0	0	0	0	0	0
1	0	0	0	0	1
2	0	0	0	1	0
3	0	0	0	1	1
4	0	0	1	0	0
5	0	0	1	0	1
6	0	0	1	1	0
7	0	0	1	1	1
8	0	1	0	0	0
9	0	1	0	0	1
10	0	1	0	1	0
11	0	1	0	1	1
12	0	1	1	0	0
13	0	1	1	0	1
14	0	1	1	1	0
15	0	1	1	1	1
16	1	0	0	0	0
17	1	0	0	0	1
18	1	0	0	1	0
19	1	0	0	1	1
20	1	0	1	0	0
21	1	0	1	0	1
22	1	0	1	1	0
23	1	0	1	1	1
24	1	1	0	0	0
25	1	1	0	0	1
26	1	1	0	1	0
27	1	1	0	1	1
28	1	1	1	0	0
29	1	1	1	0	1
30	1	1	1	1	0
31	1	1	1	1	1

Table 4-2. Voltage vectors

	V_e	V_d	V_c	V_b	V_a	V
0	0	0	0	0	0	0
1	-1/5	-1/5	-1/5	-1/5	4/5	$0.4\angle 0$
2	-1/5	-1/5	-1/5	4/5	-1/5	$0.4\angle 2\pi/5$
3	-2/5	-2/5	-2/5	3/5	3/5	$0.647\angle \pi/5$
4	-1/5	-1/5	4/5	-1/5	-1/5	$0.4\angle 4\pi/5$
5	-2/5	-2/5	3/5	-2/5	3/5	$0.247\angle 2\pi/5$
6	-2/5	-2/5	3/5	3/5	-2/5	$0.647\angle 3\pi/5$
7	-3/5	-3/5	2/5	2/5	2/5	$0.647\angle 2\pi/5$
8	-1/5	4/5	-1/5	-1/5	-1/5	$0.4\angle -4\pi/5$
9	-2/5	3/5	-2/5	-2/5	3/5	$0.247\angle -2\pi/5$
10	-2/5	3/5	-2/5	3/5	-2/5	$0.247\angle 4\pi/5$
11	-3/5	2/5	-3/5	2/5	2/5	$0.247\angle \pi/5$
12	-2/5	3/5	3/5	-2/5	-2/5	$0.647\angle \pi$
13	-3/5	2/5	2/5	-3/5	2/5	$0.247\angle \pi$
14	-3/5	2/5	2/5	2/5	-3/5	$0.647\angle 4\pi/5$
15	-4/5	1/5	1/5	1/5	1/5	$0.4\angle 3\pi/5$
16	4/5	-1/5	-1/5	-1/5	-1/5	$0.4\angle -2\pi/5$
17	3/5	-2/5	-2/5	-2/5	3/5	$0.647\angle -\pi/5$
18	3/5	-2/5	-2/5	3/5	-2/5	$0.247\angle 0$
19	2/5	-3/5	-3/5	2/5	2/5	$0.647\angle 0$
20	3/5	-2/5	3/5	-2/5	-2/5	$0.247\angle -4\pi/5$
21	2/5	-3/5	2/5	-3/5	2/5	$0.247\angle -\pi/5$
22	2/5	-3/5	2/5	2/5	-3/5	$0.247\angle 3\pi/5$
23	1/5	-4/5	1/5	1/5	1/5	$0.4\angle \pi/5$
24	3/5	3/5	-2/5	-2/5	-2/5	$0.647\angle -3\pi/5$
25	2/5	2/5	-3/5	-3/5	2/5	$0.647\angle -2\pi/5$
26	2/5	2/5	-3/5	2/5	-3/5	$0.247\angle -3\pi/5$
27	1/5	1/5	-4/5	1/5	1/5	$0.4\angle -\pi/5$
28	2/5	2/5	2/5	-3/5	-3/5	$0.647\angle -4\pi/5$
29	1/5	1/5	1/5	-4/5	1/5	$0.4\angle -3\pi/5$
30	1/5	1/5	1/5	1/5	-4/5	$0.4\angle \pi$
31	1	1	1	1	1	0

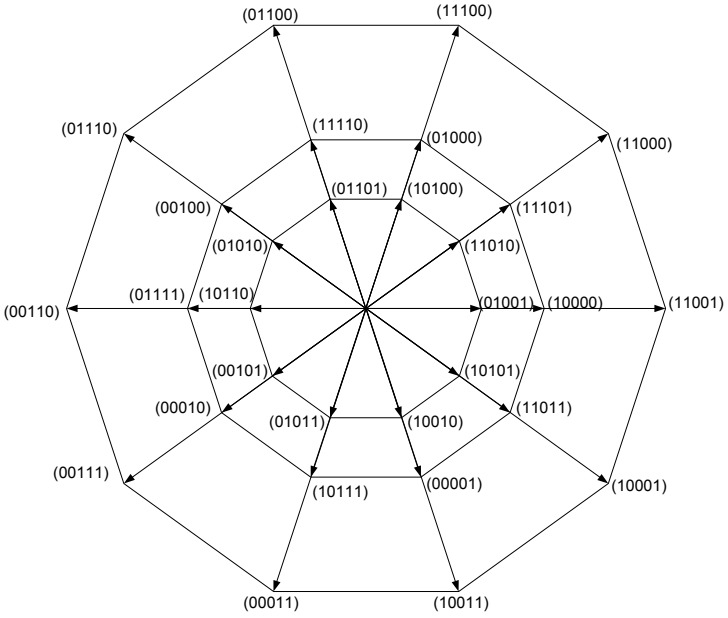

Figure 4-5 Thirty non-zero switching states for the five-phase interior permanent magnet motor drive.

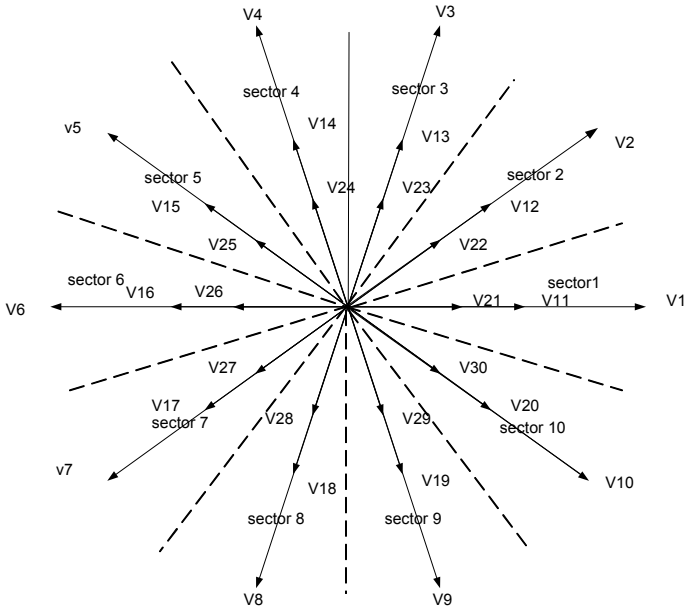

Figure 4-6 Thirty non-zero switching vectors and 10 sectors.

For example, suppose that the stator flux linkages vector is in the first sector (Figure 4-6) and only the large decagon is considered. Now, if the flux has to be increased (FI) and the electromagnetic torque has to be positive (TP), then the switching voltage vector to be selected is *V2*. On the other hand, if the stator flux linkages have to be increased (FI) and the electromagnetic torque needs to be negative (TN), then vector *V10* has to be selected. However, if the stator flux linkages has to be decreased (FD) and the electromagnetic torque needs to be positive (TP), vector *V5* is going to be selected. Similarly, if the stator flux linkages has to be decreased (FD) and the electromagnetic torque has to be negative (TN), vector *V7* is going to be applied. The voltage vectors located on the other two decagons have similar effects with respect to the larger decagon.

Based on the above, the increased number of space voltage vectors allows the generation of a more elaborate switching vector table in which the selection of the voltage vectors is made according to real-time variation of the stator flux and torque. Moreover, the different amplitudes of voltage vectors provide increased possibility to minimize the ripple in the stator flux and torque. Table 4-3 shows the optimum switching voltage vector look-up table. In this table, $d\psi = 1$ stands for FI, $d\psi = -1$ for FD, $dT_e = 1$ for TP, and $dT_e = -1$ for TN.

2. Calculating the Torque and Flux

Direct torque control of the five-phase IPM motor is being achieved based on the phase currents and the dc bus voltage measurements. According to (4-44), the stator flux linkages in the stationary reference frame can be obtained as:

Table 4-3. Optimum active voltage vector look-up table.

$d\psi$	dt_e	Sector 1	Sector 2	Sector 3	Sector 4	Sector 5	Sector 6	Sector 7	Sector 8	Sector 9	Sector 10
1	1	V2, V12, V22	V3, V13, V23	V4, V14, V24	V5, V15, V25	V6, V16, V26	V7, V17, V27	V8, V18, V28	V9, V19, V29	V10, V20, V30	V1, V11, V21
1	-1	V10, V20, V30	V1, V11, V21	V2, V12, V22	V3, V13, V23	V4, V14, V24	V5, V15, V25	V6, V16, V26	V7, V17, V27	V8, V18, V28	V9, V19, V29
-1	1	V5, V15, V25	V6, V16, V26	V7, V17, V27	V8, V18, V28	V9, V19, V29	V10, V20, V30	V1, V11, V21	V2, V12, V22	V3, V13, V23	V4, V14, V24
-1	-1	V7, V17, V27	V8, V18, V28	V9, V19, V29	V10, V20, V30	V1, V11, V21	V2, V12, V22	V3, V13, V23	V4, V14, V24	V5, V15, V25	V6, V16, V26

$$\lambda_\alpha = \int (v_\alpha - r_s i_\alpha) dt \tag{4-47}$$

$$\lambda_\beta = \int (v_\beta - r_s i_\beta) dt \tag{4-48}$$

where:

$$v_\alpha = \mathrm{Re}\left\{ \frac{2}{5} V_d \left[S_a + S_b e^{j\frac{2\pi}{5}} + S_c e^{j\frac{4\pi}{5}} + S_d e^{-j\frac{4\pi}{5}} + S_e e^{-j\frac{2\pi}{5}} \right] \right\} \tag{4-49}$$

and

$$v_\beta = \mathrm{Im}\left\{ \frac{2}{5} V_d \left[S_a + S_b e^{j\frac{2\pi}{5}} + S_c e^{j\frac{4\pi}{5}} + S_d e^{-j\frac{4\pi}{5}} + S_e e^{-j\frac{2\pi}{5}} \right] \right\} \tag{4-50}$$

Stator flux linkage is defined by its magnitude and position as:

$$\lambda_s = |\lambda_s| \prec \lambda_s \quad , \tag{4-50}$$

where

$$|\lambda_s| = \sqrt{\lambda_\alpha^2 + \lambda_\beta^2} \quad , \quad \prec \lambda_s = \tan^{-1} \frac{\lambda_\beta}{\lambda_\alpha} \tag{4-51}$$

The electromagnetic torque as derived in (4-46) is given by,

$$T_{em} = \frac{5}{2}\frac{P}{2}(\lambda_\alpha i_\beta - \lambda_\beta i_\alpha) \quad (4\text{-}52)$$

3. Speed and Position Estimations

Using a position sensor to obtain speed and position information will cancel one of the main advantages of the DTC scheme which is eliminating the position sensor and increases the cost, reduces the reliability and increases the number of connection between the motor and control interface. Therefore, it is of great importance to have a DTC drive with soft position sensor.

Techniques for sensorless control of IPM motors are based on five main categories:

- inductance variations
- flux estimators
- high frequency injection
- back-EMF detection
- state observers

Also, combinations of two different methods during low speed and high speed operations has been reported for IPM motor drives. Some of the methods indicated above, have been employed on three-phase permanent magnet motors DTC systems [60-62]. It seems that calculating position information and speed through flux estimators is easier to implement and less parameter dependent.

As mentioned earlier the electromagnetic torque can be also given by (4-42). Calculating the torque from (4-52), the load angle δ can be obtained from (4-42), and therefore the rotor position will be,

$$\theta = \prec \lambda_s - \delta \tag{4-53}$$

The rotor angular speed can be calculated as:

$$\omega = \frac{d\theta}{dt} = \frac{d\langle \lambda_s}{dt} - \frac{d\delta}{dt} = \omega_{ms} - \omega_d \tag{4-54}$$

where ω_{ms} is the speed of the stator flux linkages vector relative to the stator and ω_d is its speed relative to the rotor. In steady state condition, ω_d is equal to zero. If the rate of change of the torque is small, ω_d will be negligible. The calculated speed based on (4-54) should be filtered.

Figure 4-7 shows the block diagram of the five-phase DTC system. This system consists of three basic functions. They are: the IPM model which estimates the actual torque, stator flux linkages and shaft speed, the two level hysteresis controllers in which the torque and flux references are compared with the actual quantities calculated in the motor model, and the optimal switching logic which translates the controller outputs into the appropriate commands for the power switching devices.

E. Simulation and Experimental Results

Simulations have been performed in Matlab/Simulink to verify the feasibility of speed sensorless direct torque control of five-phase interior permanent magnet motor. Simulation has been accomplished for various cases without and with a speed loop. Figure 4-8 shows the torque response of the IPM motor to the frequent step change of command torque. Figure 4-9 shows the torque response under no load condition and triangular reference speed.

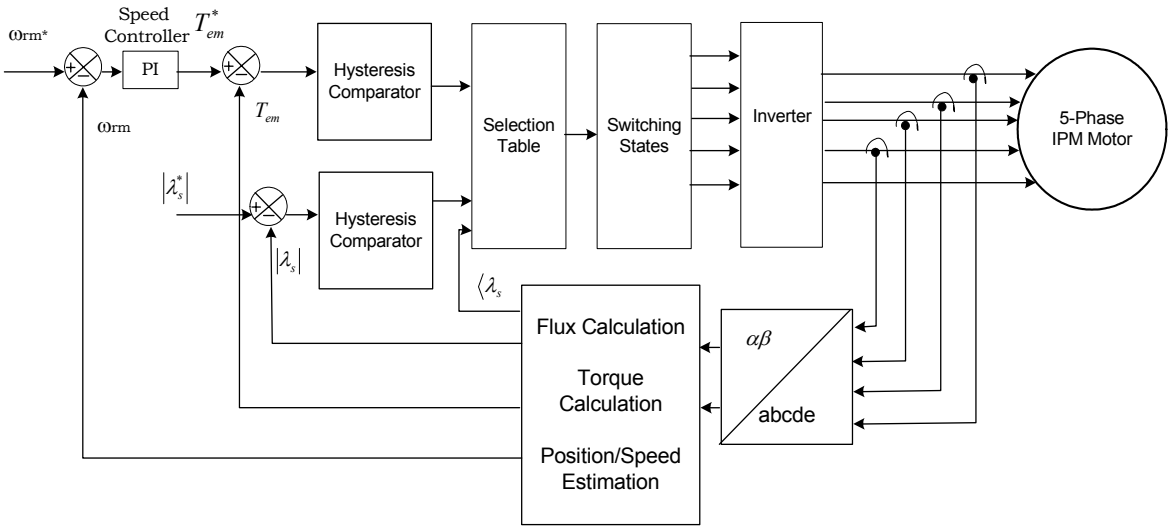

Figure 4-7 Block diagram of five-phase DTC system.

Figure 4-10 shows the simulation results, when the command speed ramps up, reaches steady state, slows down and reverses the direction under load and load removal. Figure 4-11 shows the stator flux in the stationary reference frame for this case. It is therefore understood that the five-phase DTC system provides fast torque response and fast speed reversing operation. As it is clear from the figure 4-11, the stator flux follows a predetermined path and as expected the trajectory of stator flux linkages in the stationary reference frame is a circle. Figure 4-12 shows the actual and estimated motor speed based on the stator flux position and load angle. From the figure, the actual and estimated speeds agree well with each other.

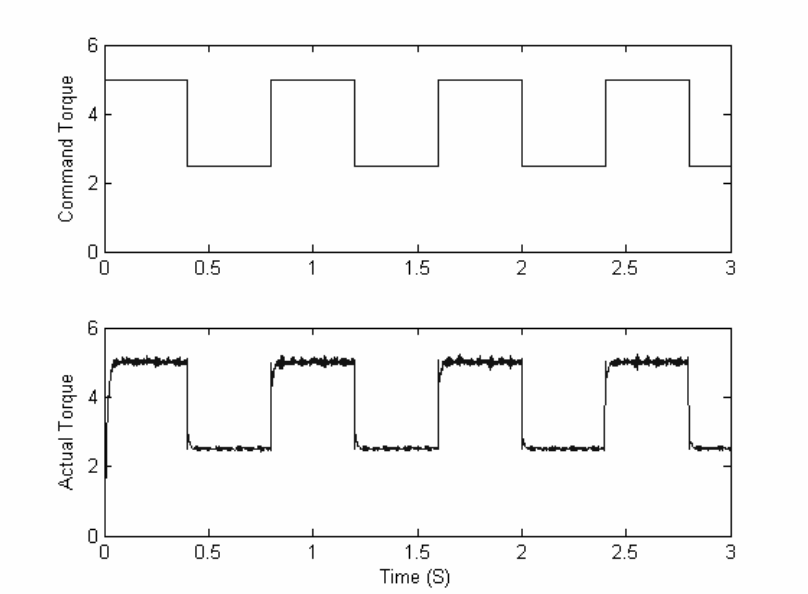

Figure 4-8 Command torque and actual torque.

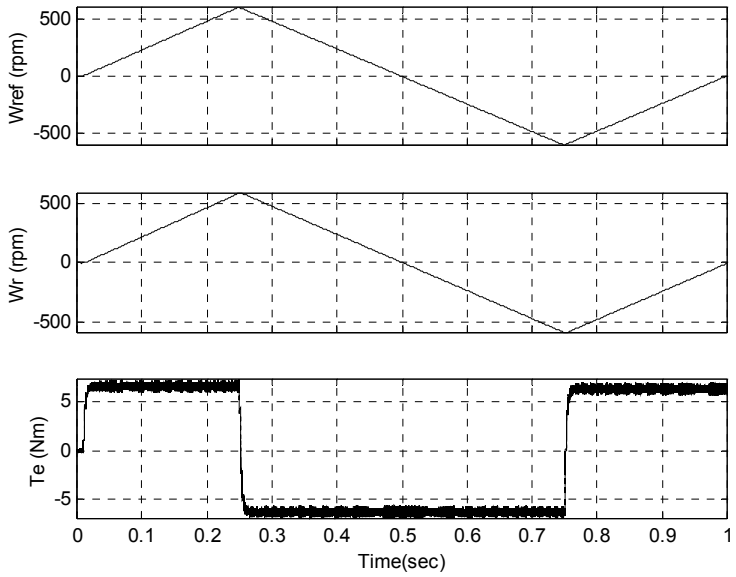

Figure 4-9 Command speed, estimated shaft speed and developed torque under no load condition.

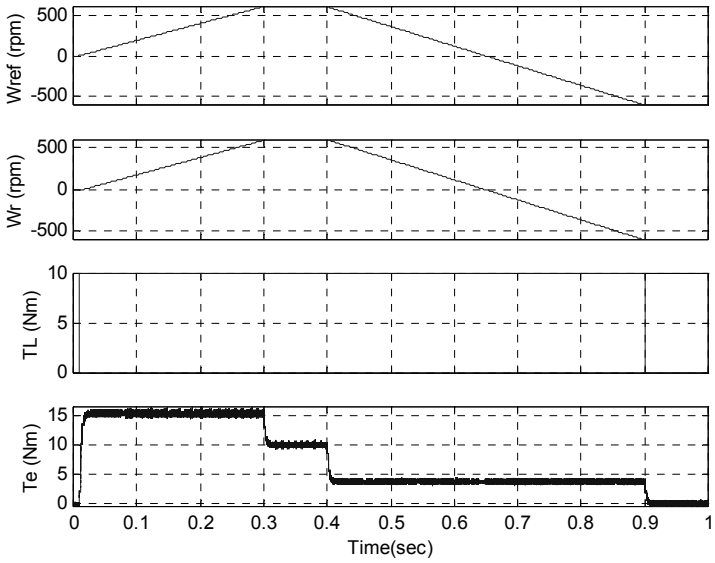

Figure 4-10 From top to bottom: reference speed, shaft speed, load torque and the electromagnetic torque.

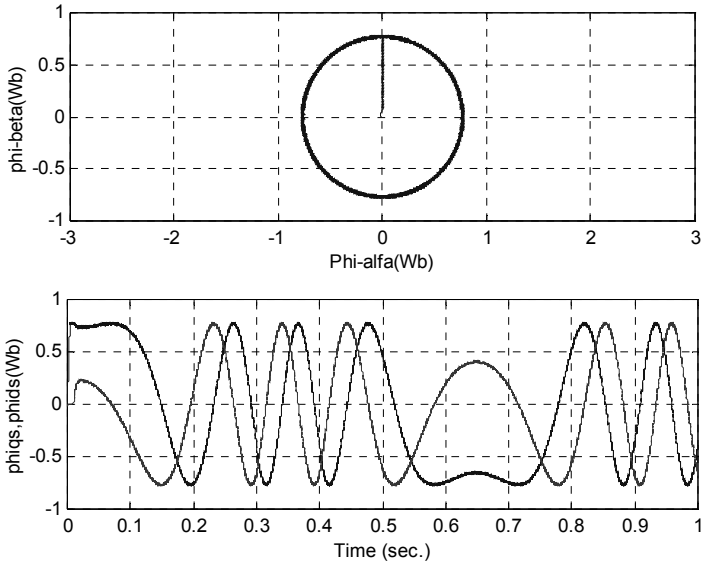

Figure 4-11 From top to bottom: α- and β-axes stator fluxes versus each other and versus time.

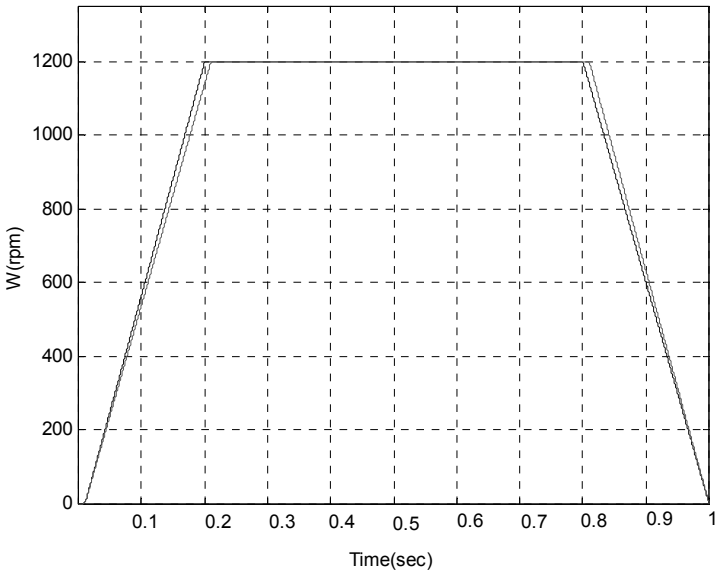

Figure 4-12 Shaft estimated and actual speed.

A five-phase IPM motor and a five-leg IGBT-based inverter were designed and fabricated in the lab. Table 4-4 shows the motor parameters. Figure 4-13 shows the cross section of the five-phase IPM motor with 15 stator slots. There are 3 coils for each phase. The magnets are Nd-Fe-Br. Figure 4-14 shows the experimental setup.

The control algorithm is being implemented on the TMS320C32 digital signal processor board. The dc bus voltage of the inverter and four phase currents are monitored through voltage isolator device and four current sensors and are fed to the analog-to-digital (ADC) channels for calculating the developed torque and stator flux. Figure 4-15 shows the calculated flux in the stationary reference frame. Figure 4-16 shows the α-axis flux versus β-axis flux that is a circle. Figure 4-17 shows the estimated position and estimated speed during steady state and in the speed of 1200 rpm.

Figure 4-18 shows the estimated and actual speed as the motor speeds up and reaches its steady state value, as it is clear from the figure estimated speed and actual speed agree well with each other.

Table 4-4. Motor parameters.

d-axis inductance	0.180 mH
q-axis inductance	0.420 mH
Stator resistance	0.7Ω
Rated voltage	120V
Rated power	3KW
Number of poles	4

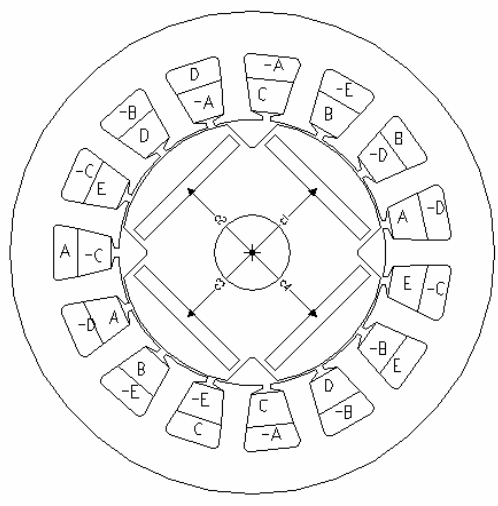

Figure 4-13 Cross section of five-phase IPM motor.

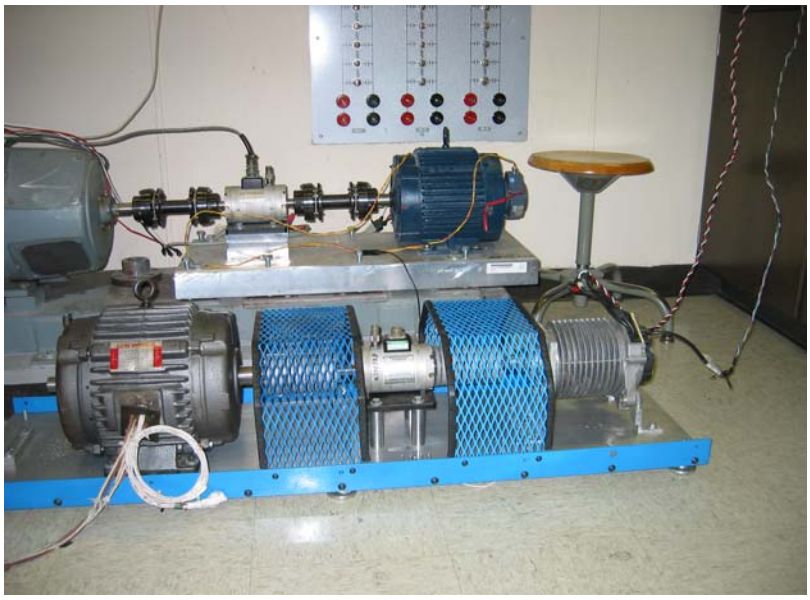

Figure 4-14 Experimental set up.

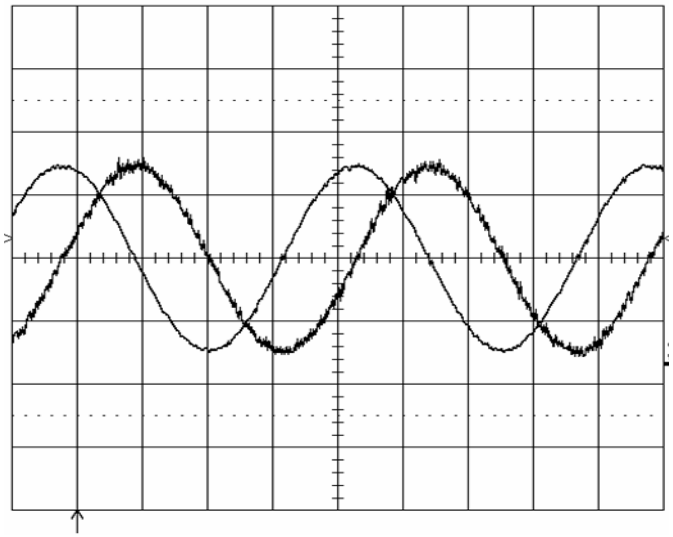

Figure 4-15 Stator flux linkages in the stationary frame. t: 5 ms/div , flux: 0.6 Wb/div

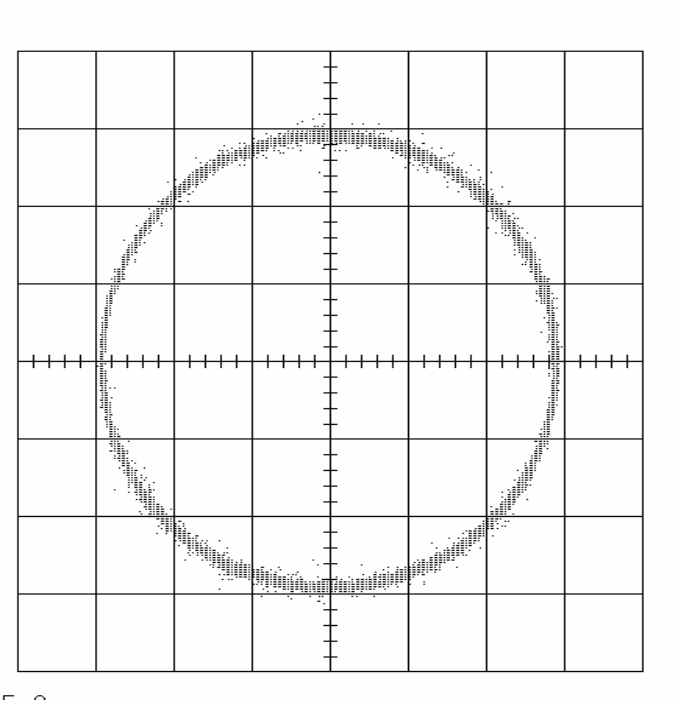

Figure 4-16 α -axis flux versus β -axis flux. flux: 0.3 Wb/div

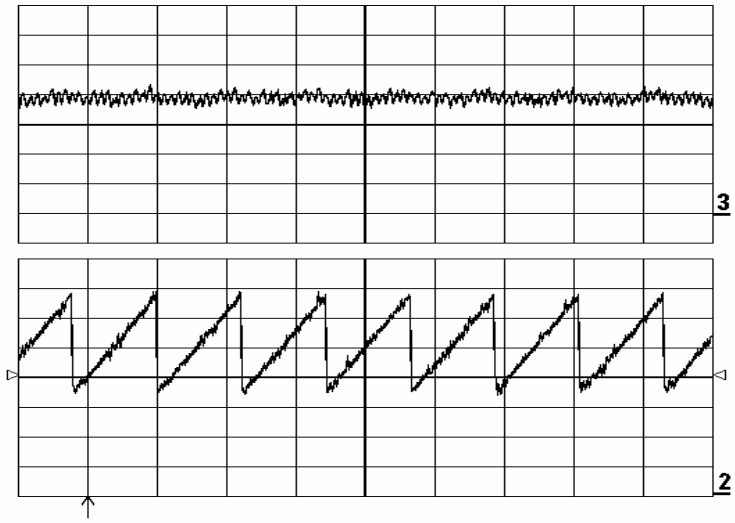

Figure 4-17 Estimated speed and position during steady state. t: 20ms/div, speed: 300 rpm/div

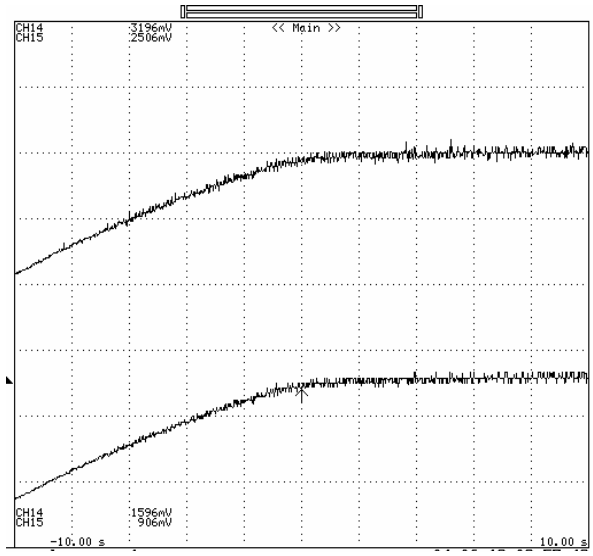

Figure 4-18 Estimated speed and actual speed when the motor speeds up and reaches steady state.

F. Conclusions

In this chapter, the speed sensorless DTC was developed for a five-phase interior permanent magnet motor based on the phase currents and the dc bus voltage measurements. First, the mathematical models governing the operation of five-phase IPM motor in the rotating and stationary reference frames were given. Then, the direct torque control of the motor was developed. Position information and speed were estimated based on the stator flux position and the load angle. Therefore, the developed DTC system works based on the stator current and dc bus voltage measurements. Due to the better flexibility offered by the 32 voltage vectors, better control of the stator flux and torque is achievable. Simulation and experimental results were included to verify the feasibility of the five-phase DTC system for IPM motor.

CHAPTER V

CONCLUSIONS AND FUTURE RESEARCH WORK

A. Conclusions

Five-phase motors are a viable alternative for three-phase motors. They have several advantages such as reducing the current per phase without increasing the voltage per phase, lowering the DC link harmonic, higher torque density, reducing the amplitude and increasing the frequency of torque pulsation and better reliability. Due to their additional degrees of freedom, these motors provide some other unique characteristics to the drive designer.

BLDC motors are known to have higher toque density compared to PMSM at low and medium speeds. However, PMSM have better controllability over a wider speed range because of the compatibility with vector control. In Chapter II, additional degrees of freedom in multi-phase machine have been used to inject higher order harmonics of current and enhance the torque producing capability of the machine. Third harmonic of current have been injected in a five-phase permanent magnet machine with quasi-rectangular back-EMF. From torque density point of view, the proposed drive approximates the behavior of a permanent magnet brushless DC machine. Harmonic effects on the three and five-phase motors were investigated based on the Fourier analysis of corresponding winding functions and excitation currents. It has been shown that time and space harmonics of the same order will contribute positively to the output

torque. For modeling and analysis of the motor a $d_1q_1d_3q_30$ frame of reference has been defined where d_1q_1 rotates at synchronous speed and d_3q_3 rotates at the three times synchronous speed. Fundamental and third harmonic components will be the DC values in this new frame of reference. Vector control is easily applicable to this motor. Therefore, the drive benefits from controllability of PMSM configuration while having the same torque density of the BLDC drives. Finite element analysis has been used to show the superior torque producing capability of the proposed motor over its three and five-phase PMSM counterparts. In this analysis, the number of turns and slots widths have been adjusted to maintain almost same copper and iron losses in all the configurations. The finite element analysis also showed that this motor has the same torque producing capability of a BLDC. Dynamic simulation results in Matlab/Simulink show the good performance of the vector control applied to this motor. A 7.5 hp surface mount permanent magnet motor with magnet type of Nd-Fe-Br and concentrated winding has been built in the laboratory. The produced back-EMF of the motor is quasi-rectangular. Five-leg IGBT-based inverter is used to drive the motor. The control algorithm has been implemented on TMS320C32 digital signal processor. Experimental results are in good agreement with the results obtained from the finite element method. Also, from the experimental results, it is clear that the vector control can be efficiently implemented on this drive.

For a three-phase motor to continue operating safely in case of loss of one phase a divided DC bus and a neutral connection is needed. However, multi-phase motors are inherently fault tolerant. In chapter III, considering that degraded performance is better

than no performance, a control strategy is introduced which allows the motor running if up to two phases are open. The algorithm is based on keeping the stator MMF unchanged at faulty condition. This is possible by adjusting the currents in remaining healthy phases. The motor will continue operating safely under loss of up to two phases without any additional hardware and just by modifying the control algorithm. Speed and load adjustment should be considered to avoid large currents flowing in the motor phases. This feature will increase the reliability of the five-phase permanent magnet motor and is of major importance in some applications such as electric/hybrid electric vehicles and ship propulsion.

In chapter IV, the direct torque control (DTC) was implemented on the five phase interior permanent magnet motor. DTC scheme has some potential advantages such as lesser parameter dependency and easier implementation of field weakening regime. The latter is because the stator flux linkages are being controlled directly in a DTC system. By using the introduced technique fast torque response with low ripple in the stator flux and torque of the five-phase interior permanent magnet motor can be achieved. The five-phase DTC system has thirty-two space voltage vectors containing thirty non-zero and two zero vectors. Theses vectors divide the plane into ten sectors. Due to more flexibility in selecting the inverter switching states, the stator flux and torque can better be adjusted. There is no need for a position speed sensor for the introduced DTC method. Position information and speed are being estimated based on the position of the stator flux linkages and load angle. The mathematical model of the five-phase interior permanent magnet motor was first derived. Later, the speed sensorless direct torque

control method of the five-phase IPM was discussed. A five-phase interior permanent magnet motor was designed and built in the laboratory. The control method was implemented on a TMS320C32 digital signal processor board. The feasibility and effectiveness of five-phase DTC system was verified through simulation and experiments.

B. Suggestions for Further Research

1. Designing a five-phase permanent magnet motor against short circuit faults is proposed as the future research work to increase the reliability of the five-phase system. In this work, proper algorithms were proposed such that the motor continues operating safely in case of open phase condition. Another major fault that happens within a drive quite frequently is the short circuit within the machine windings or power device. Special design consideration should be taken into account in order for the motor to be protected against short circuit faults. Also, optimal control strategies will be needed to avoid excessive torque pulsations after one phase or power device is shorted.

2. Estimating the position and speed information is suggested for the high torque density five-phase PM motor discussed in chapter II. This feature will provide fault tolerance to the drive against position sensor failure. On the other hand, using a position sensor increases the cost, reduces the reliability and increases the number of connection between the motor and control interface. By properly estimating the speed and position information of the five-phase system discussed in chapter II, position sensor can be eliminated.

3. Since the stator flux linkages are being controlled directly in a DTC system, implementation of field weakening regime will be much easier. On the other hand, interior permanent magnet motors are good candidates for high speed operations due to their robust structure. Based on the above, field weakening and high speed operation of the direct torque controlled five-phase interior permanent magnet motor is suggested as the future work.

REFERENCES

[1] P. Pillay and R. Krishnan, " Modeling, simulation, and analysis of permanent-magnet motor drives. I. The permanent-magnet synchronous motor drive," *IEEE Transactions on Industry Applications*, vol. 25, pp. 265 – 273, Mar./Apr. 1989.

[2] P. Pillay and R. Krishnan, " Modeling, simulation, and analysis of permanent-magnet motor drives. II. The brushless DC motor drive ," *IEEE Transactions on Industry Applications*, vol. 25, pp. 274 -279, Mar./Apr. 1989.

[3] T. M. Jahns, "Motion control with permanent-magnet AC machines" *Proceedings of the IEEE*, vol. 82, pp. 1241-1252, Aug. 1994.

[4] J. Dente, "Induction motor current source inverter systems with phase number greater than 3", in *Proceedings of First European Conference on Power Electronics and Applications,* Brussels, Oct. 1985, pp. 3.143-3.147.

[5] P. Ferraris, M. Lazzari and F. Profumo, "Phase number of inverter-fed induction motors: effects of the DC link harmonics contents", in *Proceedings of First European Conference on Power Electronics and Applications,* Brussels, Oct. 1985, pp.3.95-3.102.

[6] E. E Ward and H. Harrer, "Preliminary of an inverter fed 5-Phase induction motor", *Proeedings of Inst. Elect. Eng.,* vol.116, pp. 980-984, Jun. 1969.

[7] R. H. Nelson and P.C. Krause, "Induction machine analysis for arbitrary displacement between multiple windings," *IEEE Transactions on Power Apparatus and Systems*, vol. 93, pp. 841-848, May 1974.

[8] E. Andersen and K. Bieniek, "Six-phase induction motors for current source inverter drives", in *Conference Record of IEEE-IAS Annual Meeting,* Rome, Italy, Oct. 1981, pp. 607-618.

[9] K. Gopakumar, B. E. Sathiakumar, M. E. Biswas and J. Vithayathil, "Modified current source inverter fed induction motor drive with reduced torque pulsations", *Proceedings of Inst. Elect. Eng.,* vol.131, pt. B, pp. 159-164, Jul. 1984.

[10] E. A. Klingshirn, "High phase order induction motors-part I: Description and theoretical considerations", *IEEE Transactions on Power Apparatus and Systems,* vol. PAS-102, pp.47-53, Jan. 1983.

[11] E. A. Klingshirn, "High phase order induction motors-part II: Experimental results", *IEEE Transactions on Power Apparatus and Systems,* vol. PAS-102, pp. 54-60, Jan. 1983.

[12] M. A. Abbas, R. Christen and T. M. Jahns, "Six-Phase Voltage Source Inverter Driven Induction Motor", *IEEE Tranactions on. Industry Applicaions.,* vol. IA-20, pp. 1251-1259, Sept./Oct. 1984.

[13] K. N. Pavithran, R. Parimelalagan, and M. Krishnamurthy, "Studies on inverter-fed five-phase induction motor drive", *IEEE Transactions on. Power Electronics,* vol. 3, pp. 224-235, Apr. 1988.

[14] J. G. Dente, "Squirrel-cage induction motor with electronic commutation", in *Proceedings of International Conference on Evolution and Modern Aspect of Induction Machines,* Torino, Italy, Jul. 8-11, 1986, pp.596-599.

[15] D. F. Gosden, "An inverter-fed squirrel cage induction motor with quasi-rectangular flux distribution", in *Proceedings of Electric Energy Conference,* Adelaide, Australia, Oct. 1987, pp. 240-245.

[16] A. R. Munoz and T. A. Lipo, " Dual stator winding induction machine drive," *IEEE Transactions on Industry Applications*, vol. 36, pp. 1369-1379, Sept 2000.

[17] K. Gopakumar, T. Ranganathan, and S. R. Bhat, "Split-phase induction motor operation from PWM voltage source inverter,' *IEEE Transaction on Industry Applications*, vol. 29, pp. 927-932, Sept 1993.

[18] A. R. Bakhshai, G. Joos, and H. Jin, "Space vector pwm control of split-phase induction machine using the vector classification technique," in *Proceedings of Applied Power Electronics Conference and Exposition*, Anaheim, CA, Feb. 1998, vol. 2, pp. 802-808.

[19] L. Xu and L. Ye, "Analysis of a novel stator winding structure minimizing harmonic current and torque ripple for dual six-step converter-fed high power ac machines," *IEEE Transactions on Industry Applications*, vol. 31, pp. 84-90, Jan 1995.

[20] J. C. Salmon and B. W. Williams, "A split-wound induction motor design to improve the reliability of PWM inverter," *IEEE Transactions on Industry Applications*, vol. 26, pp. 143-150, Jan. 1990.

[21] O. Ojo and I. E. Davidson, " PWM-VSI inverter-assisted stand-alone dual stator winding induction generator," *IEEE Transactions on Industry applications*, vol. 36, pp. 1604-1611, Nov. 2000.

[22] M. S. Miranda, R. Lyra, and S. R. Silva, "An alternative isolated wind electric pumping system using induction machines," *IEEE Transactions on Energy Conversion*, vol 14, pp. 1611-1616, Dec. 1999.

[23] I. Tamrakar and O.P. Malik, "Power factor correction of induction motors using pwm inverter fed auxiliary," *IEEE Transactions on Energy Conversion*, vol. 14, pp. 426-432, Sept 1999.

[24] H. A. Toliyat, T. A. Lipo and J. White, "Analysis of a concentrated winding induction machine for adjustable speed drive applications-part II (machine design and performance)", *IEEE Transactions on Energy Conversion,* vol. 6, pp. 684-692, Dec. 1991.

[25] H. A. Toliyat, *Analysis of Concentrated Winding Induction and Reluctance Machines for Adjustable Speed Drive Application*, Ph.D. dissertation, University of Wisconsin – Madison, 1991

[26] H. A. Toliyat, L. Xu and T. A. Lipo, "A five phase reluctance machine with high specific torque", *IEEE Transactions on Industry Applications,* vol. 28, pp. 659-667, May/Jun. 1992.

[27] H. A. Toliyat, P. Waikar and T. A. Lipo, "Analysis and simulation of five phase synchronous reluctance machines including third harmonic of air-gap MMF", *IEEE Transactions on Industry Application,* vol. 34, pp. 332-339, Mar./Apr. 1998.

[28] H. A. Toliyat and T. A. Lipo, "Analysis of concentrated winding induction machines for adjustable speed drive applications-experimental results", *IEEE Transactions on Energy Conversion,* vol. 9, pp. 695-700, Dec. 1994.

[29] H. A. Toliyat, M. M. Rahimian and T. A. Lipo, "dq modeling of five-phase synchronous reluctance machines including third harmonic of air-gap MMF", in *Conference Record of IEEE-IAS Annual. Meeting,* Dearborn, MI, Oct. 1991, vol.1, pp. 231-237.

[30] H. A. Toliyat, M. M. Rahimian and T. A. Lipo, "Analysis and Modeling of Five Phase Converters for Adjustable Speed Drive Applications", in *Proceedings of Fifth European Conference on Power Electronics and Applications,* Brighton, UK, Sept. 1993, vol.5, pp. 194 –199.

[31] H. A. Toliyat, T. A. Lipo and J. White, "Analysis of a concentrated winding induction machine for adjustable speed drive applications - part I (machine analysis)", *IEEE Transactions on Energy Conversion,* vol. 6, pp. 679-683, Dec. 1991.

[32] H. Xu, H.A. Toliyat, and L.J. Peterson, "Five-phase induction motor drives with DSP-based control systems," *IEEE Transactions on Power Electronics*, Vol. 17, No. 4, pp. 524-533, July 2002.

[33] R. Shi, H.A. Toliyat, and A. El-Antably, "Field oriented control of five-phase synchronous reluctance motor drive with flexible 3rd harmonic current injection for high specific torque," in *Conference Record of IEEE-IAS Annual. Meeting*, Chicago, IL, Sept. 30 - Oct. 5, 2001, pp. 2097 – 2103.

[34] R. O. C. Lyra and T. A. Lipo," Torque density improvement in a six-phase induction motor with third harmonic current injection," *IEEE Transactions on Industry Applications*, vol. 38, pp. 1351 – 1360, Sept./Oct. 2002.

[35] Y. Kats, "Adjustable-speed drives with multi-phase motor", in *Proc. International Electric Machines and Drives Conference,* Milwaukee, WI, May 1997, pp. TC2/4.1 -TC2/4.3.

[36] M. G. Simoes, N. N. Franceschetti, and P. Vieira," Design and evaluation of a polyphase brushless DC-machine direct drive system," *Industry Applications Conference, 2001. Thirty-Sixth IAS Annual Meeting*, Chicago, IL, Oct. 2001, vol. 2, pp. 835 – 842.

[37] Q. Mingzhong, R. Xiuming, and Z. Xiaofeng, "Effect of PWM chopper on the electromagnetic torque of multi-phase PM propulsion motor," in *Proceedings of the Fifth International Conference on Electrical Machines and Systems,* Shenyang, China, Aug. 2001, vol. 1, pp. 561 – 563.

[38] R. Xiuming, Y. Bingchuan, and H. Hai, "High-power multi-phase permanent magnet (PM) propulsion motor," in *Proceedings of the Fifth International Conference on Electrical Machines and Systems*, Shenyang, China, Aug. 2001, vol. 2, pp. 835 – 837.

[39] M. G. Simoes, and P. Vieira," A high torque low-speed multi-phase brushless machine a perspective application for electric vehicles," *Industrial Electronics Society, IECON,* vol. 2, pp. 1395 – 1400, Nov. 2000.

[40] Q. Mingzhong, Z. Xiaofeng, and R. Xiuming," Research of the mathematical model and sudden symmetrical short circuit of the multi-phase permanent-magnet motor," in *International Conference on Power System Technology*, Wuhan, China, vol. 2, Oct. 2002, pp. 769 – 773.

[41] X. Xi, W. Yufei; C. Jianyun, L. Yongdong and W. Xiangheng, "Performance analysis of multi-phase PM brushless DC motor drive system," in *Sixth*

International Conference on Electrical Machines and Systems, Beijing, China, vol. 1, Nov. 2003, pp. 84 – 87.

[42] E. Levi, M. Jones, and S. N. Vukosavic, "Even-phase multi-motor vector controlled drive with single inverter supply and series connection of stator windings," *IEE Proceedings of Electric Power Applications*, vol.150, pp. 580 – 590, 2003.

[43] J. P. Martin, F. Meibody-Tabar and B. Davat, "Multiple-phase permanent magnet synchronous machine supplied by VSIs, working under fault conditions," in *Conference Record of IEEE-IAS Annual. Meeting,* Rome, Italy, Oct. 2000, vol. 3, pp. 1710-1717.

[44] A. G. Jack, B. C. Mecrow and J. A. Haylock, "A comparative study of permanent magnet and switched reluctance motors for high-performance fault-tolerant applications," *IEEE Transactions on Industry Applications*, vol. 32, pp. 889-895, July/Aug.1996.

[45] B. C. Mecrow, A. G. Jack, J. A. Haylock and J. Coles, " Fault-tolerant permanent magnet machine drives, " *IEE Proceedings of Electric Power Applications*, vol. 143, pp. 437-442, Nov. 1996.

[46] J. A. Haylock, B. C. Mecrow, A. G. Jack, and D. J. Atkinson, "Operation of a fault tolerant PM drive for an aerospace fuel pump application," *IEE Proceedings of Electric Power Applications*, vol. 145, pp. 441 – 448, Sept. 1998.

[47] W. Jiabin, K. Atallah and D. Howe," Optimal torque control of fault-tolerant permanent magnet brushless machines," *IEEE Transactions on Magnetics*, vol, 39, pp. 2962 – 2964, Sept. 2003.

[48] J. D. Ede, K. Atallah, W. Jiabin and D. Howe, "Effect of optimal torque control on rotor loss of fault-tolerant permanent-magnet brushless machines," *IEEE Transactions on Magnetics,* vol. 38, pp. 3291 – 3293, Sept. 2002.

[49] J. A. Haylock, B. C. Mecrow, A. G. Jack, and D. J. Atkinson," Operation of fault tolerant machines with winding failures," *IEEE Transactions on Energy Conversion,* vol. 14, pp. 1490 – 1495, Dec. 1999.

[50] R. Krishnan, *Electric Motor Drives: Modeling, Analysis, and Control*, Englewood Cliffs, NJ: Prentice Hall, 2001.

[51] L. Takahashi, and T. Noguchi, " A new quick response and high efficiency strategy of induction motor", in *Conference Record of IEEE-IAS Annual. Meeting*, Rome, Italy, Oct. 1985, pp. 495-502.

[52] M. Depenbrock, “Direct self control (DSC) of inverter-fed induction machines” *IEEE Transaction on Power Electronics,* Vol. 3, No. 4, pp. 420-429 Oct. 1988.

[53] M.R. Zolghadri, J. Guiraud, J. Davoine, and D. Roye, “ A DSP based direct torque controller for permanent magnet synchronous motor drives” in *Power Electronics Specialists Conference*, Fukuoka, Japan, May 1998, pp. 2055 – 2061.

[54] M.F. Rahman, L. Zhong, W.Y. Hu, K.W. Lim, and M.A. Rahman, “An investigation of direct and indirect torque controllers for PM synchronous motor drives” in *International Conference on Power Electronics and Drive Systems,* Singapore, May 1997 , vol. 2 pp. 519 – 523.

[55] S. Dan, F. Weizhong, and H. Yikang “Study on the direct torque control of permanent magnet synchronous motor drives,” in *International Conference on Electrical Machines and Systems,* Shenyang, China, Aug. 2001, vol. 1, pp. 571-574.

[56] J. Faiz, and S.H. Mohseni-Zonoozi, “A novel technique for estimation and control of stator flux of a salient-pole PMSM in DTC method based on MTPF,” *IEEE Transactions on Industrial Electronics,* vol. 50, pp. 262-271, Apr. 2003.

[57] Z. Tan, Y. Li, and M. Li, “ A direct torque control of induction motor based on three-level inverter” in *Power Electronics Specialists Conference*, Vancouver, Canada, June 2001, vol. 2, pp. 1435-1439.

[58] C. Martins, X. Roboam, T. A. Meynard, and A. S. Caryalho, “ Switching frequency imposition and ripple reduction in dtc drives by using a multi-level converter*,” IEEE Transaction on Power Electronics*, vol. 17, pp. 286-297, Mar. 2002.

[59] M. Fu, and L. Xu “A sensorless direct torque control technique for permanent magnet synchronous motors**”** *Power Electronics in Transportation*, Dearborn, MI, Oct. 1998, pp. 21 – 28.

[60] V. Comnac, M.N. Cirstea, F. Moldoveanu, D.N. Ilea, and R.M. Cernat, “Sensorless speed and direct torque control of interior permanent magnet synchronous machine based on extended Kalman filter” in *Proceedings of the 2002 IEEE International Symposium on Industrial Electronics*, L'Aquila, Italy, Jul. 2002 , pp. 1142-1147.

[61] P. Vas, *Sensorless Vector and Direct Torque Control*, NY: Oxford University Press, 1998.

[62] M.F. Rahman, M.E. Haque, L. Zhong, and M. Nagrial, " A sensorless speed estimator for the direct torque control of an interior permanent magnet synchronous motor drive" in *International Conference on Power Electronics, Machines and Drives,* Bath, UK, June 2002, pp. 504 – 509.

VITA

Leila Parsa received the B.S. degree from Khaje Nassir Toosi University of Technology and the M.S. degree with Certificate of Merit from Iran University of Science and Technology, Tehran, Iran in 1996 and 1999, respectively, both in electrical engineering. She has worked as an electrical engineer in Ghods Niroo Consulting Engineers from 1997 to 1999. From December 1999 to December 2000, she worked as a research assistant in Aachen University of Technology, Aachen, Germany. In January 2001, she joined the doctoral program of Department of Electrical Engineering at Texas A&M University and received her Ph.D. in May 2005. She can be reached c/o Prof. H. A. Toliyat, Advanced Electric Machines & Power Electronics Lab., Department of Electrical Engineering, Texas A&M University, College Station, Texas 77843 - 3128.